Impacts of fast water infiltration in fault zones and water extraction on land subsidence

vorgelegt von

ABRAHAM ISAAC MARTINEZ NOGUEZ, M.Sc.

aus Queretaro, Mexiko

von der Fakultät VI Planen | Bauen | Umwelt

der Technischen Universität Berlin

zur Erlangung des akademischen Grades

Doktor der Ingenieurwissenschaften

Dr.-Ing.

Genehmigte Dissertation

Promotionsausschuss

Vorsitzender:	Prof. Dr.-Ing. Matthias Barjenbruch, TU Berlin
Berichter:	Prof. Dr.-Ing. Reinhard Hinkelmann, TU Berlin
	Prof. Dr.-Ing. Savidis Stavros, TU Berlin
	Prof. Dr.-Ing. Rainer Helmig, Universität Stuttgart

Tag der wissenschaftlichen Aussprache: 07.02.2017

Berlin 2017

Dedicated To

My parents Abraham Martinez Baini and Cristina Noguez, my wife, children and family and to my grandfather Abraham Martinez Blanco

ACKNOWLEDGMENT

First I praise the great spirit, my God the one that his name is said as a sigh for give me this opportunity to finish this research and give me the strength and wisdom to proceed successfully.

This work would not be possible without the help of several people who were at my side helping me, encouraging me, guiding me, supporting me day by day through all these years. I would therefore like to offer my sincere thanks to all of them.

I would like to thank most specially Prof. Reinhard Hinkelmann, my supervisor, for accepting me as a PhD student in his chair and for numerous discussions that lead me to obtain a better focus of the way to develop this research, his permanent support and for the great freedom he gave me in carrying out my work. Thanks also to Prof. Savidis Stavros from the Chair of Soil Mechanics and Geotechnical Engineering, TU Berlin, for providing valuable advice and acting as advisor as well as to Prof. Helmig from the Chair, Department of Hydromechanics and Modelling of Hydrosystems, University of Stuttgart for also acting as advisor. This work would not have been possible without the excellent modeling tool (MUFTE-UG) developed by Prof. Helmig as well as the important literature published by him that I used as references. Many thanks to Dr. Mahgoub and Angela Smith for correcting my English.

I would like to express my sincere gratitude to CONACYT for providing me a scholarship to do my PhD study, without this financial support this research could not have been possible.

Also thanks to my parents for showing me the importance of academic studies, principally to my father Ing. Martinez Baini for all his help as father, professor in the university in Mexico and friend. He has been an example of a spirit of achievement. I also want to express my gratitude to my brothers and sisters Alejandro, Karen, Liz and Josué (thanks brother for offer me your house in this beautiful place in La Paz where I finished this work).

Finally, I very specially thank my wife Angela Smith and my children Yonané and Yannik for their understanding and support, thanks that they were at my side always also in the difficult times.

Abstract

Land subsidence is a complex phenomenon which occurs all around the world. The study and understanding of the phenomenon, its causes and effects, the processes, such as flow, deformation and fracturing are very important in a spectrum of approaches for predicting the consequences and future damages. Meanwhile, numerical simulation is an important and powerful tool to analyse land subsidence and predict the impact of changing conditions. It also serves to understand new processes if the conditions will change. The economical damages caused by land subsidence have brought large monetary losses to cities all around the world.

In modern times cities have grown rapidly and likewise have the agricultural and industrial activities. In order to satisfy the new demands for the vital liquid, for which the surface water bodies have not been sufficient, subterranean water has had to be exploited to such an extent that its extraction has outreached groundwater recharge.

The main objective of this research is to deeply analyse the principal conditions, associated hazards, parameters and processes that play an important role in the land subsidence phenomenon using numerical simulation. The present work contains several innovations dealing with advances in model concepts in order to investigate land subsidence processes, fracture formation as well as flow and deformation through fractured soils.

The present work analysed the flow and soil deformation behaviour due to fast water infiltration and water extraction in faulted aquifers through numerical modeling. For the flow a two-phase flow model and for the deformation elasto-

plastic models, the Mohr-Coulomb model and the Hardening Soil model, were applied and weakly coupled.

Three examples of numerical modeling of two-phase flow as well as soil deformation are presented.

The first application is a model of infiltration through a single-layer system. Here the influence of the inclination of the fracture and the inclination of the surface were investigated as well as the soil's deformation.

The second application examined a two-layered system consisting of a stratum with low permeability on its surface and a fracture that allows rapid water flow through the impermeable stratum to the lower stratum with higher permeability. A model concept for fracturing mechanism was also proposed.

The third application describes a model concept for fracturing mechanism after groundwater extraction through a well near a highly permeable pre-existing fault.

An important finding was to show that not only an inclined fault zone with low permeability could act as a hydrological barrier for the water flow in an aquifer but also an inclined fault zone with high permeability. Also the results show that this barrier effect could be a factor for triggering land subsidence.

Another important result of this research was the development of a conceptual model of a mechanism for the generation of fracturing and triggering of land subsidence: fast rain water infiltration through fault zones.

Zusammenfassung

Bodensenkung ist ein komplexes weltweit auftretendes Phänomen. Die Untersuchung und das Verständnis des Phänomens, dessen Ursachen, Auswirkungen und zugehörige Prozesse wie Wasserströmung in der ungesättigter Bodenzone, Verformung und Rissbildung sind für ein breites Spektrum von Ansätzen zur Vorhersage von Auswirkungen und potentiellen Schäden von besonderer Bedeutung. Hierbei ist die numerische Simulation ein sehr mächtiges Instrument zur Untersuchung von Bodensenkung und zur Vorhersage des Einflusses von sich ändernden Bedingungen. Auch neuartige Prozesse können mithilfe der numerischen Simulation besser verstanden werden.

In den letzten Jahren haben die Urbanisierung sowie auch Landwirtschaft- und Industrieflächen stetig zugenommen. Um der wachsenden Nachfrage nach dem lebenswichtigen Element Wasser nachzukommen, sind die Oberflächengewässer oft nicht ausreichend und es muss Grundwasser gepumpt werden. Dabei wird oft mehr Grundwasser gefördert, als sich wieder neu bilden kann.

Das Ziel dieser Arbeit ist eine auf numerischer Simulation basierende Analyse der Bedingungen, die zu Bodensenkung führen. Dies umfasst auch die damit verbundenen Gefahren, die Parameter und die Vorgänge, die mit dem Phänomen im Zusammenhang stehen. Die vorliegende Arbeit beinhaltet innovative Ansätze zur Weiterentwicklung bestehender Modellkonzepte, die Bodensenkung, Ausbildung von Störungszonen sowie Strömung und Deformation in geklüfteten Böden beschreiben.

Strömung und Bodenverformung während Wasserextraktion und schnelle Wasserfiltration in Störungszonen wurden numerisch modelliert. Es wurde ein Zwei-Phasen-Strömungsmodell mit elasto-plastischen Bodenverformungs-

modellen, dem Mohr-Coloumb Modell und dem Hardening Soil Modell, schwach gekoppelt.

In der Arbeit werden drei Fallbeispiele präsentiert:

Das erste Fallbeispiel modelliert Infiltration durch ein einschichtiges System. Dabei wurden der Einfluss der Neigung der Störungszone und der Oberfläche sowie die Bodenverformung untersucht.

Im zweiten Fallbeispiel wurde ein zweischichtiges Modell untersucht. Das Modell besteht aus einer Schicht mit geringer Durchlässigkeit an der Oberfläche und einer Störungszone, die einen schnellen Wasserdurchfluss von der gering durchlässigen Schicht zu der unteren Schicht mit höherer Durchlässigkeit ermöglicht. Es wurde ein Modellkonzept für die Ausbildung von Störungszonen vorgeschlagen.

Das dritte Fallbeispiel beschreibt ein Modellkonzept für die Ausbildung von Störungszonen nach Grundwasserextraktion durch einen Brunnen in der Nähe einer bereits bestehenden Störungszone. Hier war eine wichtige Erkenntnis, dass neben einer geneigten schrägen Störungszone mit geringer Durchlässigkeit auch eine geneigte Störungszone mit hoher Durchlässigkeit als Strömungsbarriere in einem Aquifer wirken kann. Die Ergebnisse der Modellierung zeigen, dass diese Barrierenwirkung Bodensenkung hervorrufen kann.

Eine weitere wichtige Erkenntnis dieser Forschungsarbeit ist die Entwicklung eines konzeptionellen Modells, welches den Mechanismus der Ausbildung von Störungszonen und Bodensenkungen aufgrund schneller Regenwasserinfiltration durch Störungszonen beschreibt.

Contents

Nomenclature

Terms with Latin letters

Symbol	dimension	definition
g	[m/s^2]	gravity
g	[-]	plastic potential function
h	[m]	piezometric head
h	[m]	water level
n,m	[-]	*Van Genuchten* (VG) parameter
$\underline{n}$	[-]	normal vector
c	[Pa]	cohesion
E	[Pa]	Young's modulus
E_{50}	[Pa]	stiffness modulus for primary loading
E_{ur}	[Pa]	stiffness modulus for un-/reloading stress path
$\overline{f}$	[Pa]	function of stress
f^s	[-]	yield function
f^c	[-]	cap yield surface
G	[Pa]	modulus of rigidity
P	[Pa]	pressure
P_c	[Pa]	capillary pressure
P_d	[Pa]	*Brooks-Corey* (BC) parameter, entry pressure
P_g	[Pa]	pressure of gas phase
p_p	[Pa]	isotropic pre-consolidation stress
q_f	[Pa]	ultimate deviatoric stress
q_a	[Pa]	ultimate asymptotic stress
q_w	[kg/m^{3}s]	sink or source of water
q_n	[kg/m^{3}s]	sink or source of non-wetting phase
$\tilde{q}$	[Pa]	stress measure for deviatoric stresses
t	[s]	time
v	[m/s]	flow velocity
$\underline{v}_\alpha$	[m/s]	pore velocity
$\underline{v}_f$	[m/s]	filter or *Darcy* velocity
$\underline{v}_{f\alpha}$	[m/s]	*Darcy* velocity of phase α
F_s	[N]	force

T	[Pa]	stress
$\underline{\underline{\dot{D}^e}}$	[MPa]	elastic material stiffness matrix
$\underline{\underline{K}}_f$	[m/s]	hydraulic conductivity tensor
$\underline{\underline{K}}_\alpha$	[m^2]	effective permeability tensor
$k_{r\alpha}$	[-]	relative permeability
$\underline{\underline{K}}$	[m^2]	intrinsic permeability
$\underline{\underline{M}}$	[MPa]	material stiffness matrix
Re	[-]	*Reynolds* number
S	[-]	saturation
S_α	[-]	saturation of phase α
S_e	[-]	effective saturation
S_n	[-]	non-wetting phase saturation
S_{gr}	[-]	residual gas saturation
S_w	[-]	wetting phase saturation
S_{wr}	[-]	residual water saturation
T	[°]	temperature
V	[m^3]	volume

Terms with Greek letters

Symbol	dimension	definition
α	[1/Pa]	*Van Genuchten* (VG) parameter
λ	[-]	*Brooks-Corey* (BC) parameter
λ	[-]	plastic multiplier
ν	[m^2/s]	kinematic viscosity, ν=μ/ρ
μ	[N s/m^2]	dynamic viscosity
γ^P	[-]	function of plastic strains
$\dot{\gamma}^P$	[-]	function of plastic shear strains
$\underline{\varepsilon}$	[-]	strain
$\underline{\dot{\varepsilon}}$	[-]	strain rate
ρ	[kg/m^3]	density
ρ_α	[kg/m^3]	density of air
ρ_w	[kg/m^3]	density of water
σ	[Pa]	normal stress

$\underline{\underline{\sigma}}$	[Pa]	stress tensor
$\underline{\sigma}'$	[Pa]	effective stress
$\underline{\dot{\sigma}}'$	[Pa]	effective stress rate
σ_1', σ_2', σ_3'	[Pa]	major compressive stress
τ	[Pa]	tangential or shearing stress
υ	[-]	Poisson's ratio
Φ	[-]	porosity
φ	[°]	friction angle
φ_P	[°]	failure friction angle
$\underline{\dot{\varepsilon}}^p$	[-]	plastic strain rate
$\dot{\varepsilon}_v^P$	[-]	plastic volumetric strain rate
ψ	[°]	dilatancy angle

List of figures

List of tables

1 Introduction

Land subsidence is one of the challenging issues that need to be addressed in many countries including Australia, China, Egypt, France, Germany, India, Iran, Israel, Italy, Japan, Mexico, Poland, Saudi Arabia, Sweden, the Netherlands, UK and USA.

Since prehistory, humans had to concentrate their activities close to bodies of fresh surface water. During the transition period between the Palaeolithic and the Neolithic the climate changes led to a shortage in hunting and the progressive desertification together with the factors related to the development of agriculture and domestication of animals made human-beings shift from a nomadic to a sedentary lifestyle. The first civilizations emerged close to rivers and depended totally on these water bodies, as for example Mesopotamia which in Greek etymology means *between rivers* (meso – middle, potamos – river). As shown in Figure 1.1, all civilizations in Mesopotamia were situated along the banks of the Euphrates and Tigris.

Another example is Egypt (Figure 1.2) which would be a completely arid and desert zone if the Nile river did not exist. There are many similar examples all around the world.

The use of wells enabled humans to move further away from the water bodies and to meet the needs for water during dry periods.

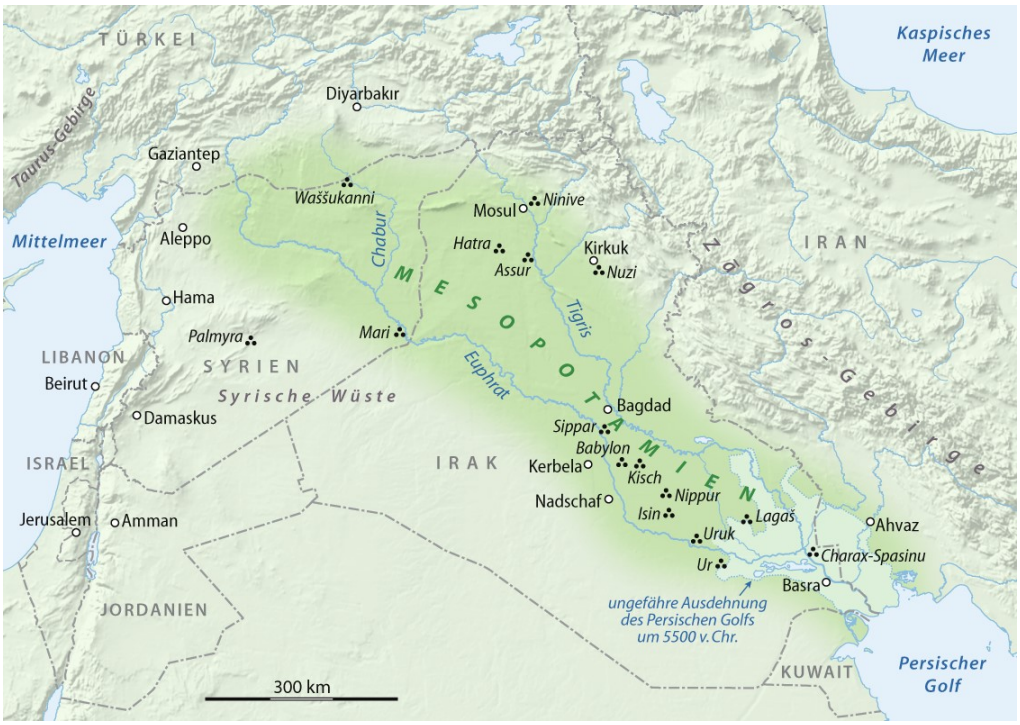

Figure 1.1 Human settlement in Mesopotamien (Wikipedia, 2015) http://de.wikipedia.org/wiki/Mesopotamien 13.05.2015

Some archaeological discoveries of wells date back to the Pre-Pottery Neolitic period (8100-7500 BC) like in the case of the well discovered in Atlit-Yam (Galili *et al*. 1993) at the coast of Israel. The use of wells has enabled the development of civilizations around the globe.

Only three percent of all the earth's water is fresh water. The majority, about 69 percent, is locked up in glaciers and icecaps, mainly in Greenland and the Antarctic. The remaining freshwater is groundwater. Only 0.3 percent of the freshwater is contained in rivers and lakes (Figure 1.3).

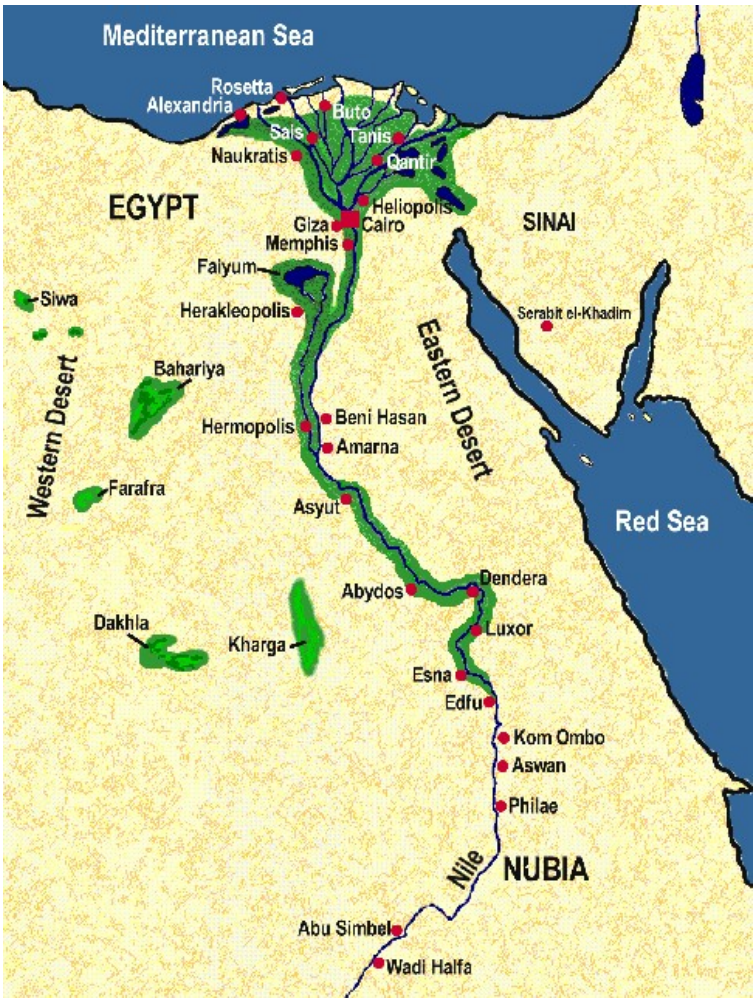

Figure 1.2 Settlements close to Nile river (Ancient Egypt, 2015) http://www.ancient-egypt.info/2012/03/egyptian-nile-river-and-god-kings-of.html

In modern times cities have grown rapidly and likewise have the agricultural and industrial activities. In order to satisfy the new demands for the vital liquid, for which the surface water bodies have not been sufficient, subterranean water has had to be exploited to such an extent that its extraction has outreached groundwater recharge. Especially in arid and semi-arid zones this has produced a deficit leading to a rapid dismantling of the groundwater table.

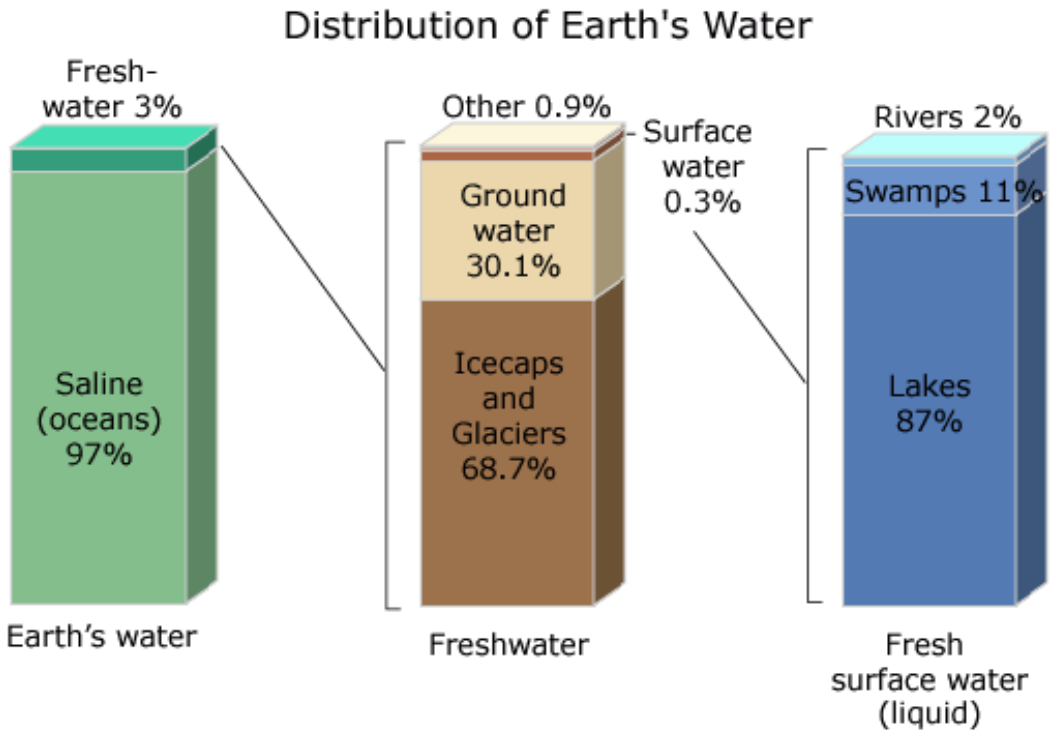

Figure 1.3 Distribution of Earth´s Water (USGS)
http://water.usgs.gov/edu/earthwherewater.html

In heterogeneous stratums the fast dismantling of the groundwater table leads to a differential settlement and in some cases to a formation of cracks and fractures on the surface of the ground. The here mentioned mechanism as well as the different conceptual models of the formation of cracks and fractures will be explained in detail in the following sections.

1.1 Motivation

Land subsidence is a complex phenomenon which occurs all around the world. The study and understanding of the phenomenon, its causes and effects, the processes, such as physical processes like flow, deformation and fracturing are very important in a spectrum of approaches for predicting the consequences and future damages. Meanwhile, numerical simulation is an important and powerful

tool to analyse land subsidence and predict the impact of changing conditions. It also serves to understand new processes if the conditions will change.

1.2 Land subsidence: definition and causes

The word subsidence comes from the Latin word subsidere (settle, sink, subside). It uses the Latin prefix sub- (under) and the Latin word sidere (settle, sink down, sit down). Land subsidence is the lowering of a portion of the earth's crust. The Oxford dictionary defines subsidence as "the gradual caving in or sinking of an area of land". Pacheco *et al*. (2007) defined land subsidence as "the phenomenon that is caused by the extraction of solids (minerals) or fluids (e.g. gas, petrol, vapour and water) from the subsoil which manifests itself in gradual or sudden sinkings of the surface and in the formation of cracks in the granular fill layer".

There are different causes of land subsidence. Some causes are natural causes but many of them are anthropogenic resulting from the exploitation of resources. The principal causes of land subsidence are aquifer-system compaction, drainage of organic soil, underground mining, hydro-compaction, natural compaction, sinkholes, and thawing permafrost (USGS 1999). Martinez-Noguez *et al*. (2012) found that also fast water infiltration through faults and fractures can produce land subsidence on the surface of the earth. Although there are many causes, the exploitation of groundwater is the most dominant around the world. Figure 1.4 shows land subsidence causes.

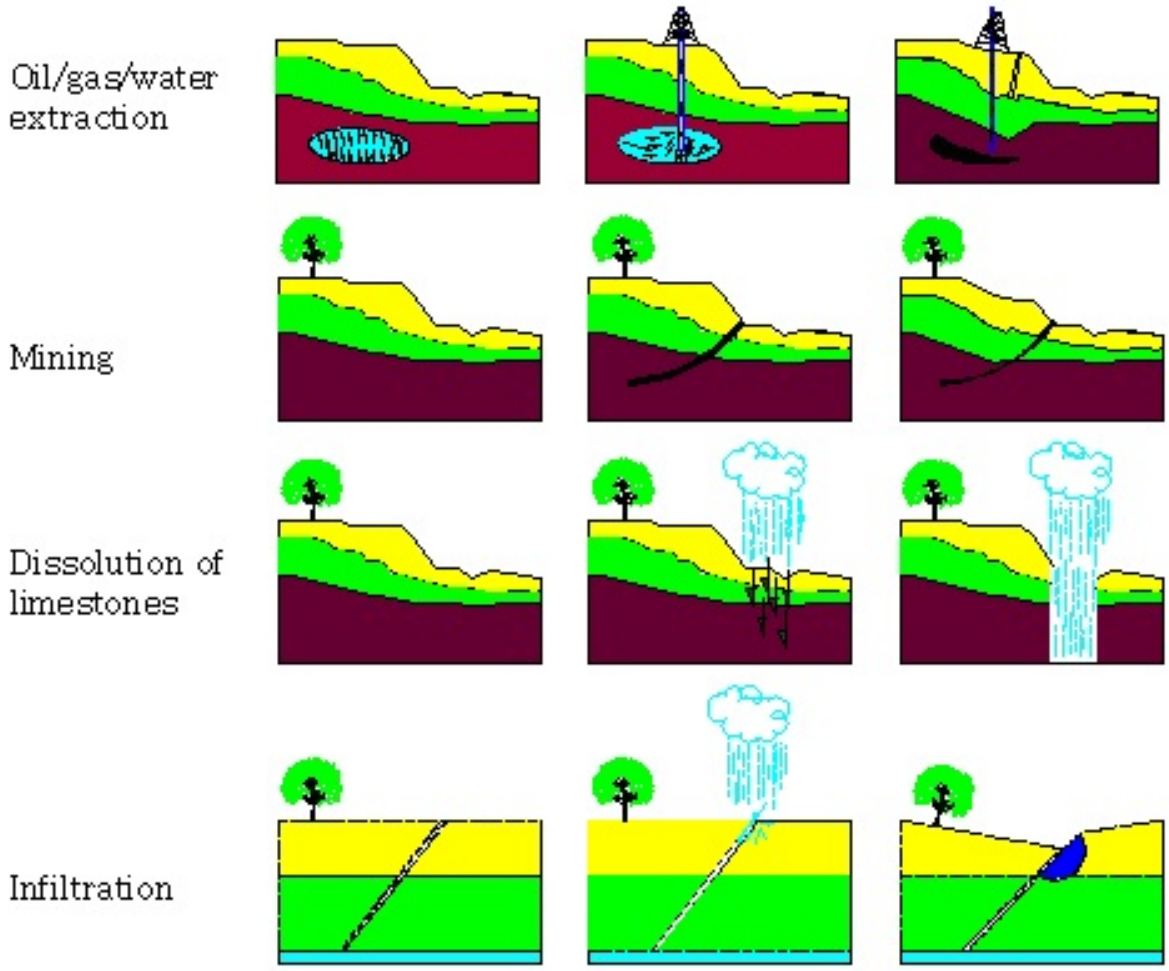

Figure 1.4 Land subsidence causes

1.3 Classification and mechanisms of subsidence

In 1979 Prokopovich presented a classification of land subsidence by origin. He divided land subsidence into two groups: endogenic, caused by processes originating within the planet associated to internal geological processes such as volcanism, folding, faulting; and exogenic, caused by processes originating near the earth´s surface. He subdivided exogenic into subsidence caused by removal or weakening of support and subsidence caused by an increase in actual or effective loading. The classification of Prokopovich is presented in Figure 1.5.

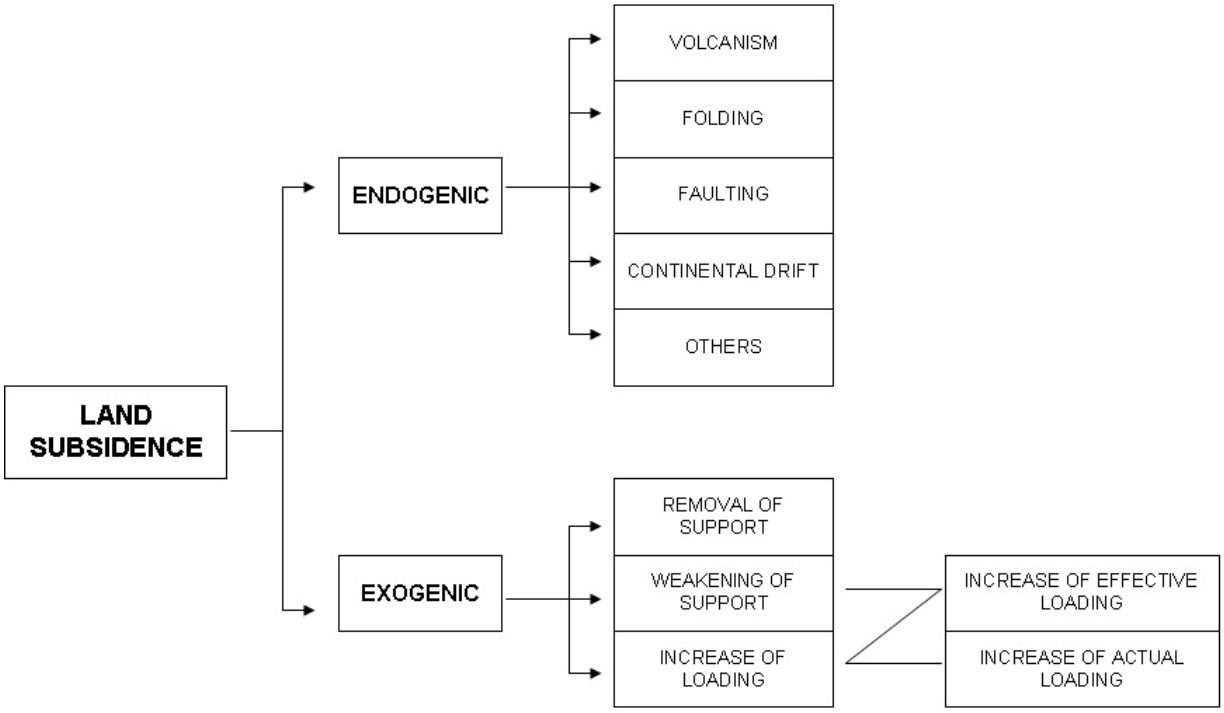

Figure 1.5 Genetic classification of land subsidence (Prokopovich 1979)

Some of the causes of the subsidence processes are the extraction activity of minerals in mining galleries, tunnel construction, fluid extraction (water, oil or gas) from natural reserve, decrease of groundwater level during prolonged dryness, natural land dissolution, compaction of soil materials or tectonic activity (Tomás *et al*. 2009).

In 2009 Tomás *et al*. explained some of the causes of land subsidence. In the following the causes are presented.

Sodium chloride (NaCI) is one of the most soluble materials in the crust of the earth. Other materials like gypsum and the carbonic rocks are also water soluble and can generate extended interconnected hole systems which lead to deformation and in extreme cases to a collapse generating subsidence (Figure 1.6).

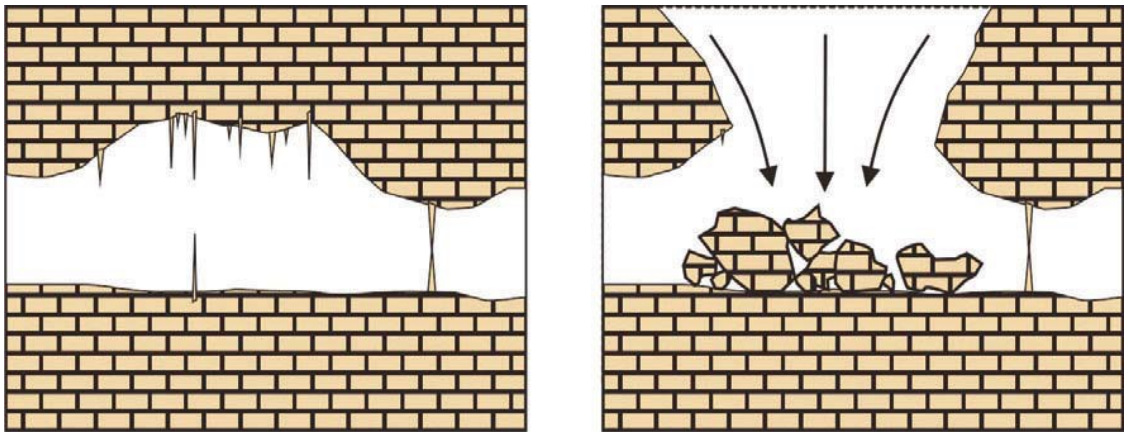

Figure 1.6 Subsidence generated by carbonate rocks dissolution (Tomás *et al*. 2009)

Subsidence produced by the excavation of ground tunnels or mining galleries leads to the lowering of the earth because of the deformation or collapse of the generated galleries resulting from the extraction of material or in the construction of tunnels (Figure 1.7).

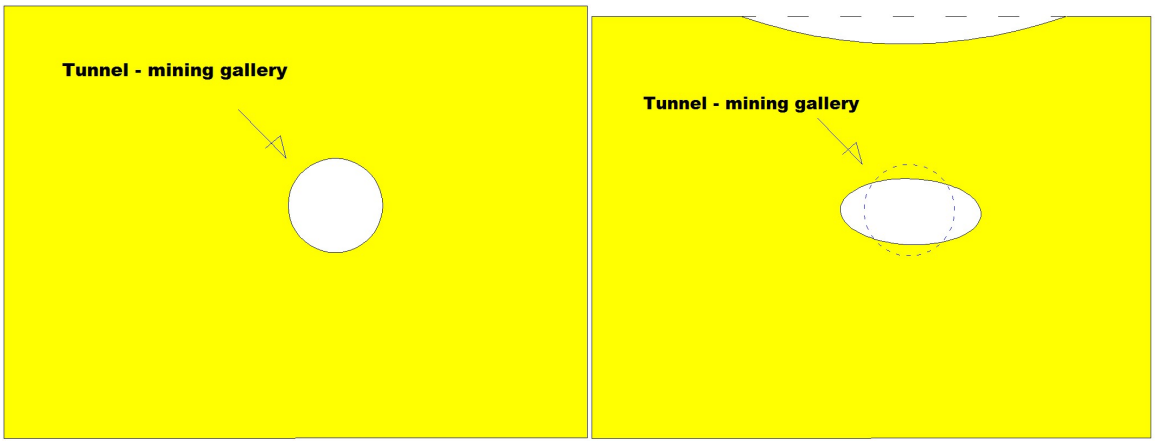

Figure 1.7 Subsidence by mining galleries (Tomás *et al*. 2009)

Subsidence produced by subterranean erosion is due to a mechanical process. When water flow transports soil particles, a system of channels is generated and these channels can collapse. This phenomenon is known as “piping” (Figure 1.8).

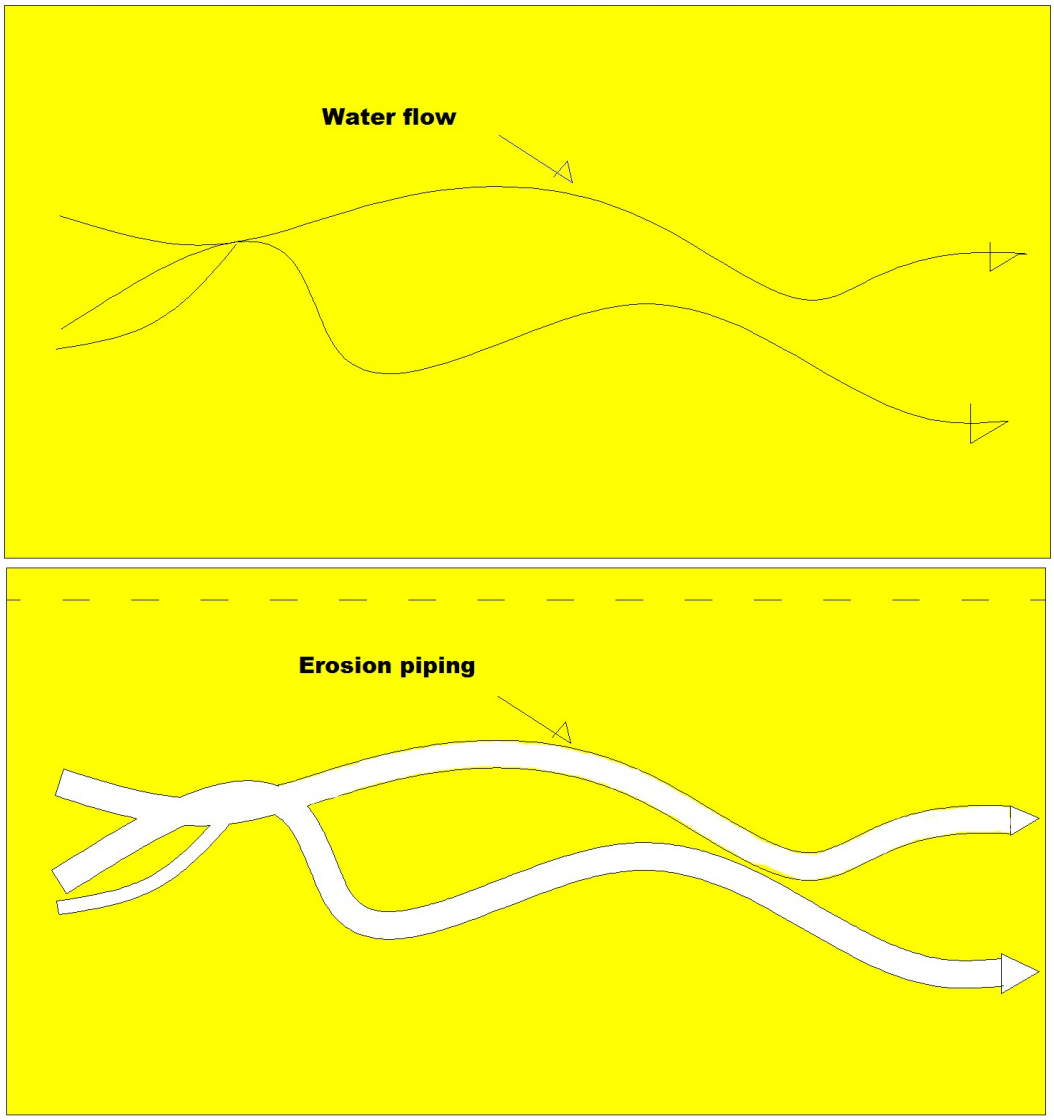

Figure 1.8 Subsidence by erosion (piping) (Tomás *et al*. 2009)

The natural excessive accumulation of sediments or some foundation types can produce soil consolidation, which is the result of extra load produced by the sediments or the constructions (Figure 1.9).

Vibrations produced by an earthquake, explosions or other causes can produce a rearrangement of particles in non-consolidated granular soils during the compaction process (Figure 1.10).

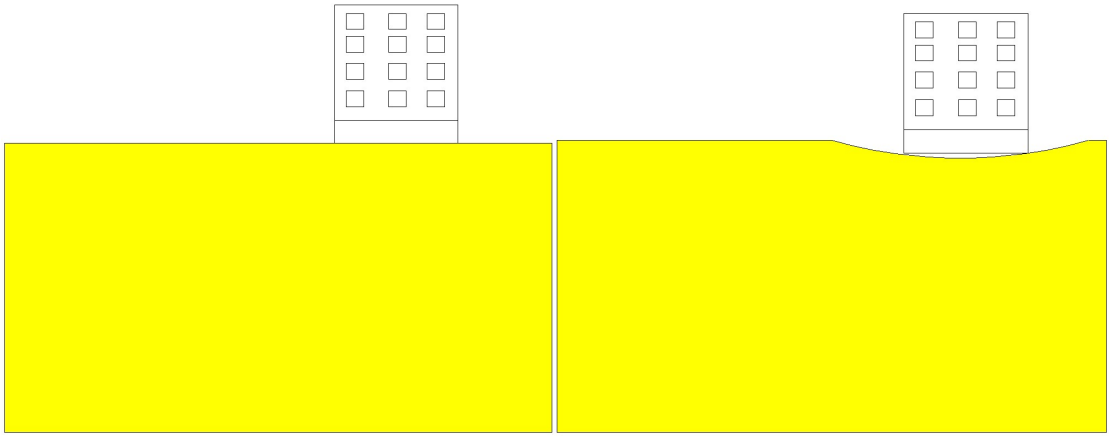

Figure 1.9 Subsidence by load (Tomás *et al*. 2009)

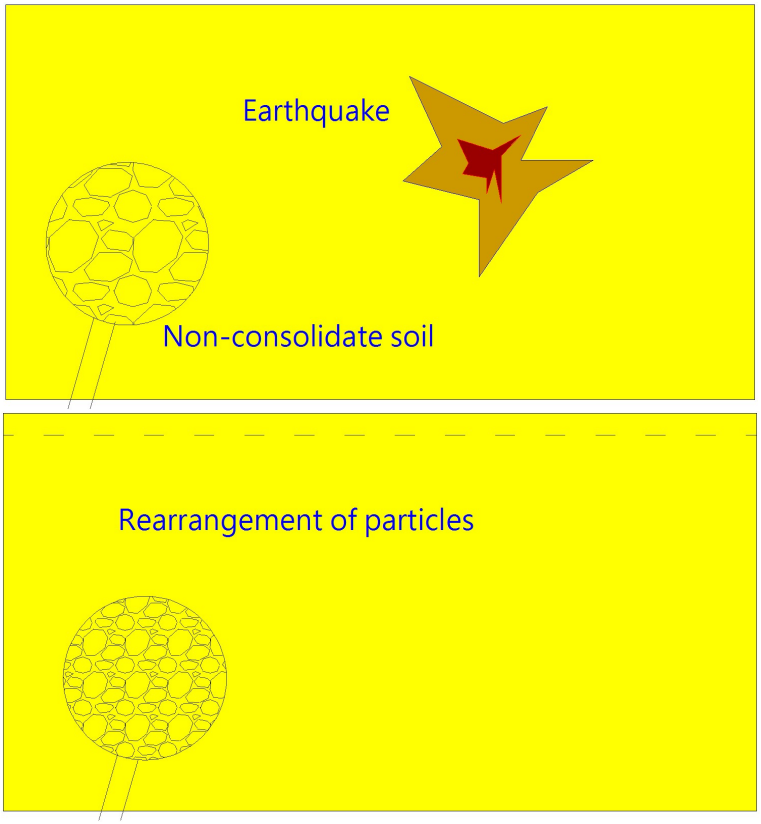

Figure 1.10 Subsidence by vibrations (Tomás *et al*. 2009)

The lowering of the earth's surface through the faults produces an effect called tectonic subsidence. This kind of subsidence is in general slow and in the range of small magnitudes (millimetres per year or less) (Figure 1.11).

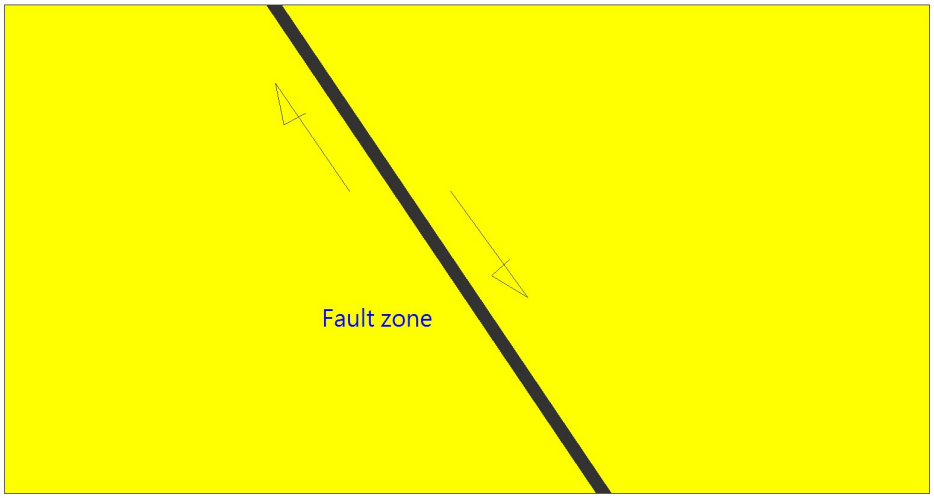

Figure 1.11 Tectonic subsidence (Tomás et al. 2009)

1.4 Unsaturated flow and deformation

The water table is generally below the land surface. It fluctuates seasonally and from year to year depending on the changes in the recharge from precipitation and surface water bodies. Groundwater occurs in two principal zones, the unsaturated zone and the saturated zone. In the unsaturated zone, the space between particle grains and cracks in rocks contain both water and gases (mainly air and some water vapour). In contrast, the voids in the saturated zone are completely filled with water. Between the unsaturated zone and the water table there is a transition zone called the capillary fringe (Figure 1.12). In this zone, the groundwater seeps up from the water table by capillary forces.

When compared to groundwater flow unsaturated flow processes are in general more complicate and difficult to describe quantitatively, since they often entail changes in the state and content of soil water during flow. The formulation and solution of subsurface flow problems very often requires the use of indirect methods of analysis, based on approximations or numerical techniques (Kumar 2002).

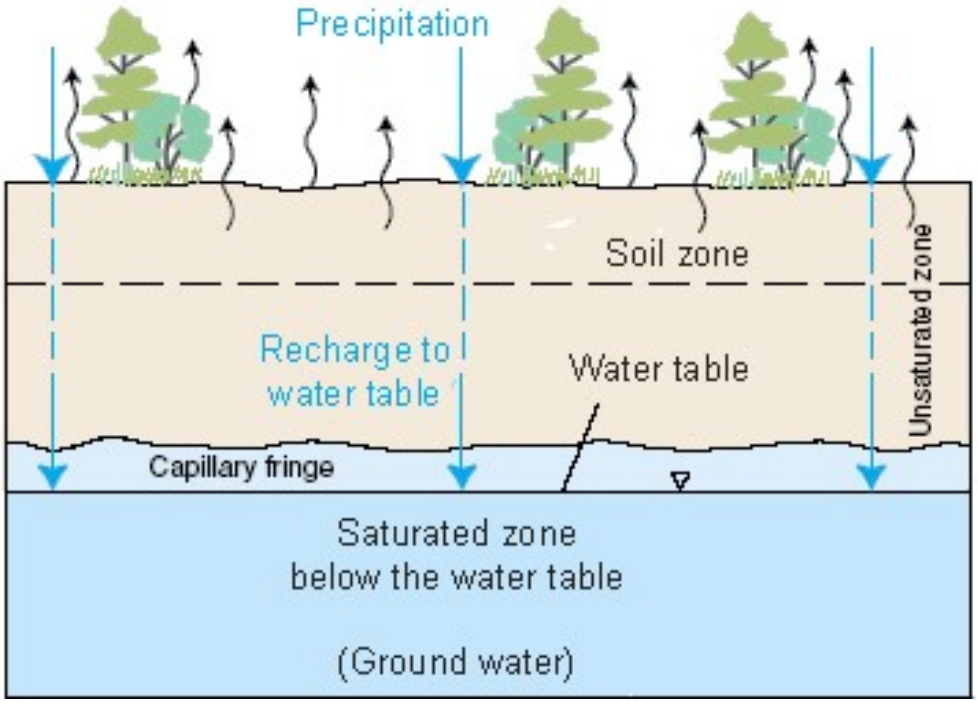

Figure 1.12 The unsaturated zone, capillary fringe, water table and saturated zone (USGS 1999)

In this research, a two-phases flow model concept for porous media was used for modeling the flow of two fluid phases that are not or only slightly miscible into each other, e.g. water, gas, air, etc. It is worth to mention that a Richards model concept is also suitable for such cases. Further information about the model concept is found e.g. in Hinkelmann (2005).

Plasticity associates irreversible strains. As soil behaviour is highly non-linear and irreversible, in this research a linear-elastic perfectly-plastic Mohr-Coulomb model and Hardening Soil model has been applied.

1.5 Impacts of land subsidence around the world

Land subsidence is not considered a natural disaster like an earthquake or a tsunami because its effects are not instantaneous, but they are perceptible in the long term. The economical damages caused by land subsidence have brought large

monetary losses to cities. For example, in 1991 the National Research Council estimated that annual costs in the United States of America from flooding and structural damage caused by land subsidence exceeded 125 million dollars (USGS 1999).

Since the middle of the 20th century, certain forms of land subsidence, related to human activities, have become widespread. Around the world there are many examples of land subsidence reported in literature.

Land subsidence not only affects visible infrastructure but also pipes, drainage and pipelines (Figure 1.13). The breaking of water pipes may add chlorine rapidly through the fracture of the earth to superficial aquifer formations. Microorganisms and organic material easily migrate from a broken drainage.

Buildings and historic monuments suffer damages due to land subsidence. An example is the Mexico City Metropolitan Cathedral which experiences differential subsidence (Figure 1.14). This is consistent with observations in past decades (Villa *et al*. 2005). Part of the Cathedral's foundations is located on top of a pre-Hispanic Aztec temple. The lack of uniformity in the degree of consolidation of the clay layers underlying different parts of its foundations generated great differential settlements of the large heavy masonry structure (Osmaniğlu *et al*. 2010, Meli & Sánchez 1997, Meli *et al*. 2001).

Land subsidence also produces a social impact (Rodríguez-Castillo & Rodríguez-Velázquez 2006). Damage to buildings and houses are covered by the owners, even in case of complete loss of the building (Figure 1.15 and 1.16).

Figure 1.13 Broken water pipe showing lateral movement (Anonym)

Figure 1.14 Mexico City Cathedral

Figure 1.15 Complete loss of a house in Querétaro, Mexico

Figure 1.16 Street damage in Querétaro, Mexico

Another example of social impact is the occurrence of a massive sinkhole opened up in the backyard of a house in the Jonesville area, west of Gainesville, USA, this forced the family to evacuate its home. (Figure 1.17, The Gainville Sun, 2012).

Figure 1.17 A large sinkhole opened up in the backyard in the Jonesville area, west of Gainesville, (McClenny 2012)

In many areas in Japan land subsidence is active. The Environmental Protection Agency of Japan reported in 1995 that principal subsiding areas are distributed in 37 prefectures with 62 regions. The 11 areas where subsiding exceeds 20 mm per year amount to 276 km^2.

In Germany Wolkersdorfer & Thiem (2006) presented a study of land subsidence caused by groundwater withdrawal in Northeastern Saxony where several large open pit lignite mines are located. Most of the open pits are 120-150 meters deep. Nevertheless, a large area is affected by groundwater withdrawal. There is concern that differential subsidence due to mine dewatering might cause vertical stress and building damage.

In 2011, Ganguli presented a work about land subsidence in Singur block, district Hoohhly, West Bengal, India, due to groundwater extraction. He found from the observation that the rate of decline of the static water table, the depth of the total aquifer system and the hydrogeological characteristics of the aquifer control the

rate of subsidence of the area. The average rate of subsidence was 0.92 mm per year during 1998 and 2002 which strongly increased to 8.7 mm per year during 2002 and 2006.

In the United States of America, as well as in many other countries in the world, land subsidence is not an isolated problem: In 1999 USGS reported that an area of more than 15,000 square miles in 45 states experienced land subsidence (Figure 1.18).

Figure 1.18 Land subsidence in USA (USGS 1999)

They reported three principal processes causing land subsidence: the compaction of aquifer systems (Ingebritsen *et al*. 1999, Galloway *et al*. 1999, Coplin *et al*. 1999, Pavelko *et al*. 1999), the oxidation of organic soils (Ingebritsen *et al*. 1999), and the collapse of cavities in carbonate and evaporate rocks (Kappel *et al*. 1999, Ingebritsen *et al*. 1999).

1.6 Objectives and structure of the research

The main objective of this research is to deeply analyse and better understand the principal conditions, associated hazards, parameters and processes that play an important role in the land subsidence phenomenon using numerical simulation. The present work contains several innovations dealing with advances in model concepts in order to investigate land subsidence processes, fracture formation as well as flow and deformation through fractured soils.

The key processes which lead to land subsidence were first analysed separately using idealized systems to understand the dominant factors. In later steps, the complexity of idealized systems as well as investigations about coupled key processes were carried out to go stepwise from idealized to natural systems. The chosen model concepts are based on fully and partially saturated flows as well as on elastic and plastic deformations in the subsurface together with a weak coupling of flow and deformation.

For this research we defined key processes which drive land subsidence for our work and they will be closer investigated within this thesis. The main areas of investigation deal with:

- fast water infiltration through faults and fractures
- dynamic groundwater table due to withdrawal and replenishment extraction
- elastic and plastic deformation processes
- simple coupling for fluid-structure interaction

The work is divided into five chapters:

Chapter 1 presents an introduction, including the motivation of this work, a definition of land subsidence, causes and classifications. Some examples of land

subsidence around the world as well as key processes investigated in this research are explained in detail.

Chapter 2 includes the main physical and mechanical concepts related to the research, those are mainly the model concept of two-phase flow and deformation in porous media, the used numerical models and coupling approach.

Chapter 3: In view of the results obtained in this investigation, of which one important result was the proposal of a conceptual model for fault and fracture formation, it was decided to add this additional chapter giving an overview of the existing models or mechanisms about fracture formation.

In **Chapter 4** three examples of numerical modeling of two-phase flow as well as soil deformation are presented. The most outstanding or important results obtained during these years investigating land subsidence are exposed here. The first example is a model of fast infiltration through a single-layer system. The second example is a study of fast infiltration and deformation of a two-layered system with a fault zone. The third example is a detailed study of water extraction through a well near a highly permeable pre-existing fault.

Chapter 5 summarizes the main conclusions of the research and gives an outlook on further research.

2 Physical and mathematical model concepts

In this chapter, first, the continuum-mechanical approach for porous media in the subsurface which makes use of the Representative Elementary Volume (REV) concept is explained. Second, a description of fluid and soil properties such as permeability, porosity, density, saturation is given. For the description of flow processes in porous media, the model concept for two-phase flow in the subsurface is described. Then the deformation models are explained, starting with the Terzaghi's one-dimensional consolidation theory, then the Mohr-Coulomb model and the Hardening Soil model. Finally, the coupling of flow and deformation is addressed.

2.1 Physical model concepts

2.1.1 Continuum-mechanical consideration

There are numerous examples of porous materials. Soils, porous or fissured rocks, ceramics, fibrous aggregates, filter papers, sand filters and loaf of bread are just a few. Bear (1972) defined porous medium as:

a) A portion of space occupied by heterogeneous or multiphase matter. At least one of the phases comprising this matter is not solid. They may be gaseous and/or liquid phases. The solid phase is called the solid matrix. That space within the porous medium domain that is not part of the solid matrix is referred to as void space (or pore space).

b) The solid phase should be distributed throughout the porous medium within the domain occupied by a porous medium; solid must be present inside each Representative Elementary Volume (REV).

c) At least some of the pores comprising the void space should be interconnected. The interconnected pore spaces are sometimes termed as the effective pore space. Certain portions of the interconnected pore space may, in fact, also be ineffective as far as flow through the medium is concerned. For example, pores may be dead-end pores, i.e., pores or channels with only a narrow single connection to the interconnected pore space so that almost no flow occurs through them.

If we describe the natural ground as a porous medium, it is not possible to describe processes in a singular pore. Instead of describing each pore we apply volume-averaged values or sizes, i.e. instead of a precise void space, geometry is only applied to a percentage of void space in the REV. Instead of a precise flow velocity distribution inside the pore, only a cross-sectional averaged flow velocity is used. The corresponding discharge can be related to the whole cross-section (filter velocity) or to the cross section of the pores (pore velocity). This depends on the porosity of the porous medium. It is possible to obtain the permeability by means of an equivalent average pore size.

Usually, the model concepts for hydrosystems (subsurface and surface water) are based on a continuum-mechanical consideration. Therefore, the processes occurring on the microscale must be averaged in space and/or time in order to serve as physical quantities, i.e. effective parameters and processes, on the mesoscale (Hinkelmann 2005) (Figure 2.1).

The length scale of a REV (Figure 2.2) is chosen so that it leads to a representative average of the property under consideration, e.g. the porosity φ. The REV must be big enough to avoid inadmissible fluctuations of the property and small enough for spatial variations of the property under consideration to be detected (Hinkelmann 2005).

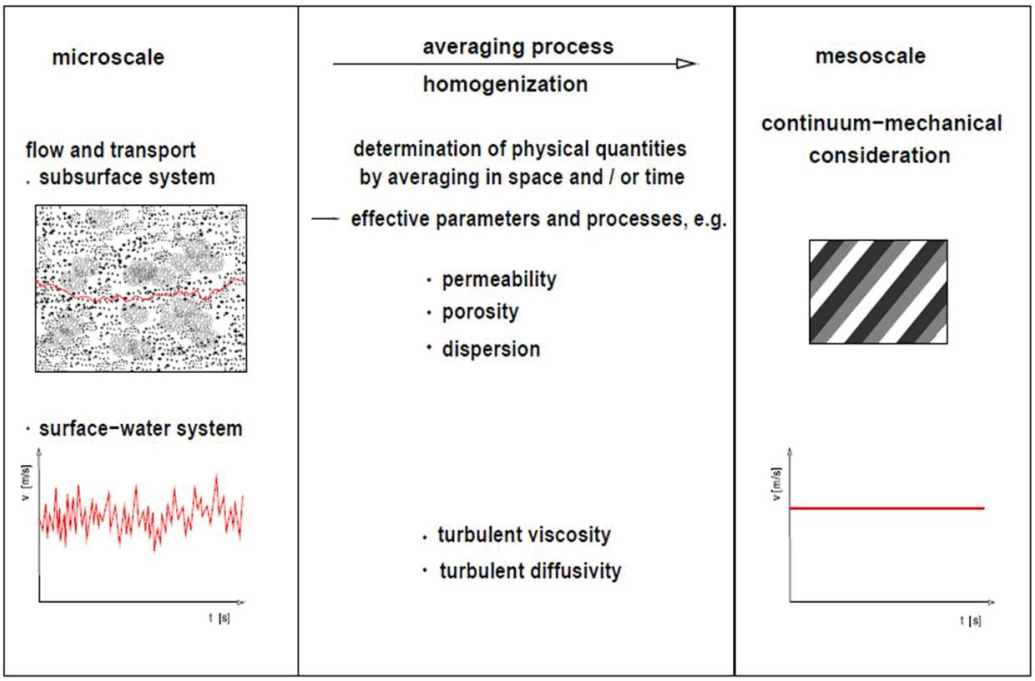

Figure 2.1 Continuum-mechanical consideration, according to Helmig, Cunningham (2002)

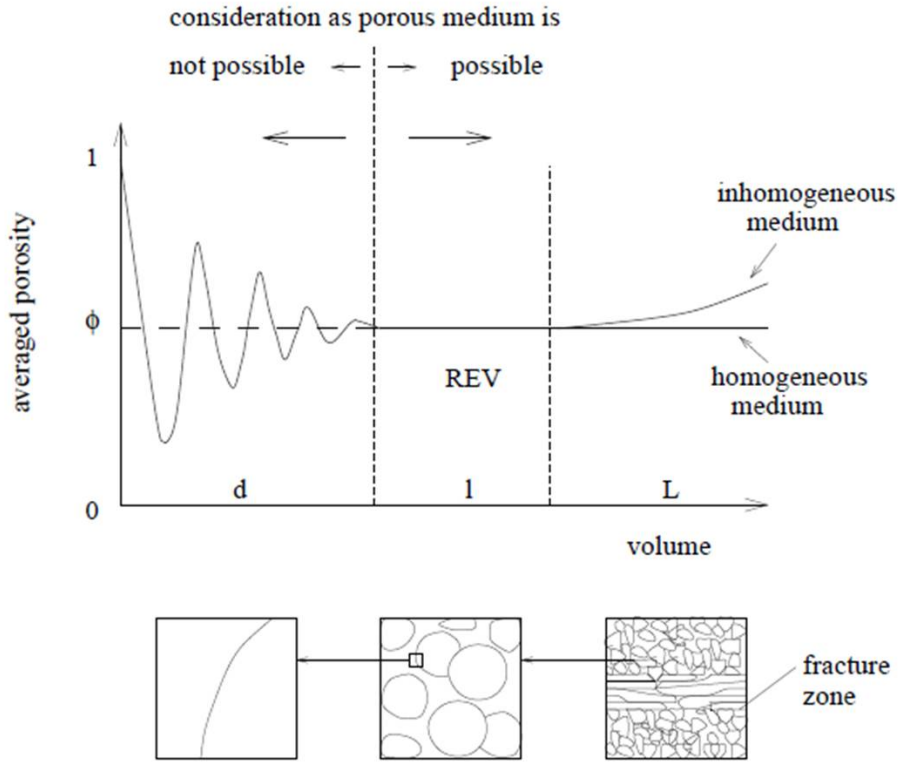

Figure 2.2 Definition of the REV, according to Bear (1972) and Helmig (1997)

2.1.2 Soil phases

In soils we can distinguish 3 phases. The solid phase formed by the mineral particles of soil; the liquid phase, for example water; the gas phase, for example air or greenhouse gases (Figure 2.3). The liquid and gas phase usually cover the void volume and the solid phase covers the solid volume.

A soil is saturated when the whole void space (pores) is filled with water. Soil below the groundwater table is saturated and soil between the ground surface and the water table is partially saturated.

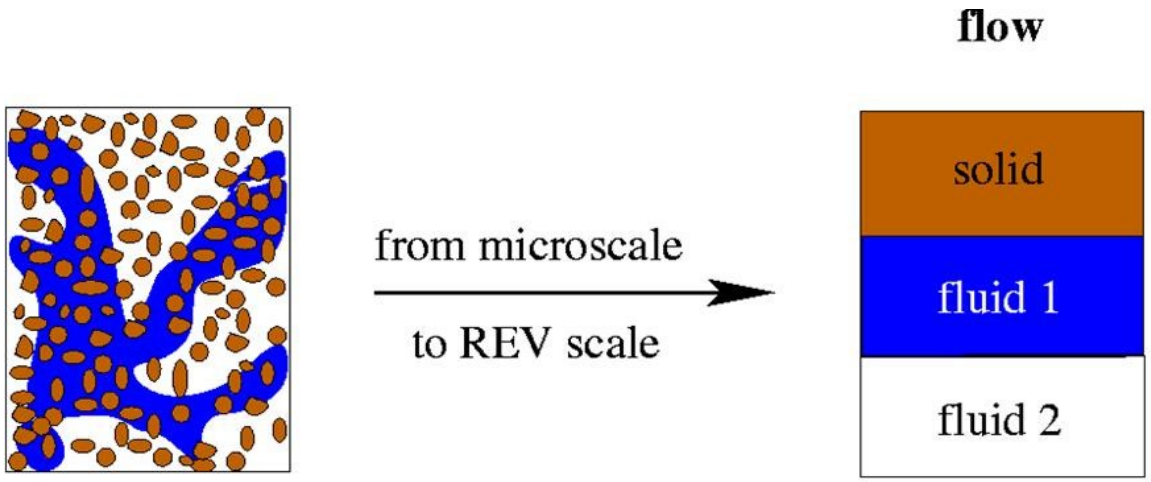

phases:
– solid, e.g. soil
– fluids, e.g. water, gas, NAPL, ..

Figure 2.3 Model concept, definition for phases (Hinkelmann 2005)

2.1.3 Fluid density

Fluid density ρ is defined as the mass m of the fluid per unit volume V. In general, it varies with pressure P and temperature T according to relations called equations of state:

$\rho = \rho(P,T)$ or $f(\rho,P,T) = 0$

$$\rho = \frac{m}{V} \qquad [2.1]$$

The unit of ρ is [Kg/m^3].

A related property is the specific weight γ defined as the weight of fluid per unit volume with the related unit [N/m^3]:

$$\gamma = \rho g \qquad [2.2]$$

Here g is the gravitational acceleration with the unit [m/s^2].

2.1.4 Dynamic viscosity

Viscosity is a measure of the resistance of a fluid which is being deformed by either shear stress or tensile stress. Informally, viscosity is the quantity that describes a fluid's resistance to flow.

The dynamic viscosity μ of a fluid phase determines the dynamics of an incompressible Newtonian fluid and is the property of the fluid phase. Dynamic viscosity is a function of temperature and dissolved constituents. The dynamic

viscosity is employed to convert the hydraulic conductivity $\underline{\underline{K_f}}$ [m/s] to the effective permeability $\underline{\underline{k}}$ [m^2] (see eq. 2.5) when using the Darcy's law.

The unit of the dynamic viscosity is the Pascal second [Pa·s]. An alternative unit of the dynamic viscosity is dyne second per square centimetre [dyne · s/cm^2].

A similar quantity is the kinematic viscosity v which is the ratio of the dynamic viscosity of a fluid to its density.

$$v = \frac{\mu}{\rho} \qquad [2.3]$$

The unit of kinematic viscosity is [m^2/s] or [cm^2/s] which is also called Stokes [St].

2.1.5 Porosity

A porous medium consists of a soil matrix and pores. The porosity Φ (a dimensionless quantity usually expressed as a percentage) can be defined as the ratio of the pore volume V_p [m^3] within the REV to the total volume V [m^3] of the REV defined as:

$$\Phi = \frac{V_p}{V} \qquad [2.4]$$

Porosity could vary between 0 (for an ideal soil with only solid phase) and 1 (empty space). Values in soils range from 0.2 (20%) to 0.95 (95%).

Effective porosity is the interconnected pore volume or void space in a soil that contribute to fluid flow. The pores which do not contribute to the flow are often called dead-end pores. Also adsorption water (water which is bound to clay particles) does not contribute to the effective porosity. When compared to the

porosity, the effective porosity is always smaller, as it does not take all water into account.

2.1.6 Hydraulic conductivity

The hydraulic conductivity tensor $\underline{\underline{K}}_f$ [m/s] is a measure of the ability of the porous material to allow fluids (gas or liquid) to pass through it under hydraulic gradients (Bear 1972).

The hydraulic conductivity tensor can be determined by experiments in laboratory or in the field and can be written as follows:

$$\underline{\underline{K}}_f = \underline{\underline{K}} \frac{\rho_w g}{\mu_w} \qquad [2.5]$$

$\underline{\underline{K}}$ represents the intrinsic permeability tensor, which is only a characteristic of the porous medium and μ_w is the dynamic viscosity of water.

The effective permeability $\underline{\underline{K}}_\alpha$ is defined as the product of the relative permeability $k_{r\alpha}$ [-] and the intrinsic permeability $\underline{\underline{K}}$:

$$\underline{\underline{K}}_\alpha = k_{r\alpha} \underline{\underline{K}} \qquad [2.6]$$

The unit is [m^2].

2.1.7 Pore velocity

The pore velocity $\underline{v}_a$ in the void space is described from the Darcy or filter velocity $\underline{v}_f$ (see eq. 2.10) by:

$$\underline{v}_a = \frac{\underline{v}_f}{\phi} \qquad \text{and the unit is [m/s].} \qquad [2.7]$$

2.1.8 Saturation

The saturation S_α [-] of the wetting liquid phase (water) α=w (see sec. 2.1.9) and non-wetting gas phase (air) α=n is defined as the quotient of the volume of the phase V_α divided by the pore volume (V_p):

$$S_\alpha = \frac{V_\alpha}{V_p} \qquad [2.8]$$

The sum of all phase saturations should be equal to one. For the case of two-phase flow with water and air phases, the pore volume is completely filled with the wetting and the non-wetting phase saturation S_w and S_n :

$$S_w + S_n = 1 \qquad [2.9]$$

It has to be taken into account that there is a mobile portion of the phase in the pore space and a residual phase quantity (residual water saturation S_{wr} and residual air saturation S_{nr}) which is not mobile in the soil, therefore we obtain the effective saturation S_e as follows:

$$S_e = \frac{S_w - S_{wr}}{1 - S_{wr} - S_{nr}} \qquad 0 \le S_e \le 1 \qquad [2.10]$$

2.1.9 Capillary pressure

Capillary pressure is generated where interfaces between two immiscible fluids exist in the pores or a fluid is in contact with a solid. It is usual to consider one phase as wetting phase and the other as non-wetting phase. The pressure discontinuities occur across the fluid-fluid interfaces due to the interfacial tension

σ [N/m]. The difference between the pressures of the non-wetting fluid and the wetting fluid is known as the capillary pressure p_c [Pa]:

$$p_c = p_n - p_w \qquad [2.11]$$

where, p_n is the pressure of the non-wetting phase and p_w is the pressure of the wetting phase.

On the microscale, the capillary pressure depends on the interfacial tension and the pore radius (Helmig 1997). The smaller the pore radius, the larger the capillarity pressure.

2.1.10 Generalized Darcy law

Generally, the momentum equation is replaced by the Darcy law in subsurface systems with the Darcy or filter velocity [m/s]:

$$\underline{v}_f = -\underline{\underline{K}}_f \, gradh \qquad [2.12]$$

$\underline{\underline{K}}_f$ is the tensor for the hydraulic conductivity [m/s] and h is the piezometric head [m] and is described as:

$$h = \frac{P}{\rho_w g} + z \qquad [2.13]$$

z [m] stands for the reference geodetic head which corresponds to the vertical spatial coordinate, P pressure [Pa] and g for gravity [m/s^2].

The Darcy law was determined experimentally. It is only valid for slow laminar flows limited to Reynolds numbers smaller than 1, because it neglects inertia terms. In this context, the Reynolds number is defined as the ratio of inertia to viscous forces. It is given by:

$$\mathrm{Re} = \frac{\underline{v}_f d}{v} \qquad [2.14]$$

d [m] denotes a characteristic length scale on the microscale, e.g. a grain diameter, and v [m^2/s] the kinematic viscosity of water. For Reynolds numbers larger 1 to 10, Forchheimer's law which represents a non-linear relationship between $\underline{v}_f$ and $gradh$, can be applied (see Bear 1972).

If the Darcy law is rearranged with Eq. 2.12 and 2.13:

$$\underline{v}_f = -\underline{\underline{K}} \frac{\rho_w g}{\mu_w} grad\left(\frac{P}{\rho_w g} + z\right) = -\frac{1}{\mu_w} \underline{\underline{K}} (gradp - \rho_w \underline{g}) \qquad [2.15]$$

Experiments have shown that a generalized form of Darcy law can describe the so-called Darcy velocity of each phase in a multiphase system:

$$\underline{v}_{f\alpha} = -\frac{1}{\mu_\alpha} \underline{\underline{K}}_\alpha (gradp_\alpha - \rho_\alpha \underline{g}) \qquad [2.16]$$

Using equation 2.6 the generalized Darcy law can be formulated as follows:

$$\underline{v}_{f\alpha} = -\frac{k_{r\alpha}}{\mu_\alpha} \underline{\underline{K}} (gradp_\alpha - \rho_\alpha \underline{g}) \qquad [2.17]$$

2.2 Mathematical model concept for two-phase flow processes in the subsurface

If two fluid phases are two immiscible fluids that flow in a porous medium, a two-phase flow model concept for a porous medium must be applied. In the following an overview of the mathematics applied for the two-phase flow in porous media is

given. For a detailed deduction it may be refered to Helmig (1997) and Hinkelmann (2005).

2.2.1 Constitutive relations

Capillary pressure-saturation relationship

As mentioned in section 2.1.9, capillary pressure p_c is defined as the non-wetting p_n phase pressure minus wetting phase pressure p_w.

The relationship between the decrease of the saturation of the wetting phase and the increase of the capillary pressure is expressed by the capillary pressure-saturation function. By convention, this function is usually expressed in terms of S_w rather than S_e:

$$p_c = p_c(S_w) \qquad [2.18]$$

In a two-phase system this fundamental relationship between the wetting and the non-wetting phase saturations S_w, S_n and the capillary pressure p_c can be determined with empirical approaches. The two most common models which formulate the capillarity pressure as a function of the saturation are the ones proposed by Brooks and Corey (1964) and Van Genuchten (1980).

$$\text{Brooks Corey: } p_c(S_w) = p_d S_e^{-\frac{1}{\lambda}} \quad \text{for} \quad p_c \geq p_d \qquad [2.19]$$

$$\text{Van Genuchten: } p_c(S_w) = \frac{1}{\alpha}(S_e^{-\frac{1}{m}} - 1)^{\frac{1}{n}} \quad \text{for} \quad p_c > 0 \qquad [2.20]$$

p_d stands for the entry pressure, which is the capillary pressure required to displace the wetting phase from the largest pores. The Brooks Corey parameter λ [-] characterizes the grain-size distribution. A small value describes a single grain size material, while a large value indicates highly non-uniform material. In the

Van Genuchten model, m=1-1/n [-] and α [1/Pa] are form parameters characterizing the pore-space geometry. The parameters of both models are determined experimentally and it is also possible to estimate these parameters from grain-sum curves (Arya & Paris 1981, Jonasson 1989). Figure 2.4 shows the capillary pressure-saturation relationship for both models in equal physical conditions.

Relative permeability-saturation relationship

Beside the capillary pressure, the relative permeability k_r represents another important quantity for multiphase flow.

Each phase α has a $k_{r\alpha}$, which can be seen as a scaling parameter. If one phase fills out the available pore space completely (disregarding the residual saturation of the other phase), the relative permeability for this phase is 1. If a phase is only present in residual saturation and therefore immobile, the relative permeability is 0.

The relationship between relative permeability and the saturation can only be described quantitatively because of the complex pore geometry in the medium. Again the two most common approaches are presented in the following.

The approach proposed by Brooks and Corey (1964) stems from the pore-network model of Burdine (1953) and is as follows:

$$k_{rw}(S_w) = S_e^{\frac{2+3\lambda}{\lambda}} \qquad [2.21]$$

$$k_{rn}(S_w) = (1 - S_e)^2 (1 - S_e^{\frac{2+\lambda}{\lambda}}) \qquad [2.22]$$

The Van Genuchten model (1980) is determined by the pore-network model of Mualem (1976) and it can be written as:

$$k_{rw}(S_w) = S_e^{1/2}\left[1-\left(1-S_e^{\frac{1}{m}}\right)^m\right]^2 \qquad [2.23]$$

$$k_{rn}(S_w) = (1-S_e)^{1/3}\left[1-S_e^{\frac{1}{m}}\right]^{2m} \qquad [2.24]$$

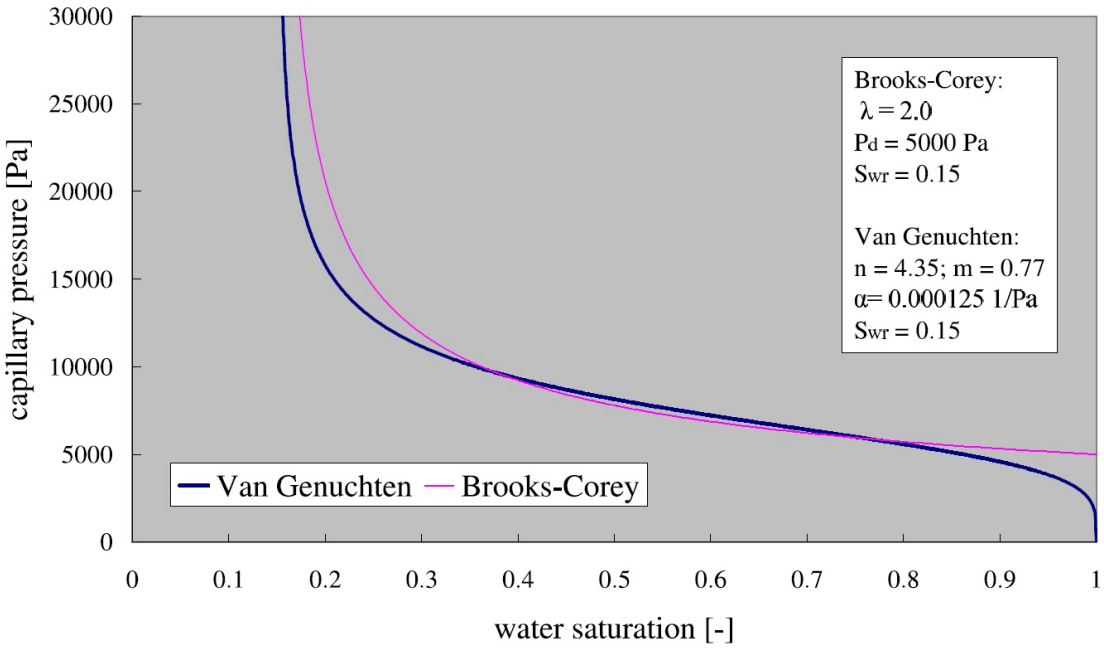

Figure 2.4 p_c-S_w relationship after Brooks and Corey and Van Genuchten, on equal physical conditions (Hinkelmann 2005)

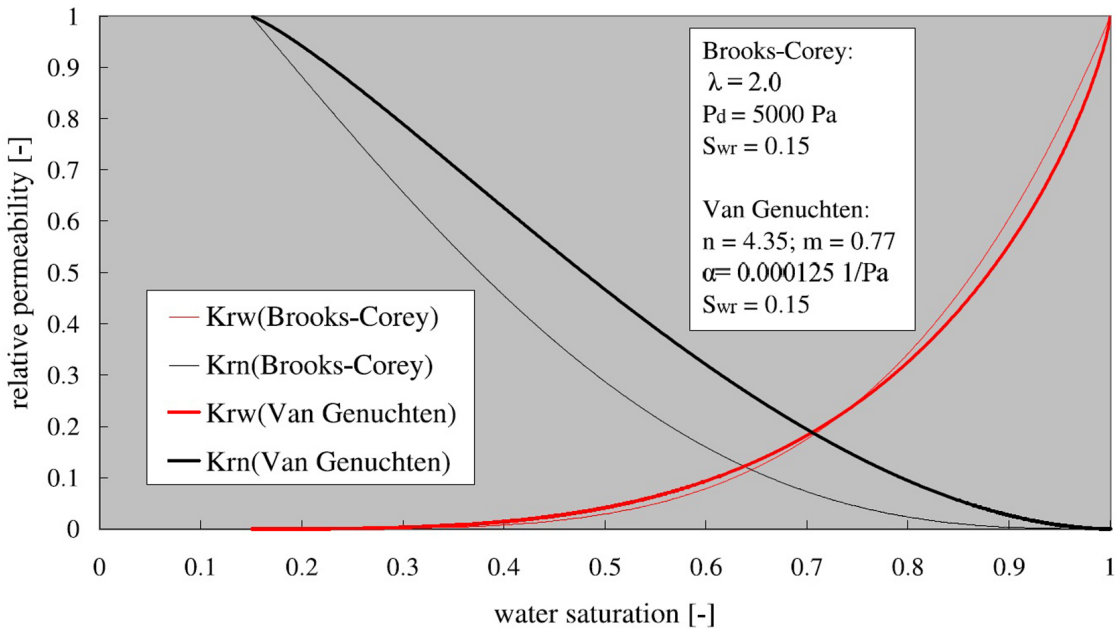

Figure 2.5 $K_r - S_w$ relationship after Brooks and Corey and Van Genuchten, on equal physical conditions (Hinkelmann 2005)

2.2.2 Two-phase flow equations

First, the two-phase flow concept is briefly introduced. The continuity equation must be fulfilled for each phase α, one for the liquid phase *w* (water) and one for the gas phase *a* (air):

$$\frac{\partial(S_\alpha \phi_\alpha \rho_\alpha)}{\partial t} + div(\rho_\alpha \underline{v}_\alpha) - \rho_\alpha q_\alpha = 0 \qquad [2.25]$$

Here, ϕ_α denotes porosity, the void space is filled with phase α, S_α is the saturation, ρ_α the density, $\underline{v}_\alpha$ the filter or Darcy velocity and q_α the sink or source of the phase. The extended Darcy law is assumed to be valid in the whole domain.

If we rearrange Eq. 2.25 with the extended Darcy law described in Eq. 2.17:

$$\frac{\partial(S_\alpha \phi_\alpha \rho_\alpha)}{\partial t} - div\left(\frac{k_{r\alpha}}{\mu_\alpha}\underline{\underline{K}}(gradp_\alpha - \rho_\alpha \underline{g})\rho_\alpha\right) - q_\alpha = 0 \qquad [2.26]$$

Here $\frac{\partial(S_\alpha \phi_\alpha \rho_\alpha)}{\partial t}$ describes the storage term, $-div\left(\frac{k_{r\alpha}}{\mu_\alpha}\underline{\underline{K}}(gradp_\alpha - \rho_\alpha \underline{g})\rho_\alpha\right)$ the flux term and $-q_\alpha$ the sink or source term.

For this research the constitutive relationships of Brooks-Corey (1964) have been chosen for the relative permeability $k_{r\alpha}$ and the capillary pressure p_c the one that we described before (see section 2.2.1).

The system is closed with two more complementary conditions: The pore volume is completely filled with the water and air phase (Eq. 2.9) and at the interface between both fluids, the difference between the phase pressure of gas and liquid phase is given by the capillary pressure (Eq. 2.11).

2.2.3 MUFTE-UG

For the simulation of water infiltration, the tool MUFTE-UG (Multiphase Flow, Transport and Energy on Unstructured Grids) (Helmig 1997, Hinkelmann 2005) was chosen. MUFTE-UG is a combination of MUFTE and UG. The MUFTE software toolbox mainly contains the physical model concepts and discretization methods for isothermal and non-isothermal multiphase/multicomponent flow and transport processes in porous and fractured-porous media (Helmig 1997, Helmig *et al*. 1998, Breiting *et al*. 2000). The toolbox UG provides the data structures and fast solvers for the discretization of partial differential equations based on parallel, adaptive Multigrid Methods (Bastian 1996, Bastian *et al*. 1997, Lang 2001). MUFTE uses UG as its fast solver. The fully Upwind Box Method, which is a combination of Finite-Volume and Finite-Element Method, is applied as

discretization method in space. This is a mass-conservative formulation on a discrete patch including a first-order upwinding scheme. For time integration it employs the forward Finite-Difference Method leading to a fully implicit formulation. As non-linear solver, the Newton-Raphson Method and as inner solver the BiCGSTAB (Biconjugate Gradient Stabilized) Method using Multigrid preconditioning are chosen.

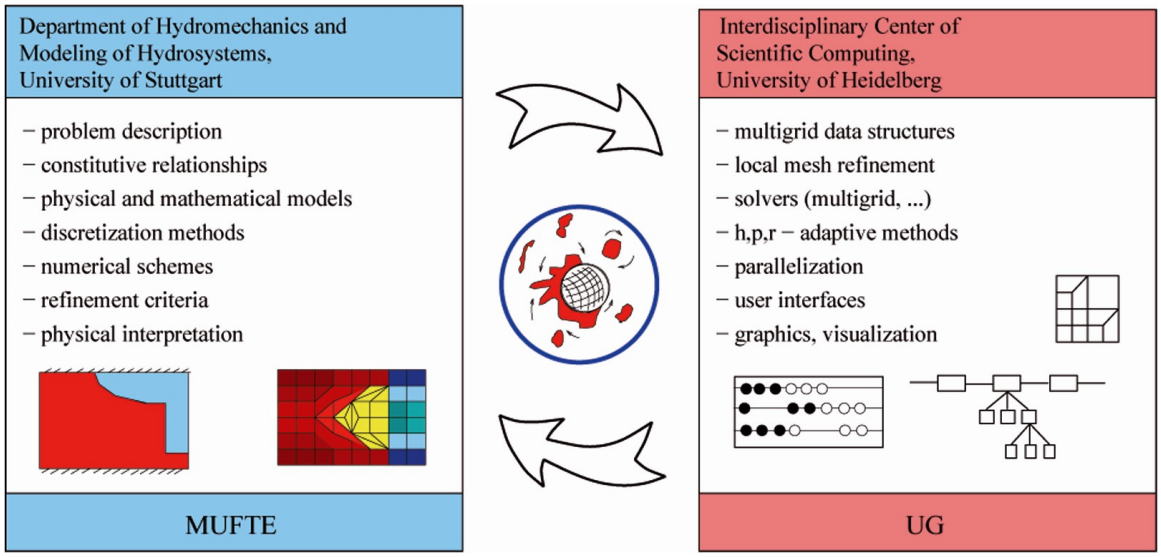

Figure 2.6 MUFTE-UG (Multiphase Flow, Transport and Energy on Unstructured Grids) (Helmig 1997, Hinkelmann 2005)

2.3 Mathematical model concept for deformation in the subsurface

The material models are described by a set of mathematical equations that give a relationship between stress and strain.

2.3.1 General definitions

Stress

If we imagine that a body is cut at the plane A–B (Figure 2.7) but its balance is conserved, a force F_s [N] distributed on the surface of the cut has to be imagined. The result of the distributed force F_s is either equal or contrary to the force F_0. The body can be considered in equilibrium under the effect of forces F_0, F_1, F_2, F_3, etc. [N] (Figure 2.8).

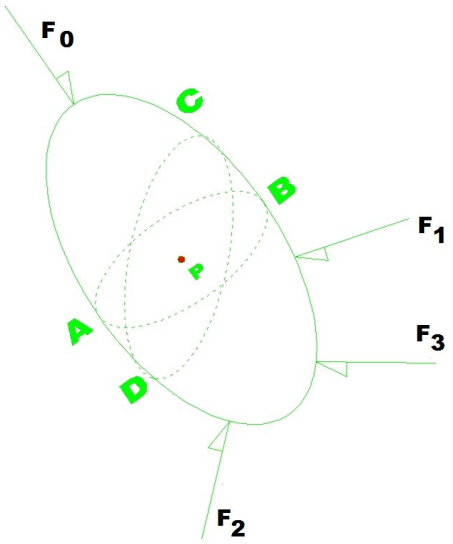

Figure 2.7 Continuum body in equilibrium under the effect of forces F_0, F_1, F_2, F_3, etc.

For a point P inside the body, the section cut AB which is perpendicular to F_0 and the body is supposed to conserve the equilibrium. We should imagine a distributed surface force Fs_1 equal to F_0 but with opposite direction (Figure 2.8).

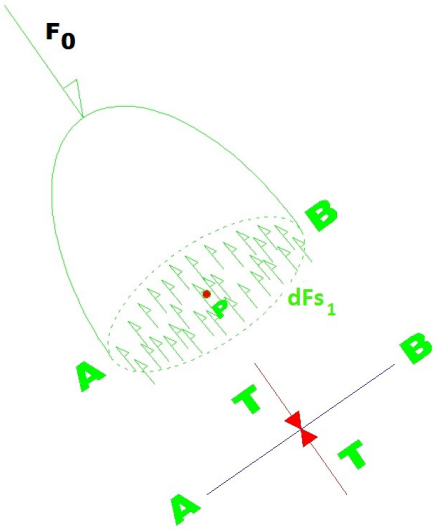

Figure 2.8 Section cut AB

The corresponding stress will be $T = dF_s/dS$ [Pa] and it will be normal to AB. If the cut CD is considered, the distributed surface force Fs_2 [N] produces a stress $T' = dF_s/dS_2$ (Figure 2.9) which is obviously minor to T because the area CD is bigger than the area AB.

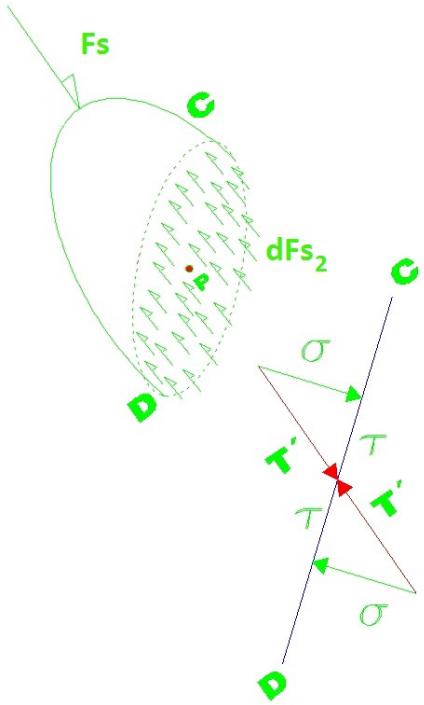

Figure 2.9 Section cut CD

Also this new stress results oblique to the surface of cut CD and can be decomposed in a normal stress σ [Pa] and a tangential or shearing stress τ [Pa].

To indicate the direction of the plane on which the stress is acting, subscripts to these letters are used.

We take a very small cubic element with sides parallel to the coordinate axes (Figure 2.10).

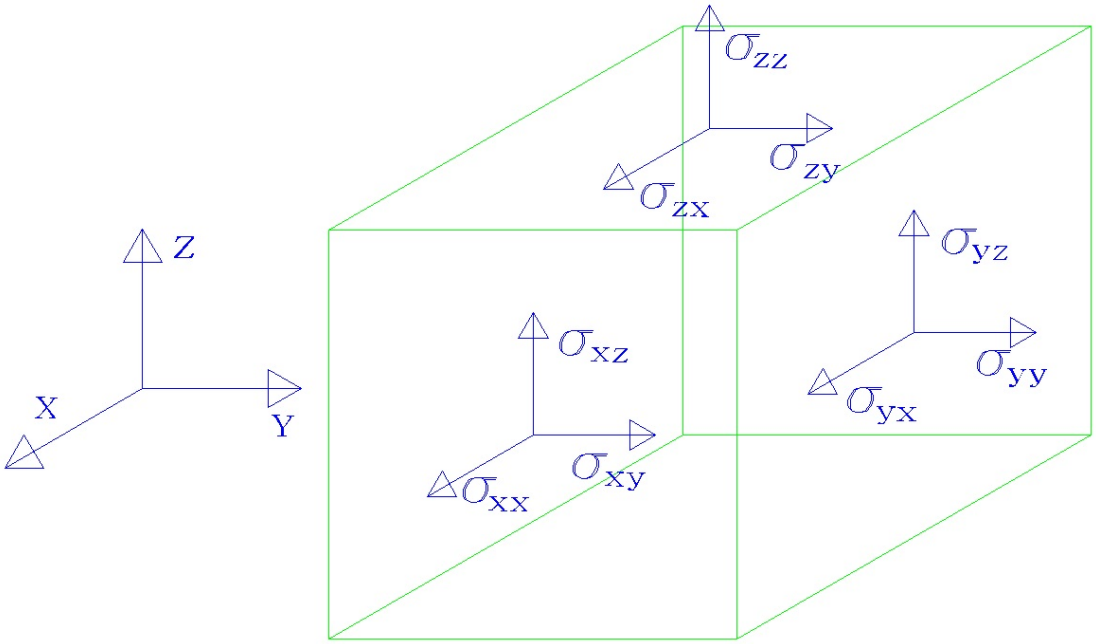

Figure 2.10 Cubic element with sides parallel to the coordinate axes

Stress is a tensor which can be represented by a matrix in Cartesian coordinates:

$$\underline{\underline{\sigma}} = \begin{bmatrix} \sigma_{xx} & \sigma_{xy} & \sigma_{xz} \\ \sigma_{yx} & \sigma_{yy} & \sigma_{yz} \\ \sigma_{zx} & \sigma_{zy} & \sigma_{zz} \end{bmatrix} \text{ or } \underline{\underline{\sigma}} = \begin{bmatrix} \sigma_{xx} & \tau_{xy} & \tau_{xz} \\ \tau_{yx} & \sigma_{yy} & \tau_{yz} \\ \tau_{zx} & \tau_{zy} & \sigma_{zz} \end{bmatrix} \qquad [2.27]$$

τ are the shear stresses and σ the normal stresses.

In standard deformation theory, the stress tensor is symmetric such that $\tau_{xy} = \tau_{yx}$, $\tau_{yz} = \tau_{zy}$ and $\tau_{zx} = \tau_{xz}$. In this situation stresses are often written in vector notation, which involve only six different components: $\underline{\sigma} = (\sigma_{xx} \quad \sigma_{yy} \quad \sigma_{zz} \quad \tau_{xy} \quad \tau_{yz} \quad \tau_{zx})^T$

If there is a plane where the shear stresses are not acting, but only the normal stresses, they are called principal stresses.

Hooke proposed a relationship between stress and strain from the stress-strain curve (Figure 2.11):

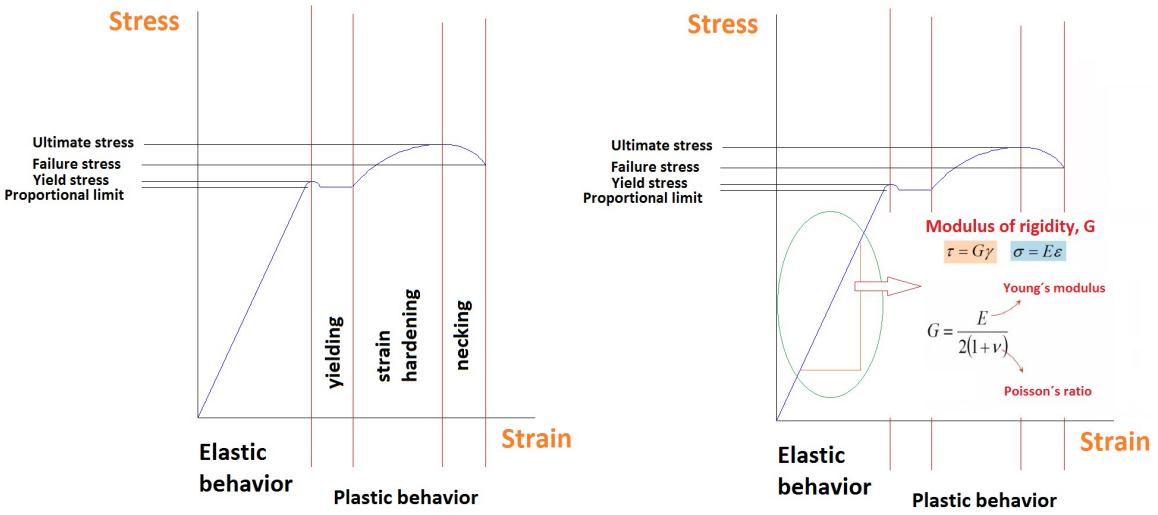

Figure 2.11 Stress-Strain relationship

From this definition applying elastic E [Pa] modulus and shear modulus G [Pa] the normal ε and shear strain γ lead to the six equations:

$$\varepsilon_x = \frac{\sigma_x}{E} - \frac{\nu}{E}(\sigma_y + \sigma_z);\ \varepsilon_y = \frac{\sigma_y}{E} - \frac{\nu}{E}(\sigma_x + \sigma_z);\ \varepsilon_z = \frac{\sigma_z}{E} - \frac{\nu}{E}(\sigma_x + \sigma_y);$$

$$\gamma_{xy} = \frac{\tau_{xy}}{G};\qquad \gamma_{xy} = \frac{\tau_{xy}}{G};\qquad \gamma_{xz} = \frac{\tau_{xz}}{G} \qquad [2.28]$$

According to Terzaghi's principle (1956), stresses in the soil $\underline{\sigma}$ are divided into effective stresses $\underline{\sigma}'$ and pore water pressures, u (Figure 2.12).

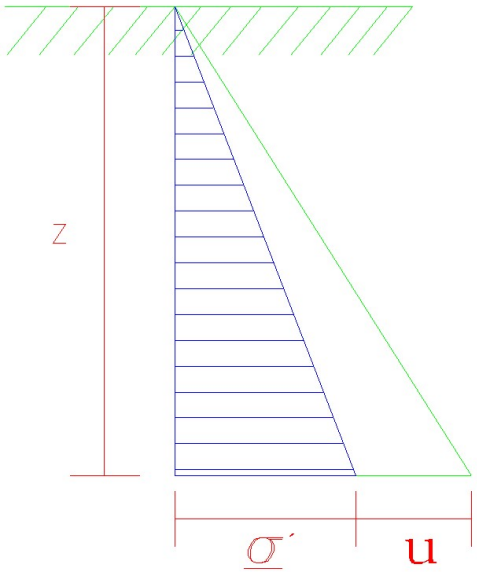

Figure 2.12 Effective stress and pore presure

$$\underline{\sigma} = \underline{\sigma}' + u \qquad [2.29]$$

Pore water pressures are provided by water in the pores. Water is considered not to sustain any shear stresses. As a result, effective shear stresses are equal to total shear stresses. Water is considered to be fully isotropic, so all pore pressure components are equal. Hence, pore pressure can be represented by a single value, p_w:

$$u = (\, p_w \quad p_w \quad p_w \quad 0 \quad 0 \quad 0 \,)^T \qquad [2.30]$$

Material models for soil and rock are generally expressed as a relationship between infinitesimal increments of effective stress and infinitesimal increments of strain. In such a relationship, infinitesimal increments of effective stress are represented by stress rates (with a dot above the stress symbol):

$$\dot{\underline{\sigma}}' = (\, \dot{\sigma}'_{xx} \quad \dot{\sigma}'_{yy} \quad \dot{\sigma}'_{zz} \quad \dot{\tau}'_{xy} \quad \dot{\tau}'_{yz} \quad \dot{\tau}'_{zx} \,)^T \qquad [2.31]$$

2.3.2 Linear-elastic perfectly-plastic model with Mohr-Coulomb failure criterion

Plasticity refers to irreversible strains. As soil behaviour is highly non-linear and irreversible, a linear-elastic perfectly-plastic Mohr-Coulomb model was applied (Waterman *et al*. 2004). This model involves five input parameters, namely Young's modulus E [Pa], Poisson's ratio υ [-], friction angle φ [°], dilatancy angle ψ [°] and cohesion C [Pa]. For simplification, in this research the dilatancy angle was taken equal to zero.

Hooke's law states:

$$\dot{\sigma}' = \underline{\underline{M}}\,\dot{\varepsilon} \qquad [2.32]$$

where $\underline{\underline{M}}$ [MPa] is material stiffness matrix.

This model decomposes strains $\underline{\varepsilon}$ and strain rates $\underline{\dot{\varepsilon}}$ into elastic and plastic parts:

$$\underline{\varepsilon} = \underline{\varepsilon^e} + \underline{\varepsilon^p} \qquad \underline{\dot{\varepsilon}} = \underline{\dot{\varepsilon}^e} + \underline{\dot{\varepsilon}^p} \qquad [2.33]$$

If Eq. 2.32 is inserted into the Hooke's law, this leads to:

$$\underline{\dot{\sigma}'} = \underline{\underline{\dot{D}^e}}\,\underline{\dot{\varepsilon}} = \underline{\underline{\dot{D}^e}}(\underline{\dot{\varepsilon}^e} + \underline{\dot{\varepsilon}^P}) \qquad [2.34]$$

$\underline{\underline{\dot{D}^e}}$ [MPa] is the elastic material stiffness matrix and $\underline{\dot{\sigma}'}$ are the effective stress rates.

A plastic potential function *g* is introduced. The plastic strain rates [-] are written as:

$$\underline{\dot{\varepsilon}^p} = \lambda \frac{\partial g}{\partial \underline{\sigma'}} \qquad [2.35]$$

in which λ is the plastic multiplier. For elastic behaviour λ is zero and for plastic behaviour λ is positive:

$$\lambda = 0 \text{ for } \quad f < 0 \quad \text{or :} \quad \frac{\partial f^T}{\partial \underline{\sigma}'} \underline{\underline{D}}^e \underline{\dot{\varepsilon}} \leq 0 \quad \text{(elasticity)} \qquad [2.36]$$

$$\lambda > 0 \quad \text{for} \quad f = 0 \quad \text{and :} \quad \frac{\partial f^T}{\partial \underline{\sigma}'} \underline{\underline{D}}^e \underline{\dot{\varepsilon}} > 0 \quad \text{(plasticity)} \qquad [2.37]$$

With these equations the relationship between the effective stress rates and strain rates can be obtained:

$$\underline{\dot{\sigma}}' = \left(\underline{\underline{D}}^e - \frac{\alpha}{d} \underline{\underline{D}}^e \frac{\partial g}{g \underline{\sigma}'} \frac{\partial f^T}{\partial \underline{\sigma}'} \underline{\underline{D}}^e \right) \underline{\dot{\varepsilon}} \qquad [2.38]$$

where:

$$d = \frac{\partial f^T}{\partial \underline{\sigma}'} \underline{\underline{D}}^e \frac{\partial g}{\partial \underline{\sigma}'} \qquad [2.39]$$

α equals to zero for elastic behaviour and equal to unity for plastic behaviour.

The full Mohr-Coulomb yield condition consists of six yield functions formulated in terms of principal stresses as follows:

$$f_{1a} = \frac{1}{2}(\sigma'_2 - \sigma'_3) + \frac{1}{2}(\sigma'_2 + \sigma'_3)\sin\varphi - c\cos\varphi \leq 0$$

$$f_{1b} = \frac{1}{2}(\sigma'_3 - \sigma'_2) + \frac{1}{2}(\sigma'_3 + \sigma'_2)\sin\varphi - c\cos\varphi \leq 0$$

$$f_{2a} = \frac{1}{2}(\sigma'_3 - \sigma'_1) + \frac{1}{2}(\sigma'_3 + \sigma'_1)\sin\varphi - c\cos\varphi \leq 0 \qquad [2.40]$$

$$f_{2b} = \frac{1}{2}(\sigma'_1 - \sigma'_3) + \frac{1}{2}(\sigma'_1 + \sigma'_3)\sin\varphi - c\cos\varphi \le 0$$

$$f_{3a} = \frac{1}{2}(\sigma'_1 - \sigma'_2) + \frac{1}{2}(\sigma'_1 + \sigma'_2)\sin\varphi - c\cos\varphi \le 0$$

$$f_{3b} = \frac{1}{2}(\sigma'_2 - \sigma'_1) + \frac{1}{2}(\sigma'_2 + \sigma'_1)\sin\varphi - c\cos\varphi \le 0$$

In addition to the yield functions, six plastic potential functions are also defined:

$$g_{1a} = \frac{1}{2}(\sigma'_2 - \sigma'_3) + \frac{1}{2}(\sigma'_2 + \sigma'_3)\sin\psi$$

$$g_{1b} = \frac{1}{2}(\sigma'_3 - \sigma'_2) + \frac{1}{2}(\sigma'_3 + \sigma'_2)\sin\psi$$

$$g_{2a} = \frac{1}{2}(\sigma'_3 - \sigma'_1) + \frac{1}{2}(\sigma'_3 + \sigma'_1)\sin\psi \qquad [2.41]$$

$$g_{2b} = \frac{1}{2}(\sigma'_1 - \sigma'_3) + \frac{1}{2}(\sigma'_1 + \sigma'_3)\sin\psi$$

$$g_{3a} = \frac{1}{2}(\sigma'_1 - \sigma'_2) + \frac{1}{2}(\sigma'_1 + \sigma'_2)\sin\psi$$

$$g_{3b} = \frac{1}{2}(\sigma'_2 - \sigma'_1) + \frac{1}{2}(\sigma'_2 + \sigma'_1)\sin\psi$$

In PLAXIS model (see section 2.4.4), all the output data, compressive stresses and forces are taken to be negative, whereas tensile stresses and forces are taken to be positive.

2.3.3 Hardening Soil model

The Hardening Soil model, developed by Schanz *et al*. 1999 uses a double-stiffness model for elasticity in combination with isotropic strain hardening. The total strains are calculated using a stress-dependent stiffness, different for both, virgin loading and un-/reloading. The plastic strains are calculated by introducing a multi-surface yield criterion. For the frictional hardening a non-associated flow is assumed whereas, for the cap hardening an associated flow rule is assumed. This model is included in the PLAXIS model (Waterman *et al.* 2004).

Hyperbolic stress-strain relation

The hyperbolic stress-strain relationship occurs under triaxial loading conditions with $\sigma_2^{'} = \sigma_3^{'}$ = constant and $\sigma_1^{'}$ being the major compressive stress. Drained triaxial tests tend to yield curves described by:

$$\varepsilon_1 = \frac{q_a}{2E_{50}} \frac{(\sigma^{'}_1 - \sigma^{'}_3)}{q_a - (\sigma^{'}_1 - \sigma^{'}_3)} \quad \text{for } q < q_f \qquad [2.42]$$

The quantities of the ultimate deviatoric and asymptotic stress q_f and q_a are defined as:

$$q_f = \frac{6\sin\varphi_P}{3 - \sin\varphi_P}(p + C\cot\varphi_P)\,; q_a = \frac{q_f}{R_f} \qquad [2.43]$$

Where C is cohesion and φ_P is failure friction angle and R_f describes the relationship between q_f and q_a. Two confining stress-dependent stiffness moduli should be used, one for primary loading E_{50} [Pa] and the second for un-/reloading stress paths E_{ur} [Pa].

Deviatoric yield surface

The corresponding plastic strain stems from a yield function of the form $f^s = \overline{f} - \gamma^P$ where $\overline{f}$ is the function of stress, γ^P is a function of plastic strains which are defined as:

$$\overline{f} = \frac{1}{E_{50}} \frac{q}{1 - q/q_a} - \frac{2q}{E_{ur}} \qquad [2.44]$$

$$\gamma^P = \varepsilon_1^P - \varepsilon_2^P - \varepsilon_2^P = -(2\varepsilon_1^P - \varepsilon_v^P) \approx -2\varepsilon_1^P \qquad [2.45]$$

The axial strain is the sum of elastic and plastic components given as:

$$-\varepsilon_1 = -\varepsilon_1^e - \varepsilon_1^P \approx \frac{1}{2E_{50}} \frac{q}{1 - q/q_a} \qquad [2.46]$$

The flow rule that involves a relationship between rates of plastic shear strain $\dot{\gamma}^P$ and plastic volumetric strain $\dot{\varepsilon}_v^P$ has the form:

$$\dot{\varepsilon}_v^P = \sin\psi_m \, \dot{\gamma}^P \qquad [2.47]$$

The mobilized dilatancy angle ψ_m is obtained by the expression:

$$\sin\psi_m = \frac{\sin\varphi_m - \sin\varphi_{cv}}{1 - \sin\varphi_m \sin\varphi_{cv}} \qquad [2.48]$$

where φ_{cv} is the critical state friction angle and φ_m is the mobilized friction angle.

At failure, when the mobilized friction angle equals to φ_p, it is found that:

$$\sin\psi_m = \frac{\sin\varphi_p - \sin\psi_p}{1 - \sin\varphi_p \sin\psi_p} \qquad [2.49]$$

To explain the plastic volume strain a second type of yield surface must therefore be introduced to close the elastic region in p-axis direction which is called cap yield surface f^c defined as:

$$f^c = \frac{\tilde{q}^2}{\alpha^2} + p^2 - p_p^2 \qquad [2.50]$$

The magnitude of the cap yield surface will be defined through the parameter α and the isotropic pre-consolidation stress P_P=-(σ_1+σ_2+σ_3)/3 and $\tilde{q} = \sigma_1 + (\delta - 1)\sigma_2 - \delta\sigma_3$ with $\delta = (3 + \sin\varphi)/(3 - \sin\varphi)$. $\tilde{q}$ is a special stress measure for deviatoric stresses. In the special case of triaxial compression $(-\sigma_1 > -\sigma_2 = \sigma_3)$ it yields $\tilde{q} = -(\sigma_1 - \sigma_3)$ and for triaxial extension (-σ_1=-σ_2>σ_3), $\tilde{q} = -\delta(\sigma_1 - \sigma_3)$. The hardening law relating p_p to volumetric cap ε_v^{Pc} states:

$$\varepsilon_v^{pc} = \frac{\beta}{1-m}\left(\frac{p_p}{p^{ref}}\right)^{1-m} \qquad [2.51]$$

α and β are cap parameters. A detailed description of the method can be found in Schanz *et al.* (1999).

2.3.4 Plaxis model

PLAXIS is a geotechnical software tool based on the Finite-Element method and intended for two-dimensional (2D) and three-dimensional (3D) geotechnical analysis of deformation and stability of soil structures. For this research only the 2D modeling was applied.

With PLAXIS 2D the geometry of the model can be easily defined in the soil and structures modes. The stage construction mode allows for simulation of soil before and after water infiltration or extraction. Since soil is a multiphase material, special procedures allow for calculation dealing with hydrostatic and non-hydrostatic pore pressure in the soil. The PLAXIS 2D is supplied as an extended package, including static elastoplastic deformation, advanced soil models, stability analysis, consolidation, safety analysis, updated mesh and steady-state groundwater flow. For detailed information please refer to www.plaxis.nl.

2.4 Coupling

The infiltration was modeled with MUFTE-UG. The saturation results were transferred to modified specific weights of the soils which were the loads for the deformation modeling with PLAXIS, i.e. the specific weight for a saturated soil γ_{wet} was set in areas where the water saturation was higher than 0.8 (blue-green shaded area in Figure 2.13) instead of the specific weight of a dry soil γ_{dry}. This procedure is a reasonable engineering estimation, especially as the transition between wet and residual saturation is relatively sharp.

The weak coupling approach used in this research did not take into account feedback effects of deformation on the flow. Therefore, it does not allow an estimation of the deformation impact on the flow. For a fully coupled approach of flow and deformation processes in partially saturated soils, it can be referred to Ehlers *et al*. (2011). However, their model has never been applied to land subsidence simulation.

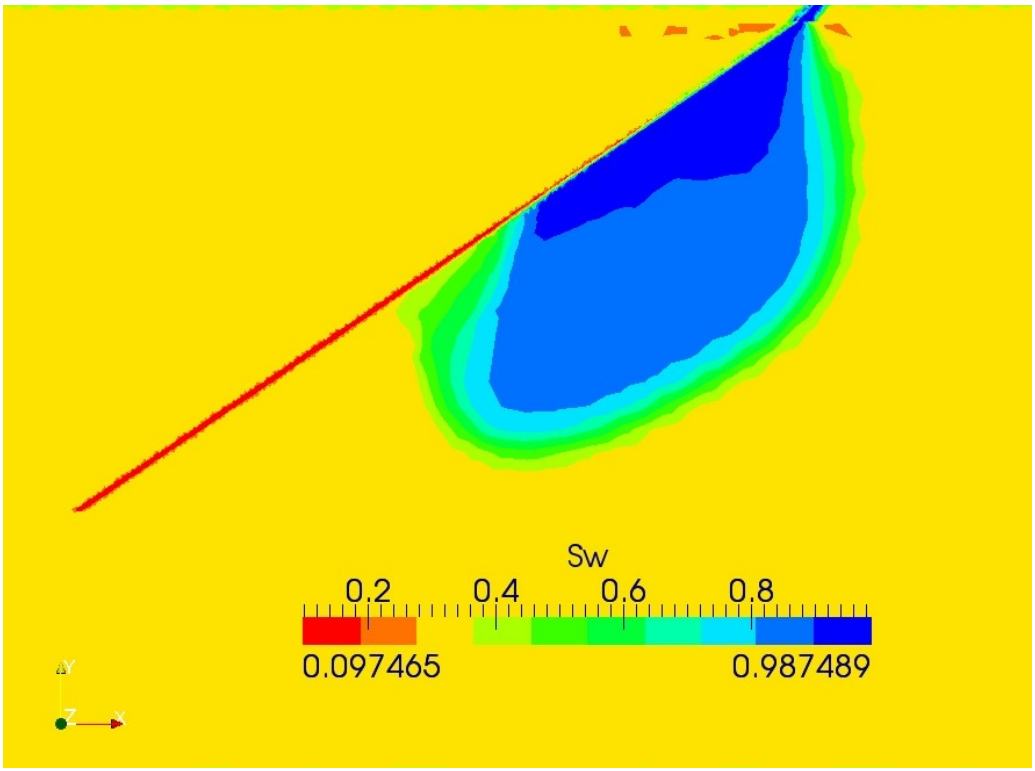

Figure 2.13 Water saturation

3 Mechanisms of fracture and fault formation

Extraction wells leading to water table decline are generally not uniformly distributed, i.e. for example, there are zones with a higher density of extraction wells. As a consequence the soil's deformation is irregular and in zones where the depression cones are larger, the magnitude of the deformation is larger.

The problem of the soil's deformation, in particular the irregularity of its magnitude, does not only depend on the volume of the extraction, but also on some of the physical properties of the strata have an influence, as for example the porosity and compressibility of the soil's strata.

Obviously, the thickness of the strata also has an influence on the subsidence. The aquifers consist of saturated porous soil mass. It is known that the bedrock, which underlies the deposits and from which the groundwater often can be extracted, is irregular. Vertical changes (faults), depressions and slopes below the deposits with different inclinations may be found. Figure 3.1 corresponds to a stratigraphic section of the aquifer in Querétaro, Mexico. This aquifer is such an example and the irregularities previously mentioned are observed.

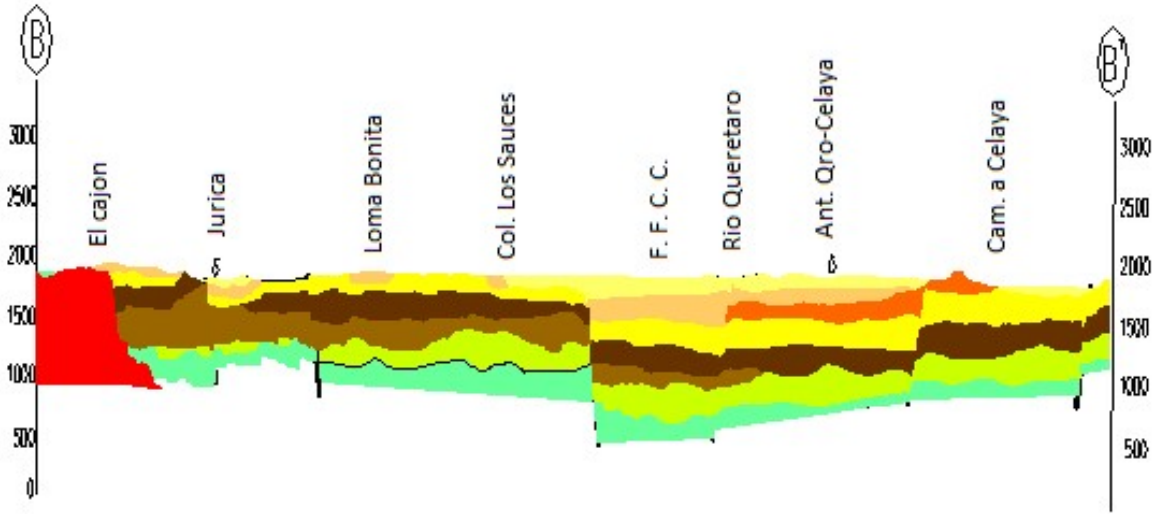

Figure 3.1 Stratigraphic section of the aquifer in Querétaro, Mexico (Arroyo *et al.*, CEA 2002)

Mechanical compression and tension stress is produced by the irregularities of the basement. As the soil's mass can not resist considerable tension stress, it is common that on the surface faults and fractures appear which coincide with the changes of the basement's level (faults or slopes of the basement with steep inclinations).

Fault and fracture formation may be predicted by means of mechanical modeling of the system: basement, fillers of saturated and partially saturated soil if the physical characteristics of the strata are known and information about the drawdown of the water table is available.

The following idealized Figure of a basement and three compressible strata (Layer 1, 2 and 3) is supposed (Figure 3.2) to explain the conditions mentioned before.

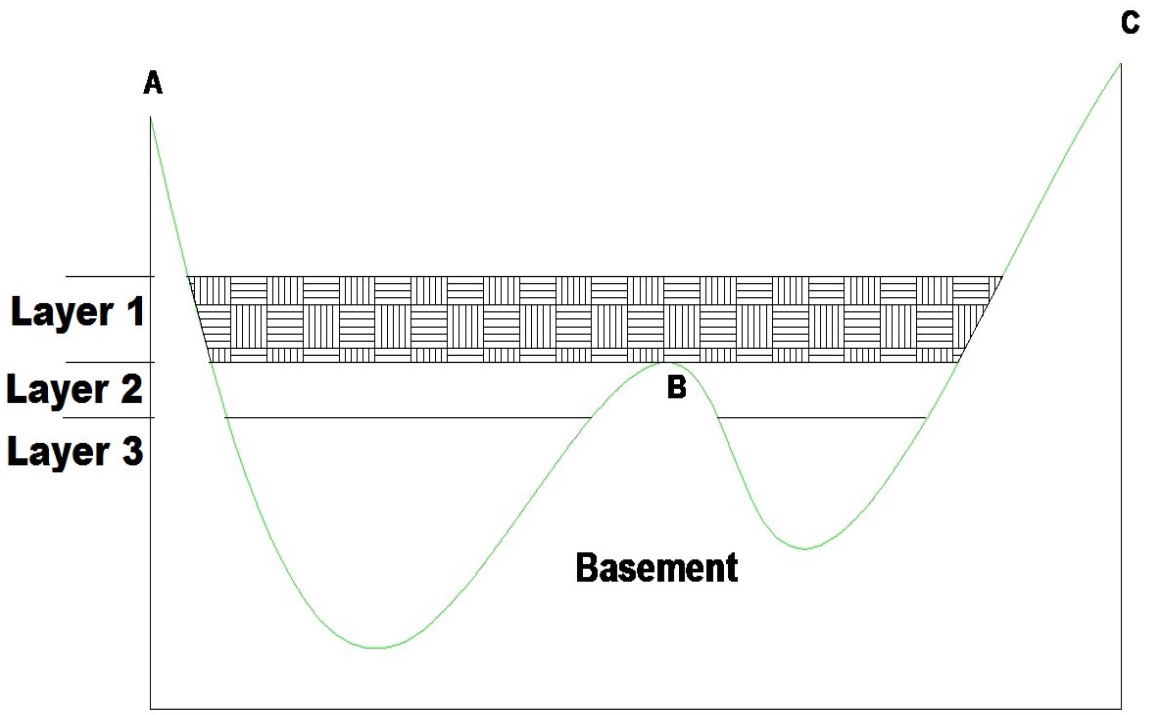

Figure 3.2 Irregular basement and deformable layers

Layer 1 is idealized as a beam and the deformation at the sides are restricted (P and P′ in Figure 3.3). In point P′′ only rotation is allowed.

If the loss of pore pressure is generated because of declined water level, deformation is produced. The soil layer will act similar as a beam bending, and this effect produces tensional stress (T) and compression (C) as shown in Figure 3.3.

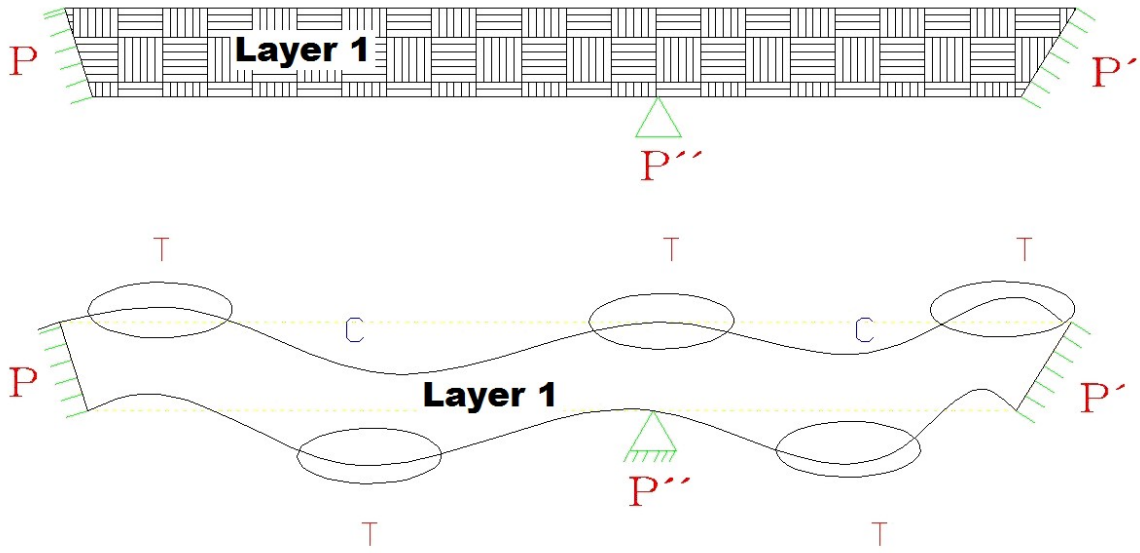

Figure 3.3 Tensile and compressive stresses for an idealized layer as a beam bending

As the soil's resistance under tension is very low, once exceeded, cut-off points appear and manifest themselves on the surface as faulting.

Several conceptual models about the mechanisms of ground failures, namely earth fissures and surface faults associated with groundwater withdrawal, have been suggested in the last years. In literature, the term “model concept” is used to describe the mechanisms of fracture and fault generation.

In 1982, Jachens and Holzer associated fracture formation caused by groundwater withdrawal with the relief on the buried interface between the alluvial aquifer and underlying bedrock. They found that all the fissure zones in Casa Grande,

Arizona, USA occurred either above ridges or above steps in the bedrock surface. These buried ridges or steps produced bending in the deformable aquifer, i.e. horizontal tensile strains on the surface leading to crack formation (Figure 3.4).

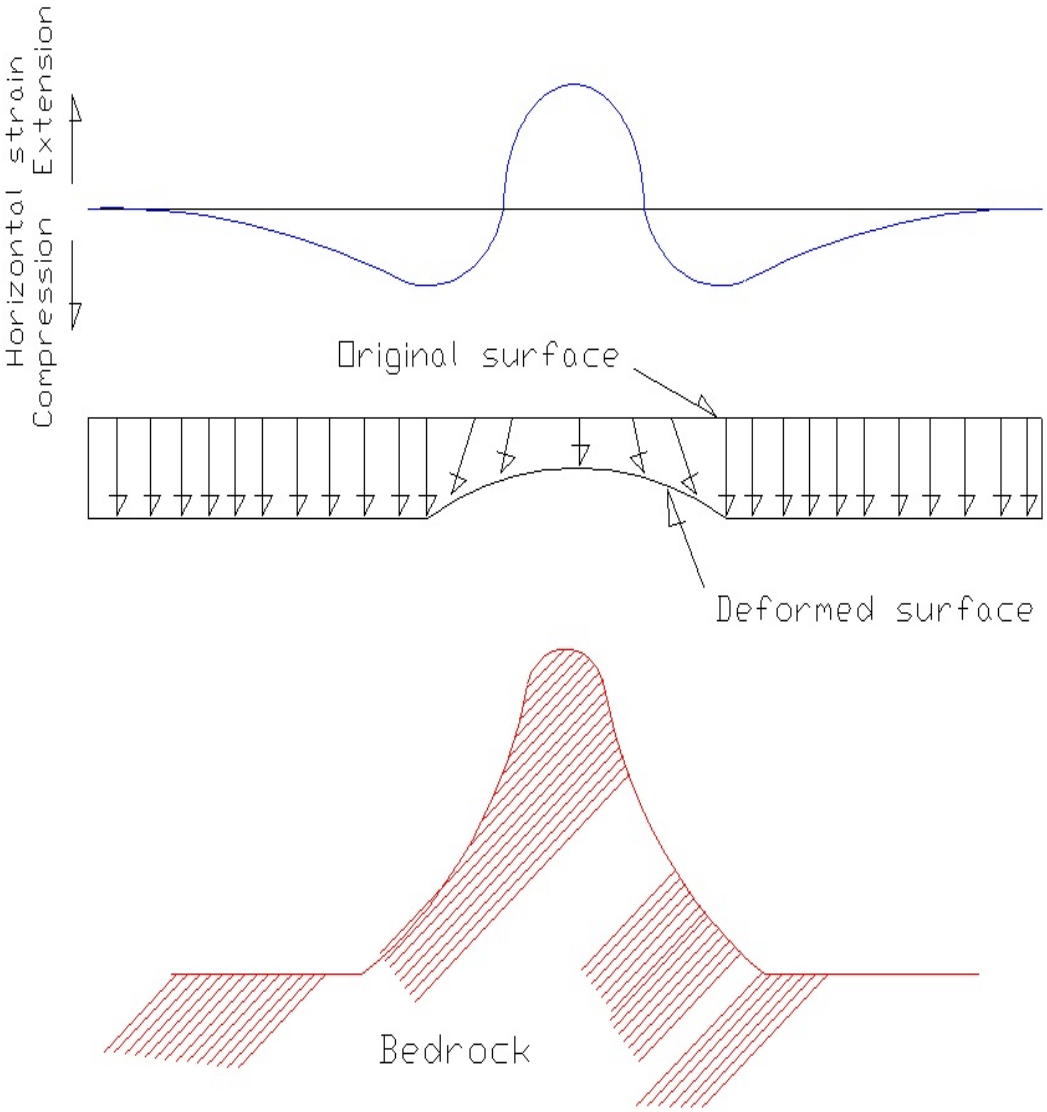

Figure 3.4 Proposed model for fissure formation after Jachens and Holzer (1982)

In 1991, Martinez-Baini and Trejo-Moedano proposed two possible mechanisms for fracture formation on the surface. For the first mechanism they proposed that a combination of dehydration of the superficial layer, non-uniform consolidation

because of the applied extra weight caused by constructions, and the extraction of water in a heterogeneous aquifer produced tensile fractures on the surface.

The second mechanism demonstrated that when the water table of an aquifer with sinusoidal underlying bedrock declines, this leads to settlements because of the increase of vertical effective stresses (Figure 3.5). The magnitude of these settlements depends on the compressibility and thickness of the affected strata. Because of the sinusoidal underlying bedrock, the thickness of the deposits affected by the increase of vertical effective stresses varies causing non-uniform settlement and flexion on the superjacent material. This flexion results in horizontal tensile strains perpendicular to the settlement axe (Figure 3.6).

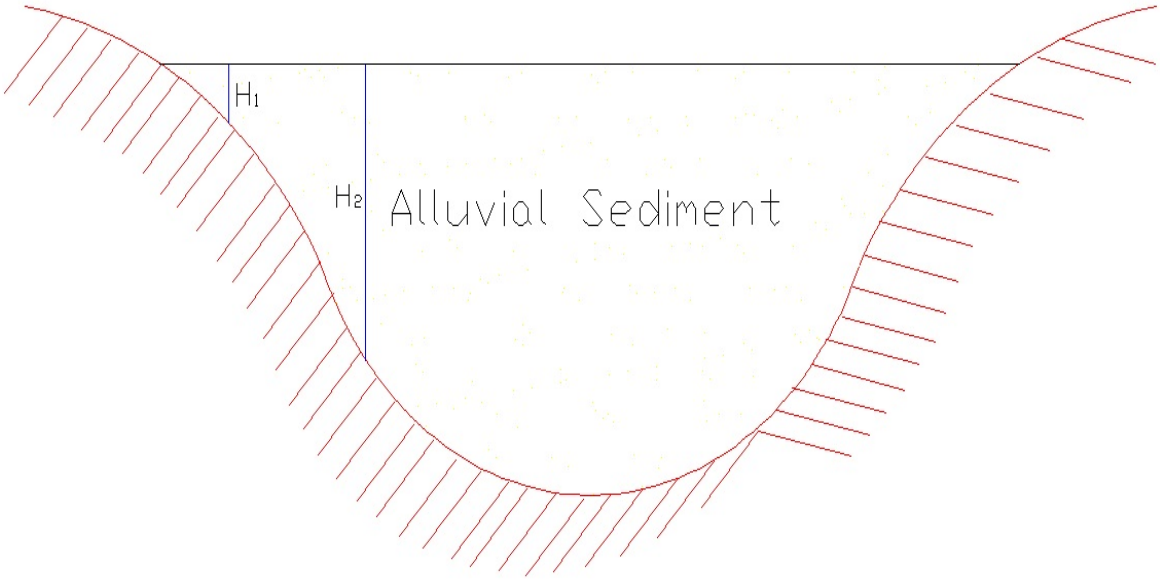

Figure 3.5 Aquifer with sinusoidal underlying bedrock (Martinez-Baini & Trejo-Moedano 1991)

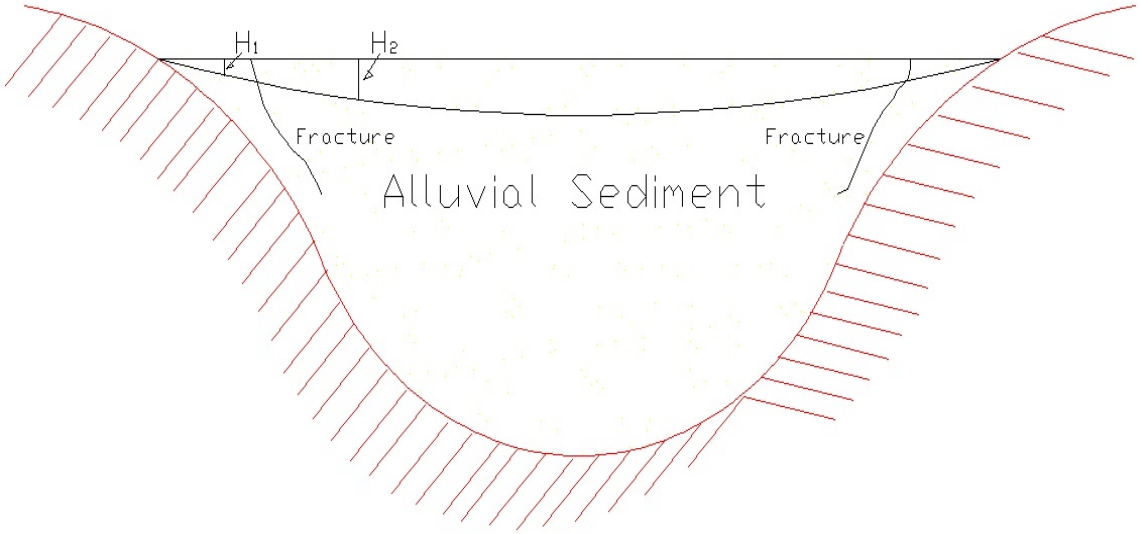

Figure 3.6 Non-uniform settlement and flexion on the superjacent material because of the sinusoidal underlying bedrock (Martinez-Baini & Trejo-Moedano 1991)

Burbey (2002) presented another scenario. In an aquifer of granular material with pre-existing faults, he represented faults as a discontinuity for horizontal water flow. Such a barrier leads to a non-uniform water table decline when water is withdrawn. This non-uniform water table decline leads to differential settlement and to subsequent faulting because of horizontal displacements.

In 1995, Sheng and Helm presented two new mechanisms for earth fissuring. They emphasized the effect of hydraulic forces and pre-existing geologic structures.

Model 1 assumed an aquifer with horizontal weakness planes. In stratified materials the interface between layers forms weakness planes. Non-uniform vertical compaction of the aquifer could induce slips along them. Horizontal hydraulic forces produced by water withdrawal cause shear stresses along these weakness planes. Shear failure occurs along the weakness planes when the accumulated shear stress has reached the shear strength of the weakness plane. A

potential tensile zone is formed and tensile failure propagates upwards to the land surface (Figure 3.7).

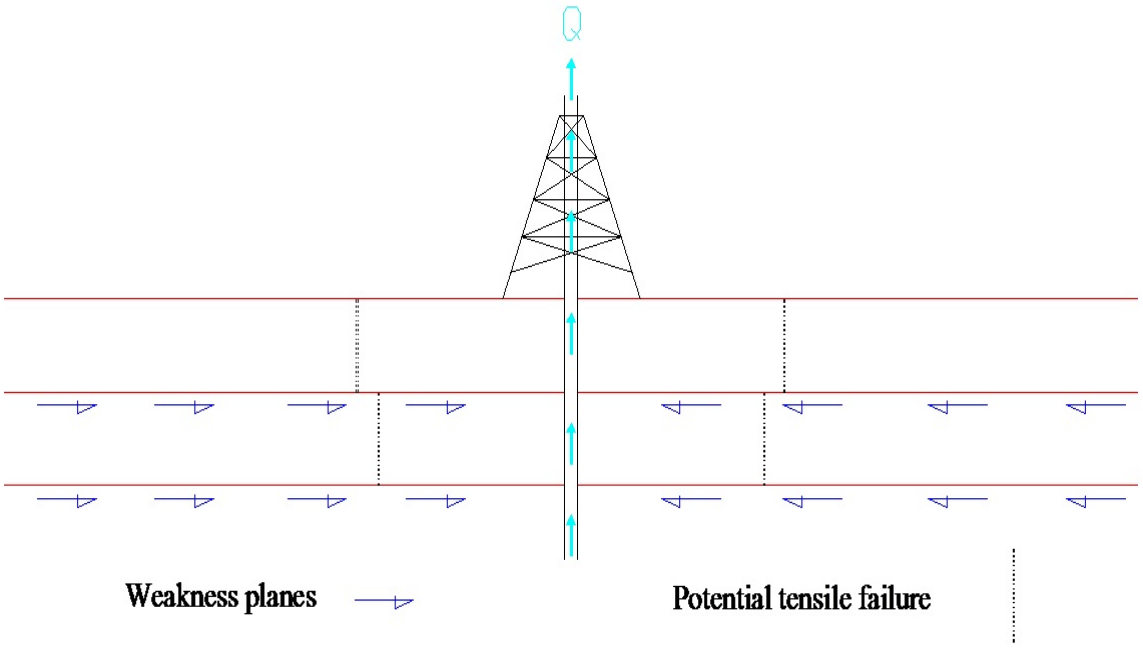

Figure 3.7 Aquifer with shear stresses along weakness planes and potential tensile failure (Sheng & Helm, 1995)

Model 2 assumed an aquifer with a partly pre-existing fault (a barrier for horizontal flow). Then, aquifer movement may correspondingly induce differential displacement on the two walls of the fault. Such differential displacement could trigger re-shearing or opening of the fault and generate new sub-cracks (Figure 3.8).

Hernandez-Marin & and Burbey (2010) expound a numerical simulation study about the conditions that favour the occurrence of earth fissures in faulted basins under continuous pumping. The hydrostratigraphy of the model was made up of alternating aquifers and aquitards including an upper 100 m thick vadose zone.

The entire analyzed sedimentary sequence is cut by a normal sub-vertical NE-SW trending fault system. The research shows that the simulated patterns of compression and tension are controlled largely by the zone of pumping, the

pumping rate, and the fault. Their results show significant contrast in magnitudes between the saturated and unsaturated regions, which may lead to the generation of horizontal fissures at this transition.

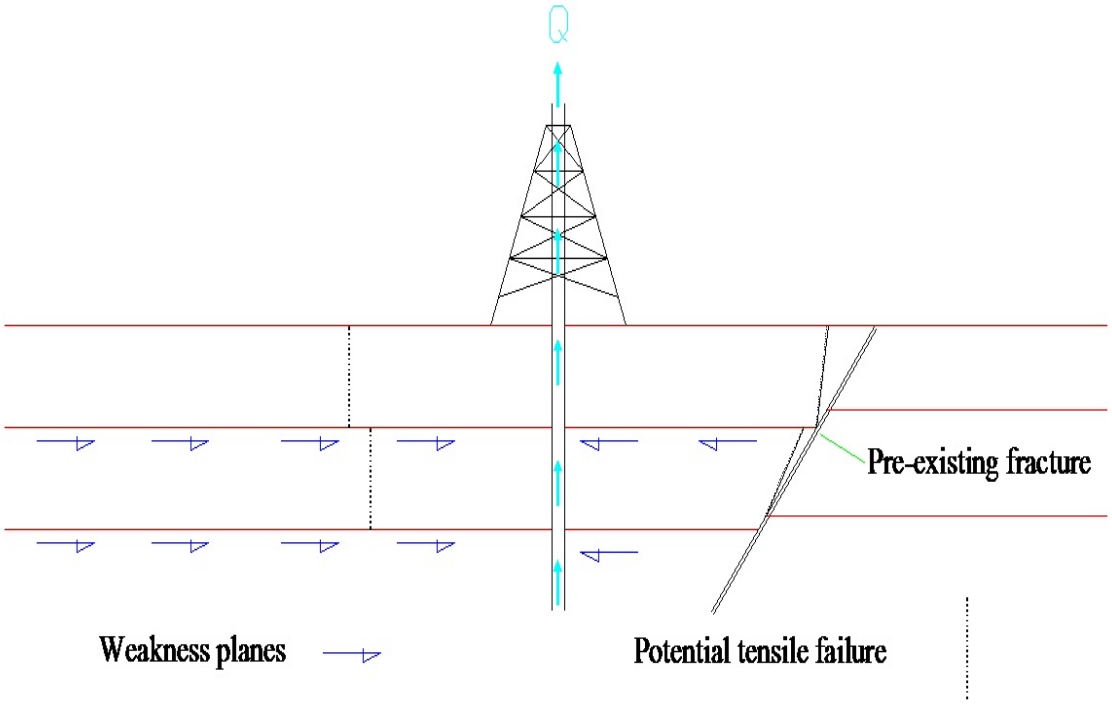

Figure 3.8 Aquifer with pre-existing fracture, shear stresses along weakness planes and potential tensile failure (Sheng & Helm, 1995)

All these mechanisms dealt with groundwater withdrawal and showed that land subsidence was closely related to the formation of fractures.

In 1999, Carpenter and in 2005 Suarez-Placencia *et al*. presented a model focusing on rainfall water infiltration as trigger for the fracture formation. They proposed that in a pre-existing fracture, rainwater infiltrates through the pre-existing fracture eroding and increasing it within a few minutes.

Martinez-Noguez *et al*. in 2013 presented an article with some results that are exposed here. They also present a mechanism focusing on fast water infiltration

through a pre-existing fault (Figure 3.9). Erosion is not taken into account, but the increase of the water saturation proceeds in the deposits.

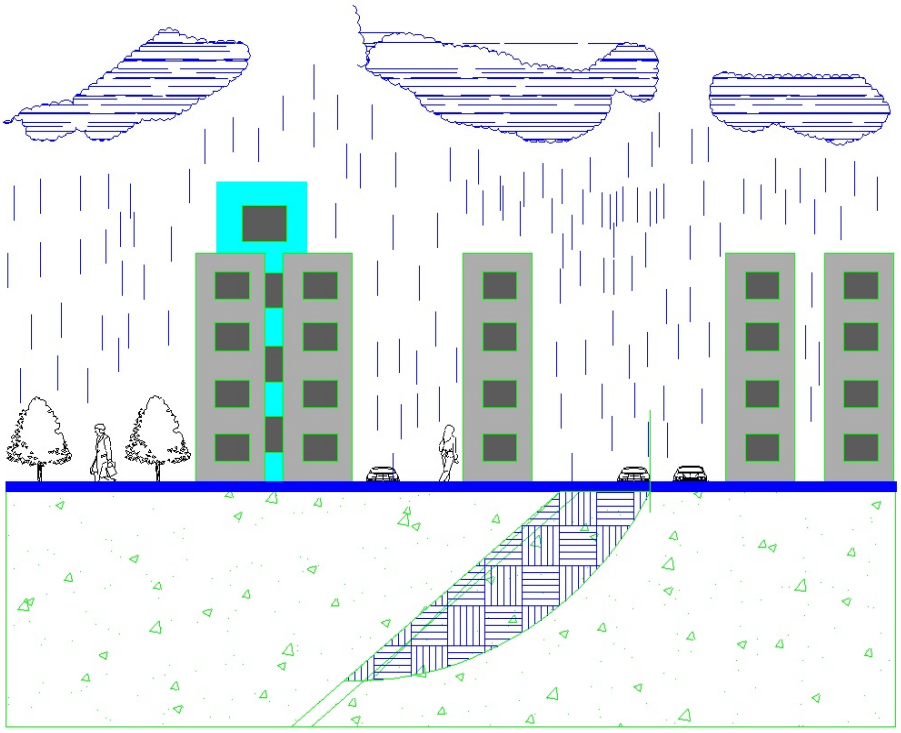

Figure 3.9 Fast water infiltration, a mechanism for fracture formation during land subsidence (Martinez-Noguez *et al*. 2013)

This mechanism focusing on fast water infiltration through a pre-existing fault is described in detail in section 4.2.

4 Applications

In this chapter three examples of numerical modeling are presented. These results were published in Martinez-Noguez *et al*. (2010), Martinez-Noguez *et al*. (2012), Martinez-Noguez *et al*. (2013) and Martinez-Noguez *et al.* (2015).

The first application is a model of infiltration through a single-layer system. Here the influence of the inclination of the fracture and the inclination of the surface were investigated as well as the soil's deformation.

The second application is a more detailed study of the infiltration and deformation of the soil. In this case a two-layered system consisting of a stratum with low permeability on its surface and a fracture that allows a rapid water flow through the impermeable stratum to the lower stratum with higher permeability was examined. A model concept for fracturing mechanism was also proposed.

The third application describes a model concept for fracturing mechanism after groundwater extraction through a well near a highly permeable pre-existing fault. The irregular drawdown of the water table on both sides of the fracture and its relation with the boundary condition was also analysed.

Since the water table in arid and semi-arid zones is found several meters under the surface, the infiltration occurs in partially saturated soil, i.e. two phases are present (water and air). Hence for all three examples, the numerical simulation of flow and infiltration are based on a two-phase (water-air) flow model concept for porous media (see sec. 2.2). The stress-strain analysis is carried out for the first example with the Hardening Soil model (elasto-plastic model) using a double stiffness concept for elasticity in combination with isotropic strain hardening. For the second and third example a linear-elastic perfectly-plastic model with Mohr-Coulomb failure criterion was applied (see section 2.3). The results of numerical

infiltration, i.e. saturation, are used for the stress-strain analysis. Flow and deformation processes are weakly coupled (see section 2.4).

Fault zones show a wide variety of geometrical, physical and fracture patterns. In this work a fault zone was represented as a porous medium damage band with higher permeability compared to soil matrix. Therefore, 2D high-resolution grids with higher resolutions in and around the fault zone were chosen as shown in Figure 4.1 4.13 and 4.28. The fault was defined as a continuous porous media, the Darcy law was considered valid for this first approximation, in other words: it is valid only for laminar flow with Reynolds number not bigger than 1 to 10 (see sec. 2.1.10).

The flow parameter used in all the numerical simulations for the matrix and the fault zone are described in Table 1. For the second example, fault parameters are varied, they will be shown in section 4.2.

Table 1 Soil parameters for two-phase flow modeling

	Sand	Clay	Fault Zone
S_{wr} [-]	0.15	0.18	0.05
S_{nr} [-]	0.01	0.01	0.01
$\boldsymbol{K}$ [m^2]	$5*10^{-11}$	$3.5*10^{-13}$	Variable
λ [-]	2.3	3.5	2.2
p_d [Pa]	700	2400	200
φ [-]	0.37	0.43	0.32

(S_{wr}, S_{nr}: residual water, air saturation; *K:* permeability, λ, p_d: Brooks-Corey parameters, φ: porosity)

4.1 Fast water infiltration into a single-layer system

The purpose of this study is to analyze rapid infiltration and fluid flow through unsaturated soil with faults and its mechanical involvement in the propagation of land subsidence. Generally, the most important reason for land subsidence is the fluid withdrawal from a reservoir responsive to stress variation. However, this

research focuses on another important aspect of land subsidence, fast rainwater infiltration. When land subsidence phenomenon is present, in most of the cases it is accompanied by fault formations and these faults are usually also present in the soil layers on the top. These pre-existing faults serve as highly conductive waterways. During strong rainfalls, fast water infiltration is produced through these “channels”, inducing high hydraulic pressure and a rapid increase of the soil‘s weight. This aspect becomes even more important when these faults transport the liquid phase through superficial layers with low permeability into layers with higher permeability and this rapid infiltration then produces a fast change in the soil saturation conditions (see section 3).

The aim of this work is to better understand dominant parameters and processes during fast infiltration and fluid flow through faults, specially the role of the fault characteristics and capillary pressure, as well as to couple the results with an analysis of the mechanical deformation.

In this first example, two numerical studies are presented. The first numerical study is a principle investigation of infiltration into the unsaturated zone through a vertical as well as an inclined fracture zone. The second numerical study considers a system with an inclined surface which is close to real natural conditions. Different parameter studies are presented. The results show the important role of rapid infiltration during strong rainfall on the propagation of subsidence and fracturing.

4.1.1 Idealized system and parameters

Two-dimensional (2D) numerical simulations applied to an idealized homogeneous matrix with a high permeable fault zone were investigated, one in a 42 x 90 m rectangular system with a 40 cm fracture zone and one with an inclined surface (Figures 4.2 and 4.3). The system was discretized with 16666 cells with higher resolutions in and around the fault zone (Figure 4.1).

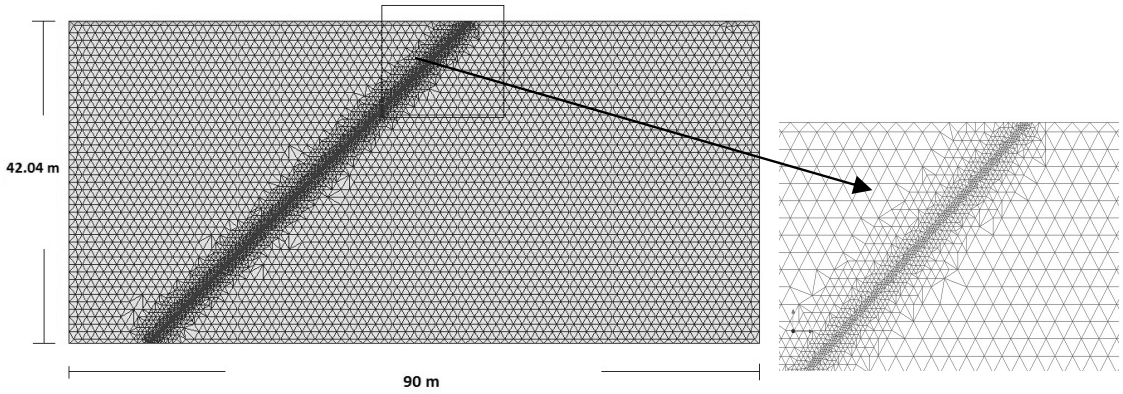

Figure 4.1 Mesh with 16666 cells and a higher resolution in and around the fault

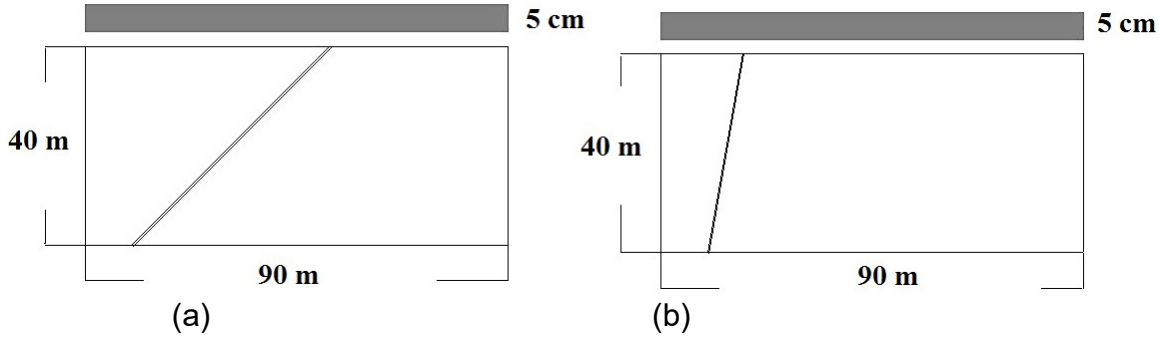

Figure 4.2 Idealized system: (a) 45° inclined fault; (b) 80° inclined fault (Martinez-Noguez *et al.* 2010)

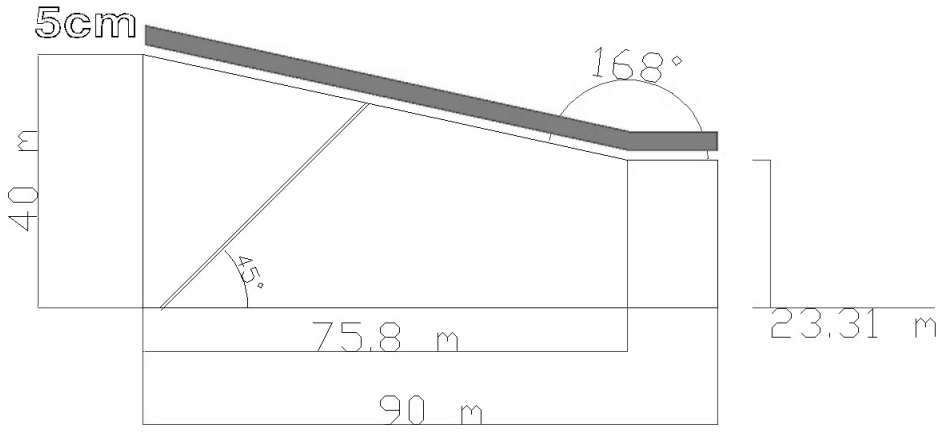

Figure 4.3 Idealized system with an inclined surface and an inclined fault of 45° (Martinez-Noguez *et al.* 2010)

The flow parameter used in the numerical simulation for the matrix and the fault zone are described in Table 1. The boundary condition (BC) at the top of the system is a Dirichlet BC with a fixed water pressure $p_w = p_{atm} + \rho g h$ with $h = 5$ cm simulating an accumulation of a 5 cm water column caused by a runoff after a strong rainfall (Figures 4.2 and 4.3). At the bottom, left and right side of the domain a fixed Neumann no flow BC was chosen. The residual saturation of material was used as initial saturation.

For the mechanical simulations the soil properties are defined in Table 2. The parameters are typical for a clay-sand material. Displacements are possible along the surface boundary. The other boundaries are non-deformable.

Table 2 Soil properties for mechanical modeling.

	Matrix soil	Fault zone
Material Model	Hardening soil	Elastic
Unsat. soil weight [kN/m^3]	16	16
Sat. soil weight [kN/m^3]	20	20
E_{50}^{ref} [kN/ m^2]	10000	---
E_{eod}^{ref} [kN/ m^2]	10000	---
E_{ur}^{ref} [kN/ m^2]	30000	---
E [kN/ m^2]	---	1000
m [-]	0.5	---
P_{ref} [kN/ m^2]	100	---
Poisson's ratio [-]	0.2	0.3
K_o^{nc} [-]	0.44	---
Cohesion [kN/ m^2]	1	---
Friction angle φ [°]	25	---

4.1.2 Results

When the fault zone tends to be vertical the water infiltrates mainly through the fault zone directly into the partially saturated soil (Figure 4.4), but when the fault zone has a considerable inclination the water infiltrates fast through the discontinuity and also propagates into the matrix because of gravity, as shown by Figure 4.5 a and b. The fast infiltration leads to a rapid increase of the soil's weight because of the increased water saturation in the soil. The surface inclination has a minor influence on the load increase.

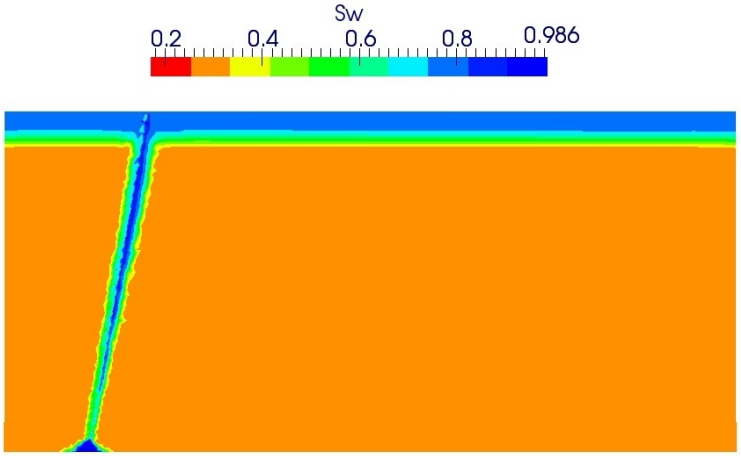

Figure 4.4 Saturation after 90 min water infiltration through an 80° inclined fault zone (Martinez-Noguez *et al.* 2010)

The results of infiltration after 180 min were used for the mechanical modeling and, in addition, the weight of the 5 cm water column on the top was also considered. A deformable material was supposed for the system and the fault zone was defined in this model as a highly elastic material in order to allow deformations and conserve a continuum medium.

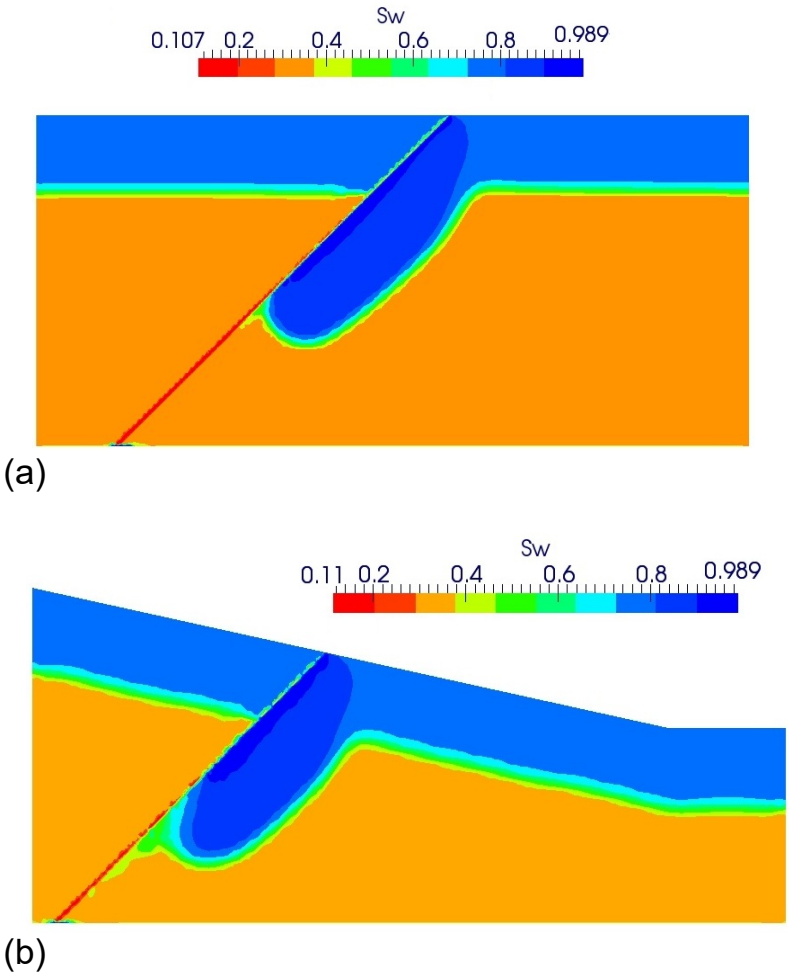

Figure 4.5 (a) Saturation after 180 min water infiltration through a 45° inclined fault zone. (b) Saturation after 180 min water infiltration through a 45° inclined fault zone with a slope on the surface (Martinez-Noguez *et al.* 2010)

The mechanical modeling of the 80° fault system (Figure 4.4) was not carried out as the water infiltrates directly into the saturated zone. When the infiltration was only in the matrix and not in the fault zone, a maximum horizontal displacement of 0.012cm ≈ 0 (Figure 4.6 b) and a maximal vertical displacement of 5.2 cm (Figure 4.6 a) were obtained.

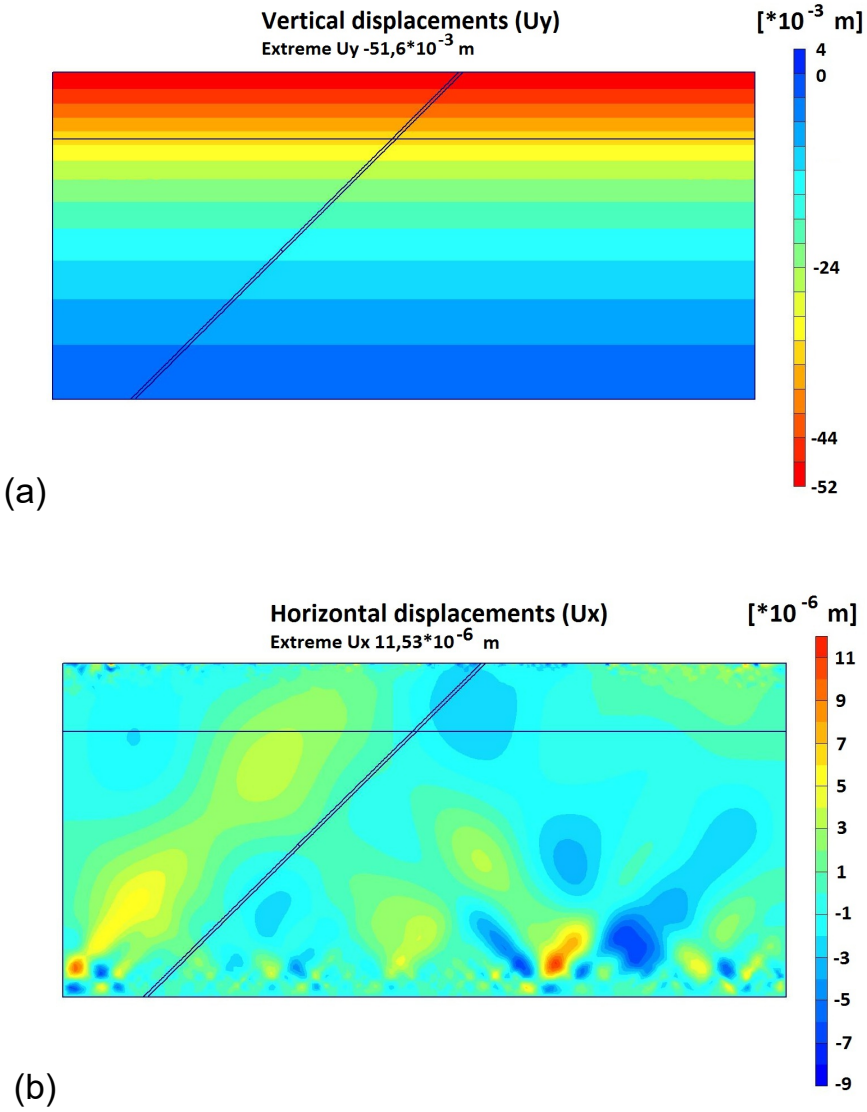

Figure 4.6 Displacements after 180 min of uniform water infiltration (on the surface, not in the fault zone) (Martinez-Noguez *et al.* 2010): (a) Vertical, (b) Horizontal

When infiltration in matrix and fault zone in the rectangular system with a 45° fault zone was considered, a maximum horizontal displacement of 1.2 cm (Figure 4.7 b) and a maximum vertical displacement of 6.6 cm (Figure 4.7 a) were obtained. The horizontal displacement resulted 100 times and the vertical one ~28% bigger compared to the simulation with infiltration only in the matrix.

This deformation increased considerably when there was a certain slope on the surface, as shown in the Figure 4.8 a and b where there was a maximum horizontal displacement of 4.4 cm and a maximal vertical displacement of 12.6 cm.

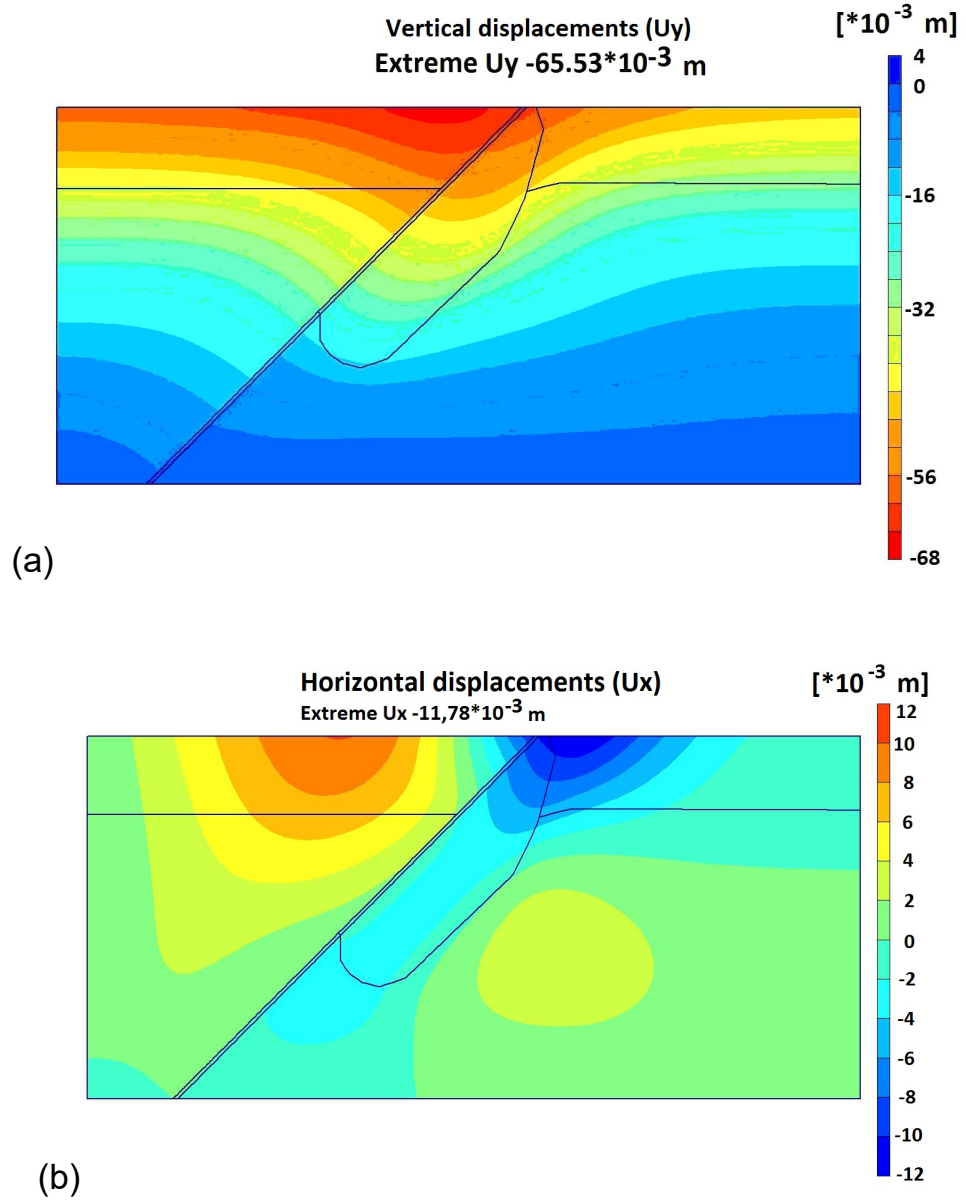

Figure 4.7 Displacements after 180 min water infiltration through 45° inclined fault zone (Martinez-Noguez *et al.* 2010): (a) Vertical, (b) Horizontal

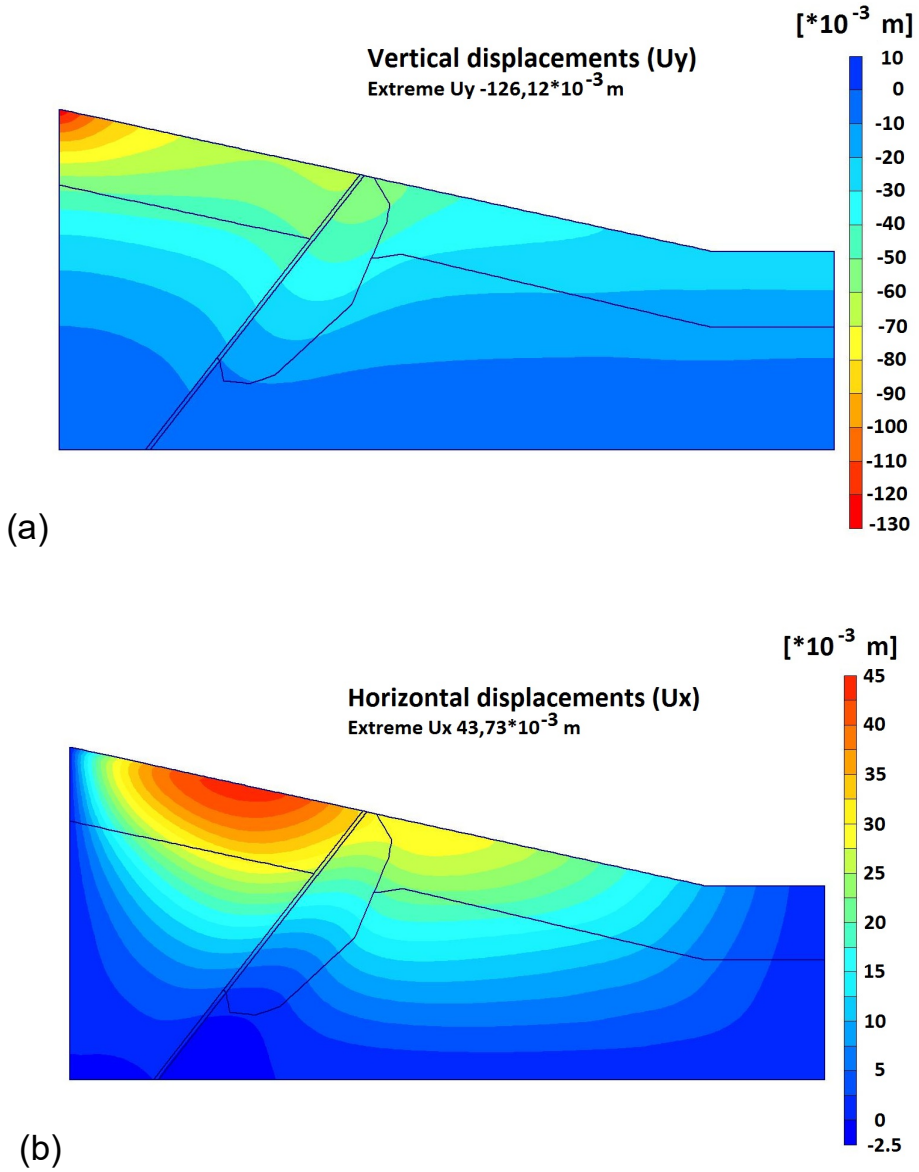

Figure 4.8 Displacements after 180 min water infiltration through 45° inclined fault zone with slope on the surface (Martinez-Noguez *et al.* 2010): (a) Vertical , (b) Horizontal

4.1.3 Conclusions

The numerical studies show that infiltration into a system with a horizontal surface and with a vertical fault zone has no considerable influence on deformation because the water infiltrates directly into the saturated zone.

Infiltration into a system with a horizontal surface and without a fault zone produces linear vertical displacements and the horizontal displacements are negligible. If water infiltrates through the inclined fault zone, the displacements, especially the horizontal one, increase strongly. If there is an inclination on the surface (slope), both horizontal and vertical displacements are considerably increased.

The results of the numerical simulations presented in this first example show that subsidence can be increased considerably by a fast water infiltration through fault zones.

4.2 Fast water infiltration into a two-layer system

The motivation of this example was a fault of one kilometre length and up to 5 meters depth in some parts which appeared in Chalco, Mexico suddenly in the night of 1 June 2009 after a strong rainfall.

Figure 4.9 Fracturing in San Martin Chalco, Edo. De Mexico, Juni 2009
http://www.jornada.unam.mx/2009/06/03/estados/032n1est

In order to understand and to explain possible causes of this sudden faulting after a strong rainfall, different simulations were performed with varying parameters and boundary conditions.

In this section a mechanism of the generation of faults, which can trigger land subsidence, is presented. The results in this example show that a fast infiltration in a partially saturated aquifer leads to land subsidence, extension of pre-existing fault zones and the generation of new cracks.

Infiltration through a fault into a two-layered system, consisting of a clay layer on the top (as it usually occurs in arid or semi-arid regions) and a sand layer as well as the soil deformation on the surface were numerically investigated. Faults serve as highly conductive waterways through layers with low permeability into permeable layers inducing hydraulic pressure and a rapid increase of the soil's weight as a result of the changing soil saturations. Also the results of the water infiltration modeling show that the clay layer acts like a barrier. The reason is that the water is strongly sucked in the clay layer because of the strong capillarity effect. The aim of this example is to better understand the dominant hydrogeological parameters in the evolution of the subsidence on the surface. The mechanical analysis was carried out using the Mohr-Coulomb model (see sec. 2.3.2). Different studies with variations of the fault parameter as well as the infiltration conditions have been carried out. Some unexpected results were obtained and interesting conclusions could be drawn. The most important results have been published (Martinez-Noguez et al. 2013)

4.2.1 Introduction

A series of works about land subsidence induced by fluid extraction from reservoirs (e.g. Jachens *et al.* 1979, Holzer 1984, Carreón-Freyre *et al*. 2005) have been undertaken. Because of the heterogeneous strata, associated with an uneven course of the underlying bedrock surface (for detailed explanation see section 3),

tensional stresses are produced in the soil resulting in fault zone formations in the soil on the surface of the earth. In addition to faults and fractures, soil often exhibits a variety of heterogeneities, such as fissures, cracks and macropores or interaggregate pores (Gerke & van Genuchten, 1993). These fault zones can significantly affect water and solute movements in soils because the flow and transport is accelerated (Novák *et al.* 2000). Infiltration processes in soils with fractures and faults have been investigated for example by Pham Van (2009) and Novák *et al.* (2000).

During strong rainfalls, fast water infiltration occurs through these fault zones inducing hydraulic pressure and a rapid increase of the soil's weight because of the change of soil saturation conditions. A previous numerical study (Martinez-Noguez *et al*. 2010) described in chapter 4.1 has shown, that subsidence can be increased considerably by a fast water infiltration through fault zones. This aspect becomes even more important when such fault zones transport the water through superficial layers with low permeability into layers with higher permeability.

Therefore, such a system with a superficial layer which consists of sand and clay layer and is close to real field conditions is investigated in this example. The main infiltration is limited to a small area where the fault intersects the surface of the earth. Further, real data from a natural system in Queretaro city, Mexico have been chosen. In Queretaro land subsidence has occurred in the last years due to intensive groundwater withdrawal for domestic and industrial use. There, the soil properties have been analysed and the deformation processes have been monitored (Trejo-Moedano 1989, Arroyo *et al. 2002*, Álvarez 1999).

In order to understand the relevant parameters and processes for land subsidence induced by fast rainwater infiltration into a fault zone, a number of numerical simulations are presented varying the fault zone width, the permeability as well as the boundary conditions on the top.

As soil behaviour is highly non-linear and irreversible, a linear-elastic perfectly-plastic model (Mohr-Coulomb model) has been applied to determine the infiltration induced deformation (see section 2.3).

As initial condition, it is assumed that an unconfined aquifer is completely saturated and the underlying bedrock contains a buried ridge (Figure 4.10, left). If the water table declines because of water withdrawal (Figure 4.10, right), the soil's buoyancy is reduced and a strong increase of the grain-to-grain stress is produced. This increase of the effective stresses produces a rearrangement of the soil's particles. In such cases, this compaction of deposits is not uniform.

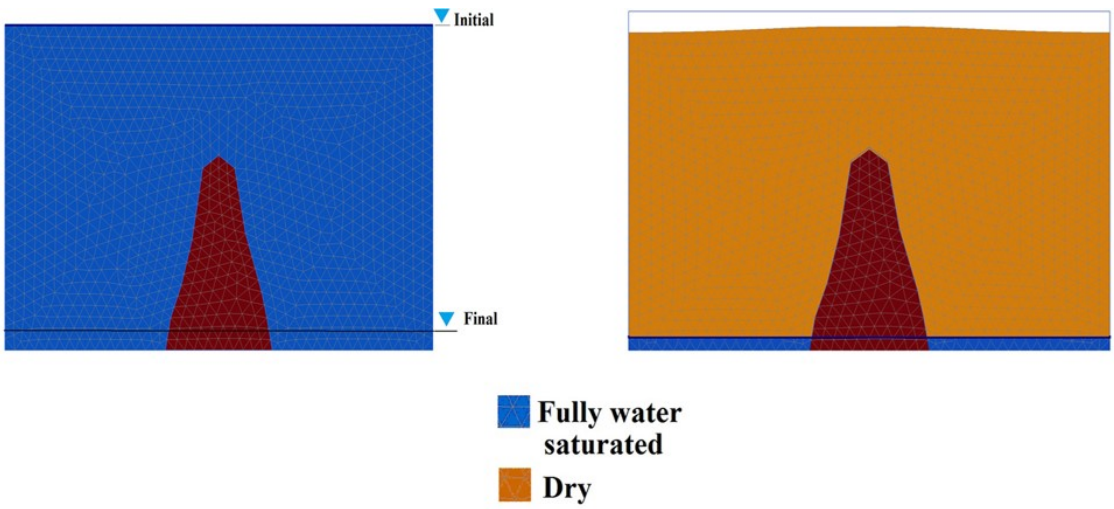

Figure 4.10 Idealized system with a buried ridge (left), and deformed mesh after water decline (right)

Heterogeneous strata, associated with an uneven course of the underlying bedrock surface and groundwater withdrawal leads to tensional stresses in the soil resulting in plastic zones (Mohr-Coulomb points) and the formation of fault zones (tensional cut-off points) on the surface (Figure 4.11).

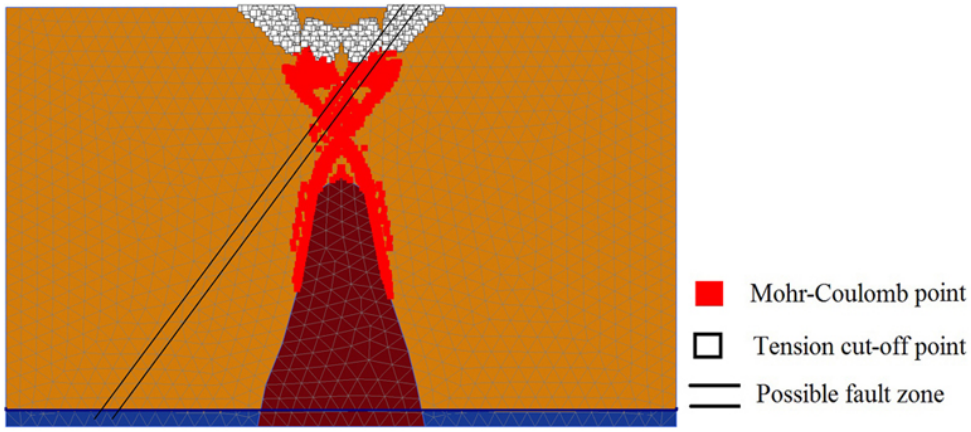

Figure 4.11 Plastic and tension cut-off zones and fault zone

Up to this point, the classical models of faults and fracture formation caused by groundwater withdrawal have been briefly explained (for detailed explanation see section 3). In the following a new mechanism for fault formation induced by fast water infiltration is introduced.

In arid and semi-arid zones, rainfalls are characterized by short intensive rainstorms (Verheye 2002). An example is Mexico City with more than 20 mm/hr (Magaña *et al*. 2002). During strong rainfalls, fast water infiltration occurs through fault zones inducing hydraulic pressure and a rapid increase of the soil's weight because of the increase in soil saturation (Figure 4.12, left) which produces deformation and possibly new faulting on the surface (tension cut-off points in Figure 4.12, right). In section 4.1 it was shown that subsidence can be increased considerably by fast water infiltration in a homogeneous layer through fault zones. This effect can be intensified when such faults transport the water through a superficial layer with low permeability into layers with higher permeability.

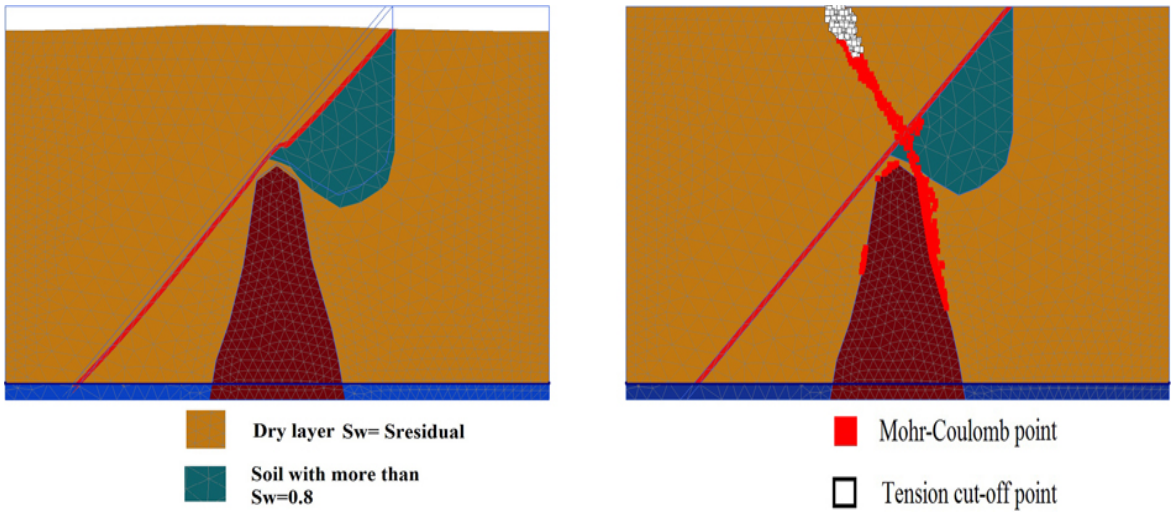

Figure 4.12 Deformation after infiltration (left), plastic and tension cut-off zones (right)

4.2.2 Idealized system and parameters

A model of a two-layered system with a clay layer on the top, a sand layer underneath and a high permeable fault zone was set up in form of a rectangle with 40 m length and 30 m depth (Figure 4.13, left). In this study, a 45° inclined fault zone (blue in Figure 4.13, right) was chosen and idealized as a porous medium damage band with a much higher permeability compared to the sand and clay layers (green, red in Figure 4.13, right). An unstructured grid was generated with 21762 cells with a higher resolution around the fault zone as shown in Figure 4.13, right. It is pointed out that the fault zone, which has a considerable width in the range of several decimetres, is also discretized by triangular elements.

Typical parameters for sand and clay were chosen for the two-phase flow simulation (Table 1). The boundary condition (BC) at the top of the system is a Dirichlet BC with a fixed water pressure $p_w = p_{atm} + \rho g h$ with h = 5 or 1 cm represents an accumulation of a 5 or 1 cm water column caused by a runoff after a strong rainfall, p_{atm} is atmospheric pressure, ρ is water density and g is gravity. At the bottom, left and right of the domain a fixed Neumann no flow BC was chosen.

For deformation modeling real data of a natural system in Querétaro, Mexico, were available for the piroclastic non-consolidated deposits (TpPyLac) and the Quaternary Alluvium (Qal) sediments (Pacheco-Martinez *et al*. 2007, Trejo 1989, see Table 3). Displacements are possible along the surface boundary. The other boundaries are non-deformable. Different set-ups were analysed varying the width and permeability of the fault zone as well as the boundary condition on the top, see Table 4.

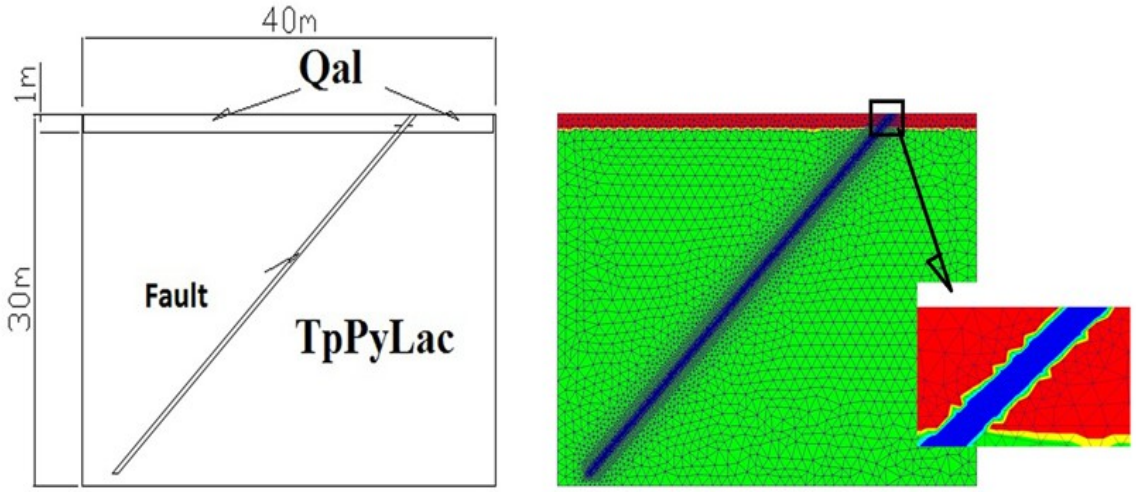

Figure 4.13 Two-layered idealized system with a fault zone (left), and mesh with detail (right)

For all simulations, as initial condition the initial water saturation was set to 0.3. The water column of 5 and 1 cm was applied for the deformation analysis as a distributed load.

Table 3 Soil properties in Queretaro for deformation modeling after Trejo (1989)

Material	υ	E	φ	C	γ_{wet}	γ_{dry}
	[-]	[kN/m^2]	[°]	[kPa]	[kN/m^3]	[kN/m^3]
Qal	0.2	28200	28	12.7	18.5	16
TpPyAl	0.21	45000	34	25	20	18.5
Fault Zone	0.3	1000	--	--	20	16

Young's modulus E, Poisson's ratio υ, friction angle φ, cohesion C, specific weight for a saturated soil γ_{wet} and dry soil γ_{dry}, piroclastic no consolidated deposits (TpPyLac) and the Quaternary Alluvium (Qal) sediments

Table 4 Parameters to be varied

Fault width [cm]			Fault permeability [m2]		Boundary condition on the top (Water column)	
20	40	80	10-9	10-10	5 or 1 cm	on complete surface or only on fault

4.2.3 Results

In section 4.2.3 the results of parameter variations for the water infiltration are described. For selected cases it was investigated the impact of the water infiltration on the soil deformation which is described in section 4.2.3.2.

4.2.3.1 Water infiltration

Case 1: Barrier effect: Variation of fault zone permeability and water column height only on the fault zone

For a 20 cm fault width and a water column only on the fault zone, there is neither a remarkable difference in the results if the fault permeability is 10^{-9} or 10^{-10} m^2 nor if the water column on the top of the fault zone is of 5 or 1 cm. The reason for this is that water is strongly absorbed horizontally in the low permeable layer because of the strong capillarity effect. Only a small part of water infiltrates through the high permeable fault into the sand (Figure 4.14). The clay layer acts like a barrier. Similar results have been obtained by Kung (1990).

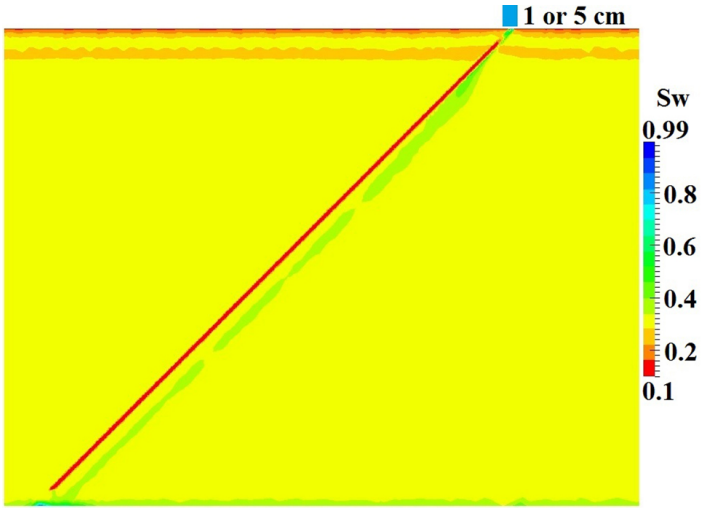

Figure 4.14 Results of water saturation after 2 hours in a system with a 20 cm fault zone with a permeability of $K = 10^{-9}$ m^2 and 5 or 1 cm water column only on the fault zone

Case 2: Variation of the water column on the complete surface

If a 5 cm water column is on the complete surface, it infiltrates slightly into the low permeable layer, however it strongly infiltrates through the fault into the sand. The barrier effect is overcome which is indicated by only small red parts of the water saturation in the clay layer in Figure 4.15, left. Hence the deformation modeling is performed for this case (see section 4.2.3.2) since the infiltration is not uniform and the water pressure is much stronger on the right side of the fault zone leading to deformations on the surface.

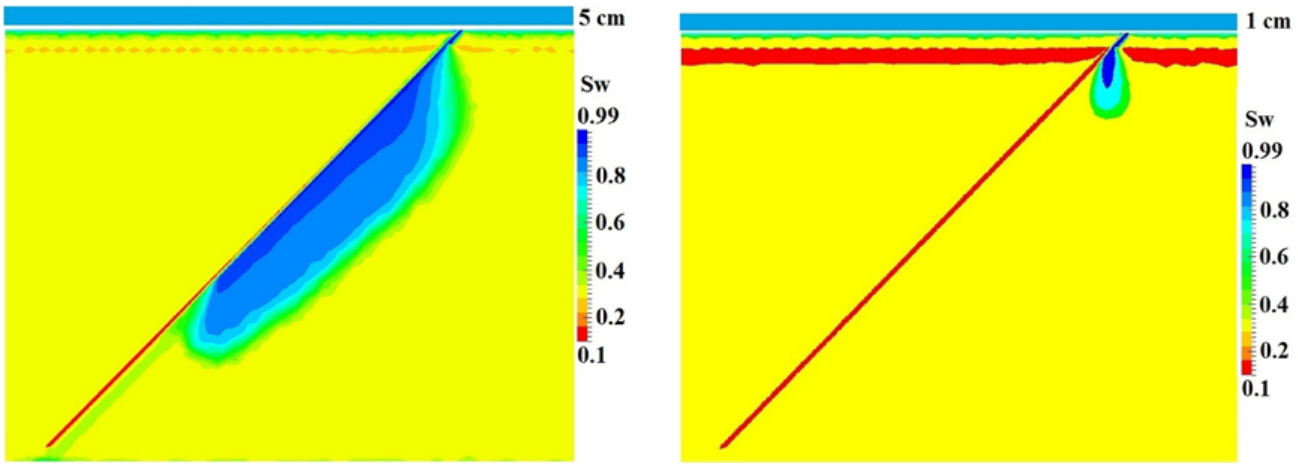

Figure 4.15 Results of water saturation after 2 hours in a system with a 20 cm fault zone width with a permeability of $K = 10^{-9}$ m^2: a 5 cm water column on the complete surface (left), a 1 cm water column on the complete surface (right)

If the water column on the top boundary is only 1 cm, the barrier effect still occurs (red colour in clay layer in Figure 4.15, right) which in addition to the smaller water column contributes to a considerably smaller infiltration compared to Figure 4.15, left, however to a bigger infiltration compared to Figure 4.14.

Case 3: Variation of fault zone width

If we use the same parameters as for Figure 4.14, left (fault zone permeability of $K=10^{-9}$ m^2, 5 cm water column on the complete surface) and extend the fault zone width from 20 cm to 40 cm, the water reaches the bottom of the system (where a groundwater table could be) much faster. Here after about 30 min (Figure 4.16, left), while in Figure 4.15, left, the bottom has not been reached after 2 hours. For an 80 cm fracture width, the water arrives at the bottom after about 15 minutes.

If the water column is only set on the fault zone, for a 20 cm fault zone width the infiltration is minimal (Figure 4.14). For a 40 cm fault zone the infiltration ratio increases considerably but not enough to produce notable deformation on the surface. In the case of an 80 cm fault zone width, the infiltration considerably

increases and this produces deformation (Figure 4.16, left). Therefore, mechanical simulation is performed (see sec. 4.2.1.2).

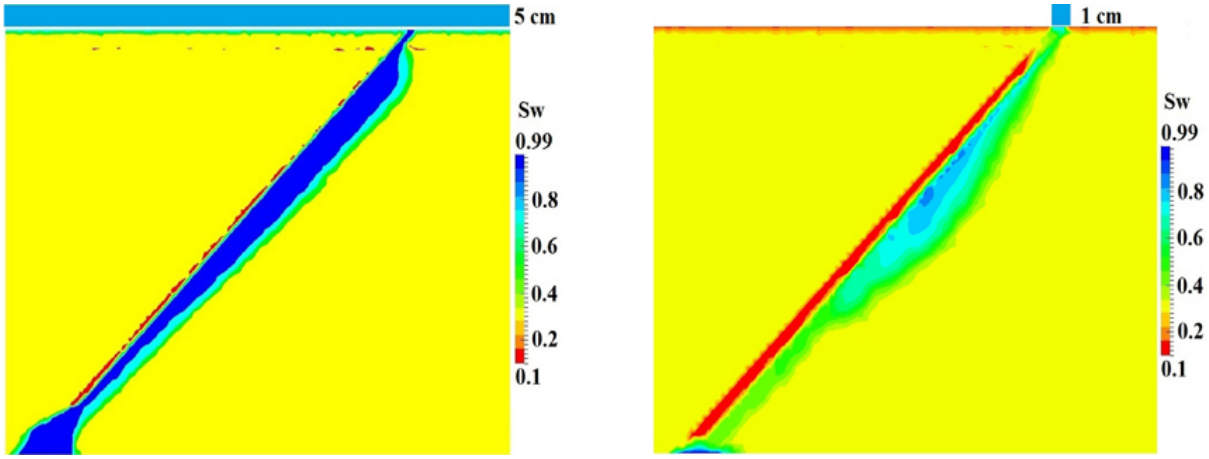

Figure 4.16 Water saturation after 2 hours in a system with a 40 cm fault zone width with a permeability of $K=10^{-9}$ m^2 and a 5 cm water column on the complete surface (left), water saturation after 30 min in a system with a 80 cm fault zone width with a permeability of $K=10^{-9}$ m^2 and a 1 cm water column only in the fault zone (right)

4.2.3.2 Water infiltration and soil deformation

Subsidence occurs in many parts of the world as a result of the heavy groundwater withdrawal. In Querétaro city (region where the data for the modeling are used) the annual average water decline is of 3 m per year and in some areas the decline reaches 6 m per year (State Water Commission, CEA 2006). This water table decline has produced land subsidence as well as fracture and fault formations through the years. During strong rainfalls the water infiltrates through the fault zone leading to soil deformation within just a few hours.

The results of the infiltration modeling of three cases have been considered for the soil deformation analysis. First, a reference case was defined where we investigate a system without fault zone. In the following we compare these deformation results with results of 3 cases of a system with a fault zone.

In the reference case without a fault, it is first assumed as an idealized condition, that the water table was initially at the surface and then declined 30 m in 10 years to the bottom of our system. Only vertical displacements occurred with a maximum of 7.5 cm on the surface (Figure 4.17, left) corresponding to 7.5 mm per year. In the reference case without a fault, next we set a 5 cm water column on the surface leading again only to vertical displacements with a maximum of about 0.5 mm on the top after 2 hours (Figure 4.17, right).

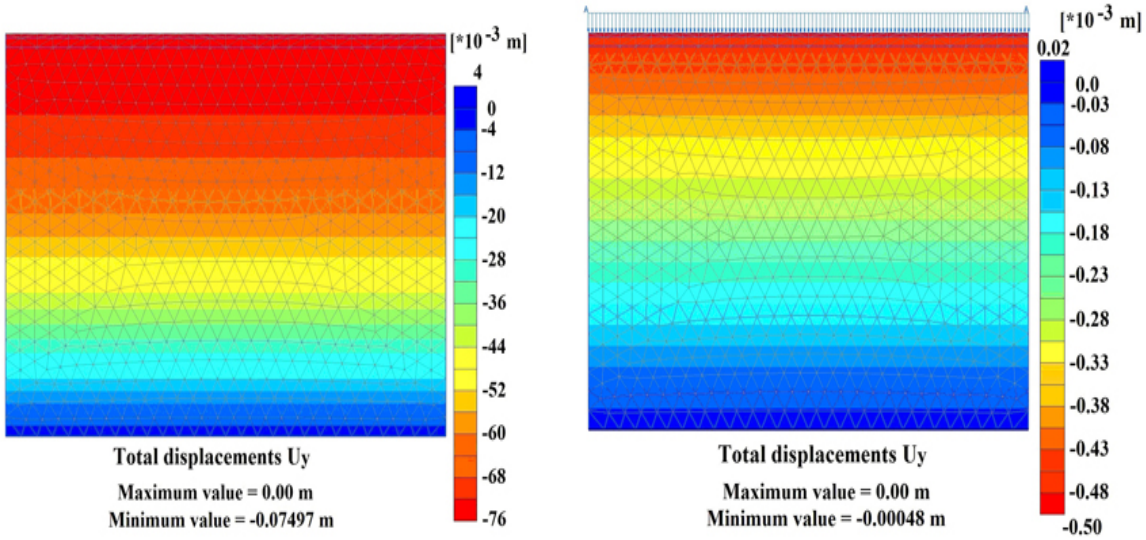

Figure 4.17 Reference case for deformation modeling: vertical displacements for 30 m water table decline in 10 years (left); vertical displacements for a 5 cm water column on the complete surface after 2 hours (right)

Case 1: Deformation modeling of water table decline and fast infiltration with a 5 cm water column on the complete surface and a 20 cm fault zone width

First the deformation for the water table decline in the system with the fault was investigated. The maximum vertical displacement was ~ 10 cm at the surface (Figure 4.18, left) corresponding to 1 cm per year and this was about 25 % higher if compared to the reference case (see Figure 4.17, left). The maximum horizontal displacement was about 1 cm corresponding to about 1 mm per year (Figure 4.18,

right). Overall it had a two-dimensional deformation field due to the fault. If the loads of Figure 4.15, left (5 cm water column on complete surface and water infiltration of 2 hours) were taken, this resulted in a maximum vertical displacement of 3.3 mm being more than 5 times bigger compared to the reference case (Figure 4.17, right) and a maximal horizontal displacement of 0.7 mm (Figure 4.19, right). When comparing case 1 with the reference case, we point out that the fault led to a substantial relative increase of the maximal vertical displacement for the fast infiltration case (0.5 mm → 2.6 mm), while this relative increase is smaller for the water table decline (7.5 cm → 10 cm).

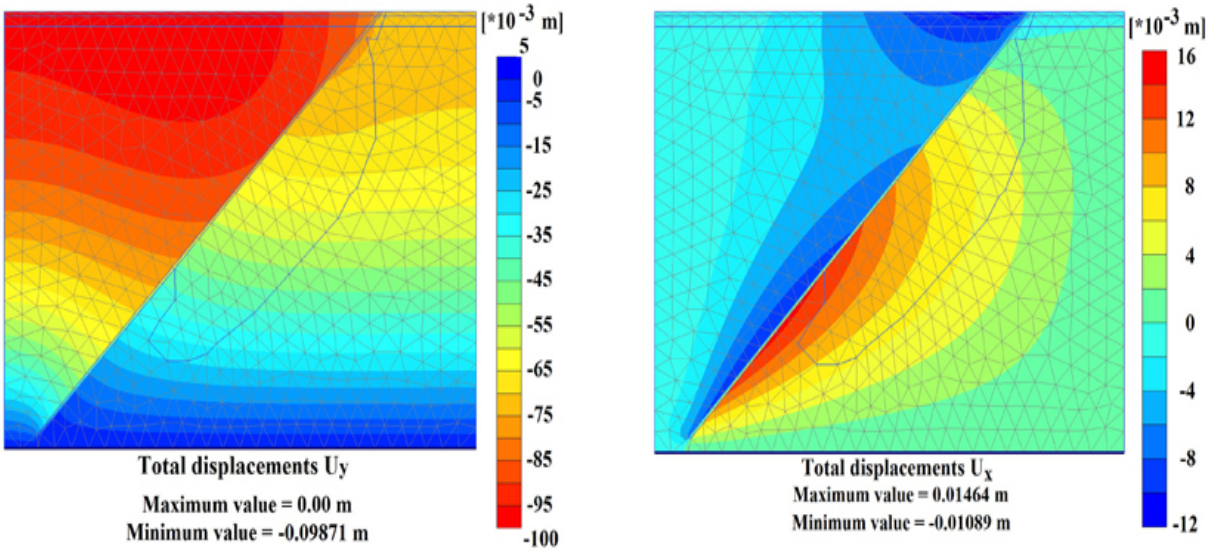

Figure 4.18 Displacements for 30 m water table decline in 10 years: vertical displacements (left); horizontal displacements (right)

Comparing the results of Figure 4.19 to the yearly subsidence obtained in Figure 4.18, the vertical displacements caused by infiltration in 2 hours were more than about 30 % of the yearly displacement caused by the water table decline in 10 years. The horizontal displacements in two hours were approximately 70 % of the yearly displacement due to the water table decline in 10 years.

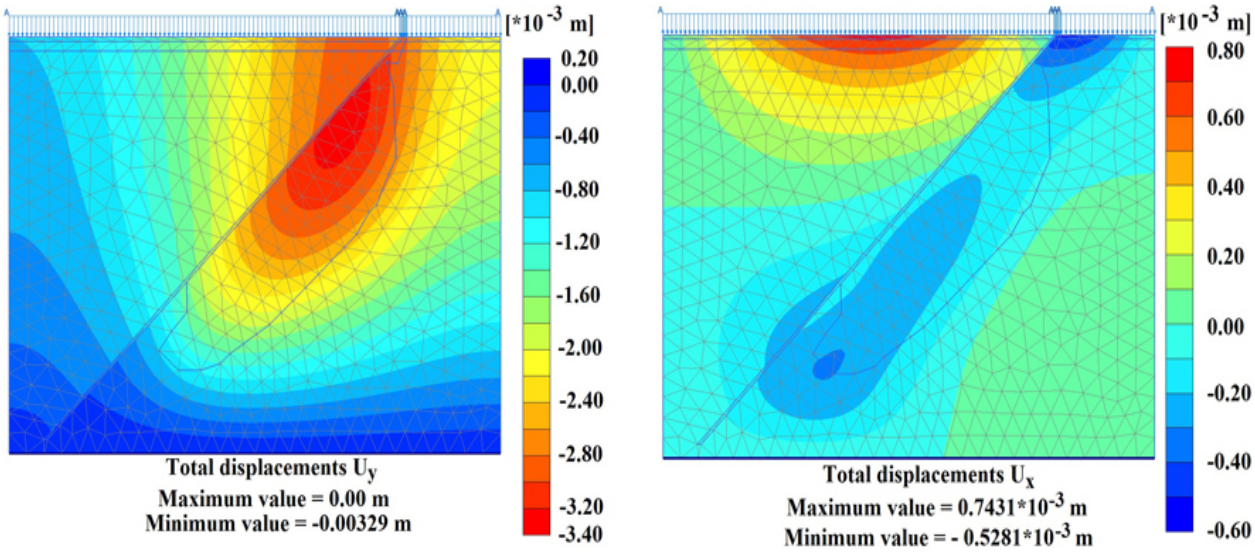

Figure 4.19 Displacements for water infiltration after 2 hours: vertical displacements (left); horizontal displacements (right)

For the case of the water table decline, Mohr-Coulomb points in plastic zones occurred around the fault close to the surface as well as close to the bottom (Figure 4.20, left). The plastic zone on the surface led to an enlargement of the fault. Further, zones with tension cut-off are seen around the fault close to the surface leading to the formation of new cracks. The fast water infiltration also led to plastic and tension cut-off zones. Plastic zones occurred around the fault at the bottom of the system and tension cut-off zones at the interface between the clay layer and the sand which are called “weakness planes” (Figure 4.20, right).

If we compare the water table decline (Figure 4.17, left) with the fast infiltration (Figure 4.17, right), less plastic and cut-off zones occurred in the latter case.

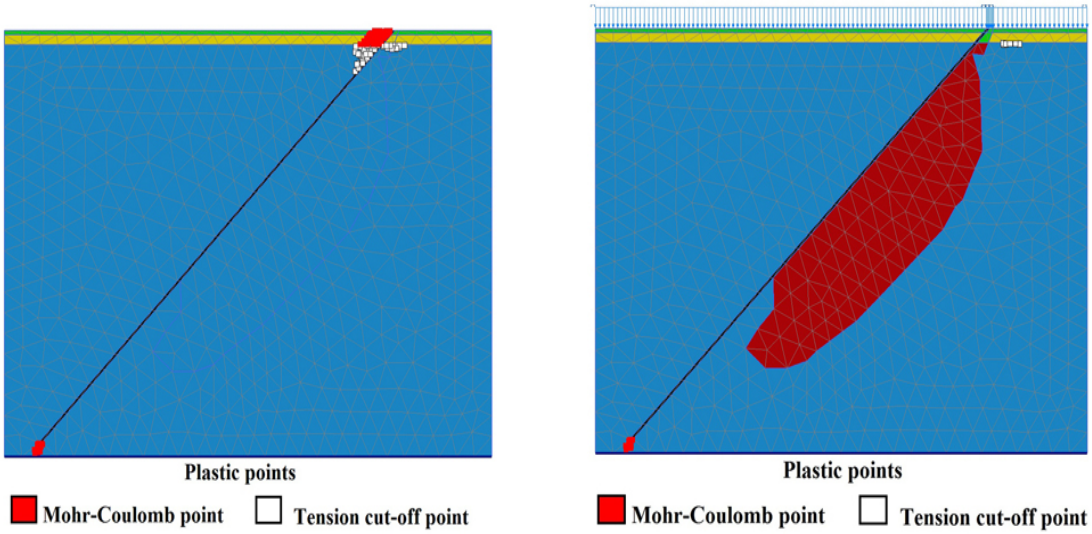

Figure 4.20 Plastic and tension cut-off zones caused by: water table decline (left); fast infiltration (right)

Case 2: Deformation modeling of water table decline and fast infiltration with a 1 cm water column on the top of a fault zone with 80 cm width

As in the previous case, the deformation simulation was performed when the water table declined 30 m in 10 years. A maximum vertical displacement of 14 cm (1.4 cm per year) and a maximum horizontal one of 2.6 cm were obtained (2.6 mm per year) (Figure 4.21).

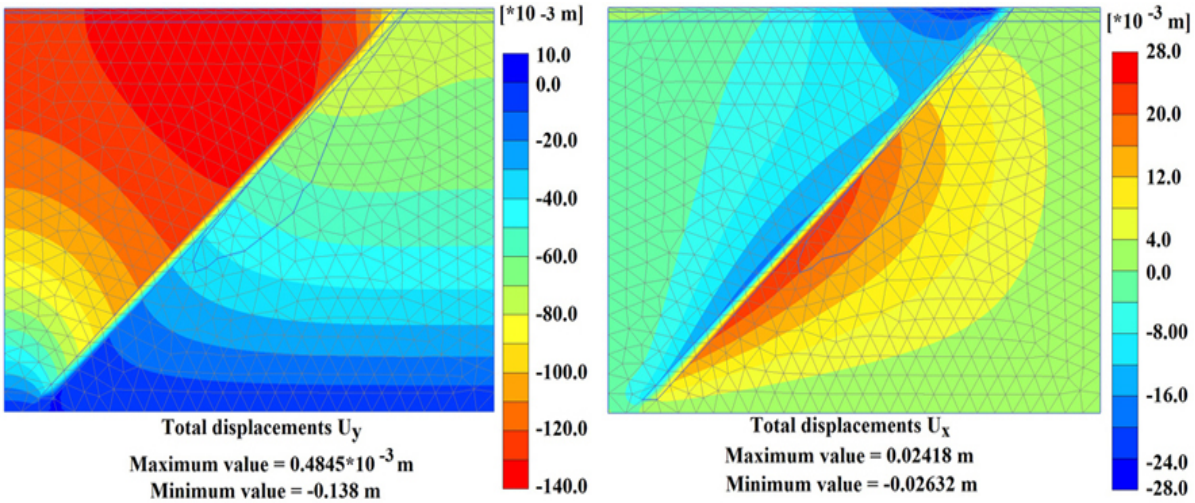

Figure 4.21 Displacements for 30 m water table decline in 10 years: vertical displacements (left); horizontal displacements (right)

When using the infiltration results shown in Figure 4.16, right, in the case of fast infiltration through a system with an 80 cm fault zone width and a 1 cm water column on the top of the fault zone, a maximum vertical displacement of 3.3 mm and a maximum horizontal displacement of 0.5 mm were obtained after 2 hours of infiltration (Figure 4.22). Comparing the case water table decline and fast infiltration, the maximum vertical and horizontal displacements of the fast infiltration were about 25 % and 20 % of the corresponding displacements of the water table decline (Figure 4.23, 4.24).

If we compare case 1 and case 2, the results are quantitatively similar. For the water table decline, the maximum displacements are bigger for case 2, the maximum horizontal displacements are ever much bigger (Figure 4.19, right, 4.22, right).

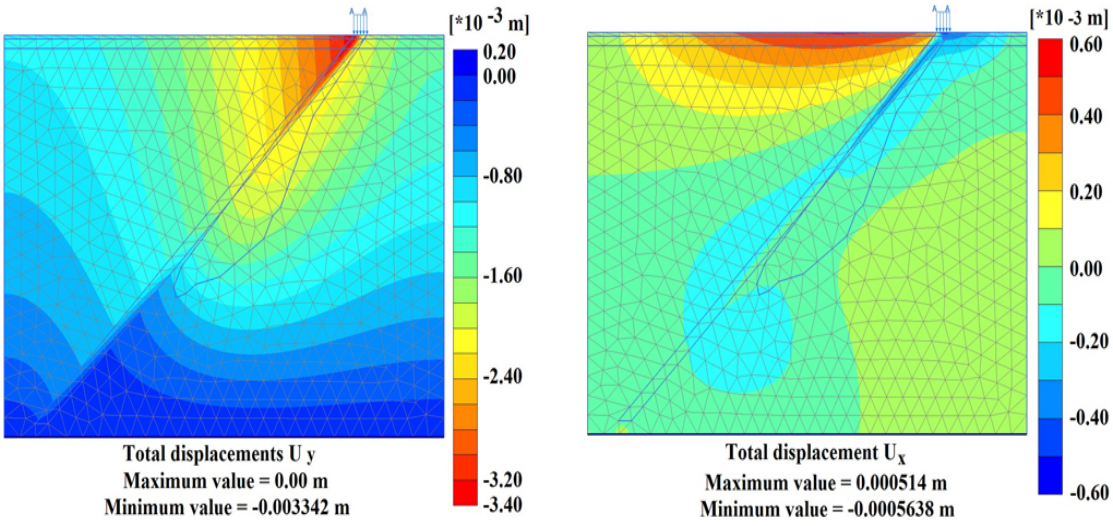

Figure 4.22 Displacements for water infiltration after 2 hours in a system with a 1 cm water column on the top of a fault zone with 80 cm width: vertical displacements (left); horizontal displacements (right)

For the fast infiltration, the maximum displacements are very similar (Figure 4.19, left, Figure 4.22, left). This circumstance indicates that neither the fault zone width nor the water column on the complete surface or only on the fault have a

remarkable influence on the maximal deformation, if the water column is 5 cm as the barrier effect is no more important in such cases.

Case 3: Deformation modeling of water table decline and infiltration of a 5 cm water column on the complete surface and a 40 cm and 80 cm fault zone width

If the fault zone had a width of 40 cm, the water table decline of 30 m in 10 years produced a vertical displacement of 7.5 cm (7.5 mm per year) and a horizontal one of 0.4 mm (a yearly displacement of almost zero) (Figure 3.23).

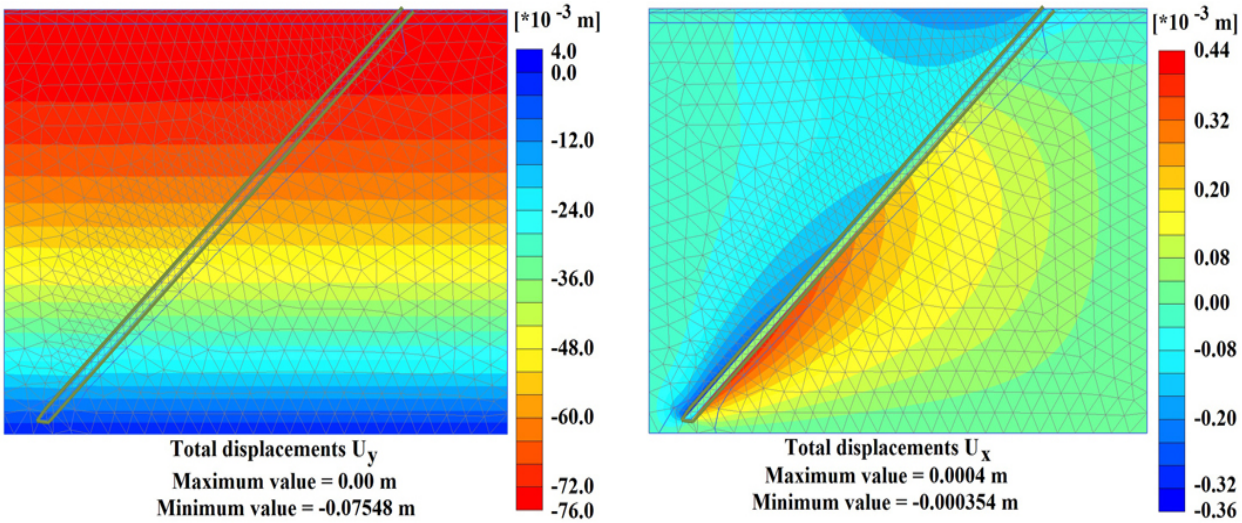

Figure 4.23 Displacements for 30 m water table decline in 10 years: vertical displacements (left); horizontal displacements (right)

If the fault zone is 40 cm wide, a 5 cm water column is set on the complete surface and the infiltration after 30 minutes obtained in Figure 4.16, left is used, the mechanical simulation shows a maximal vertical displacement of 1 mm and a horizontal displacement of 0.1 mm (Figure 4.24). In this case the infiltrated water reaches the groundwater in less than 30 min. Therefore, the saturation in the soil

caused by this infiltration does not count as an extra weight any more; i.e. the soil's buoyancy is recovered. If the fault zone is 80 cm wide the infiltrated water reaches the groundwater in less than 15 min.

If we compare the results obtained for a 20 cm fault zone (Figure 4.19) with the results for a 40 cm fault zone (Figure 4.24) there is a notable difference in the infiltration and deformation. In a 40 cm fault zone the infiltrated water reached the bottom after 30 min and most of infiltrated water flowed through the fault and not into the sand layer. In a 20 cm fault zone after 2 hours the infiltrated water had not reached the bottom and the water infiltrated into the sand layer on the right side of the fault which produced deformation on the surface.

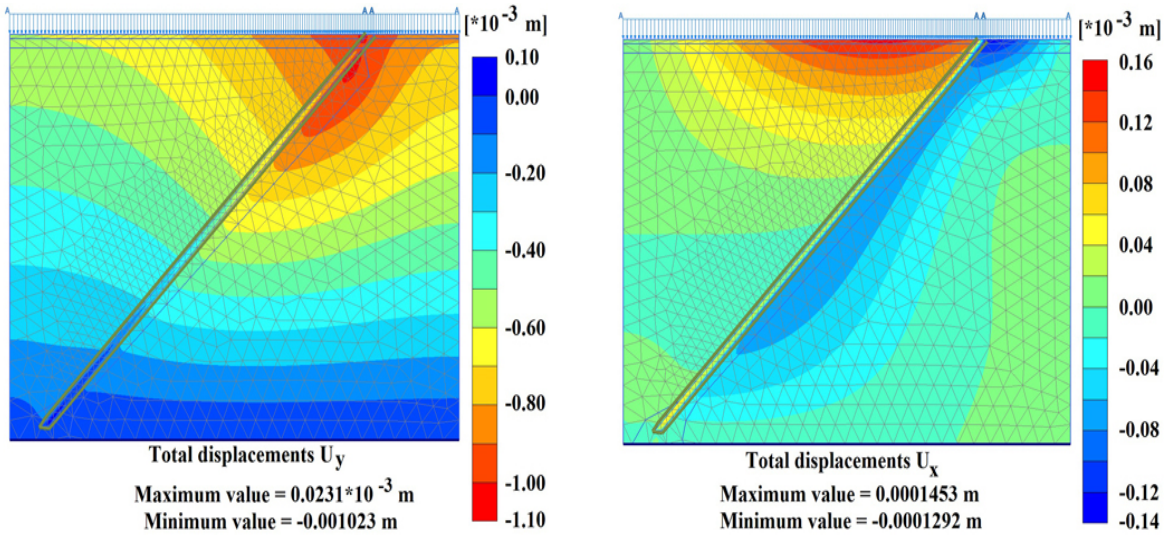

Figure 4.24 Infiltration after 30 min in a system with 40 cm fault zone with a permeability of $K = 10^{-9}$ m^2

4.2.3.3 Comparison

The results show that fast water infiltration through an inclined fault zone produces vertical and horizontal deformation. Especially vertical deformation plays an important role in fracture and fault formation. As Figure 4.25 shows,

case 1 and 2 have similar vertical deformation although the conditions are different. The horizontal deformations, which also can lead to new fracture and fault formation, are smaller.

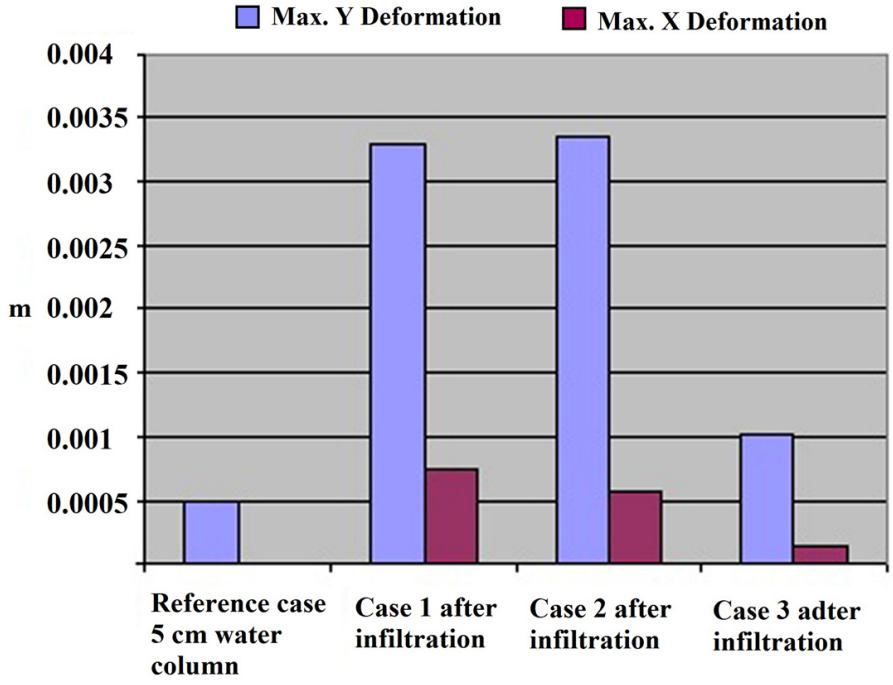

Figure 4.25 Horizontal and vertical deformation for reference case and case 1, 2 and 3

4.2.3.4 Conclusions

This example described a new conceptual model of a mechanism for the generation of fracturing and faulting and triggering of land subsidence: fast rain water infiltration through fault zones.

Numerical simulations were performed in order to explain the new mechanism and to obtain an understanding of the dominant hydrogeological parameters in the evolution of the deformation on the surface caused by a rapid water infiltration. A two-layered system consisting of a sand layer, a small clay layer on the top and an inclined fracture was investigated.

If the water column is set only on the fault zone, the numerical studies showed that there is no considerable difference if the permeability in the fault zone is 10^{-9} or 10^{-10} m^2 (one or two orders minor than the surrounding sand layer). Also the water column of 1 or 5 cm made nearly no difference in the infiltration and this infiltration did not produce considerable deformation.

If a water column of only a few centimetres (1 and 5 cm) is set on a narrow fault zone (in our simulation 20 cm), there is no remarkable infiltration through the fault zone because the capillary suction in the clay layer is much stronger than the one of the fault and gravity causing a barrier effect.

A water column set on the complete surface produced fast infiltration through the fault which propagated horizontally and vertically because of capillarity and gravity. The rapid change of the water content in the soil increased the soil's weight resulting in deformation on the surface. This rapid infiltration could produce 70 % or more of the annual subsidence ratio. If an extreme rainfall leads to a 5 cm water column close to the surrounding area of the top of the fault, it will produce a rapid increase in the land subsidence, fracture and fault formation and might damage buildings that are close-by.

The results of a fault zone width of 20 cm also showed infiltration into the partially saturated zone and deformation of the soil. If the fault zone width is 40 cm or more, very fast infiltration is produced predominantly through the fault zone reaching the groundwater table quickly. Therefore pore water pressure is generated. The increase in the water content in the partially saturated zone is minimal and so is the soil deformation. This case is an interesting option if the recharge of an aquifer is proposed through a fault zone.

4.3 Numerical study about hydrologic barrier effects caused by a high permeable fault

In natural systems faults can act as hydrologic barriers in aquifers and as a result different behaviours (water levels) on both sides of the discontinuities in the same aquifer are observed. This difference can be of the magnitude of several meters, as for example in the aquifer in Querétaro, Mexico, where it presents a difference of more than 10 meters.

This example presents a numerical study about the influence of structural soil discontinuities on unsaturated flow in the presence of water extraction. The aim of the study is to simulate the dynamic groundwater table of a homogeneous aquifer with a fault zone caused by a single water extraction well.

Typically, a fault can act as a barrier when it has a low permeability, but the results of this study showed that also a fault zone with high permeability can act as a hydrologic barrier and it can be a triggering factor for land subsidence. It was also noticed that not only the extraction ratio affects the flow, but also the well's position with respect to the fault zone and the boundary. So, the presence of a hydrologic barrier can detonate land subsidence.

4.3.1 Introduction

Groundwater overexploitation, may cause land subsidence and produces fracture and fault formation around the world (Jachens & Holzer 1982, Trejo & Martinez-Baini 1991, Burbey 2002, Shen & Helm 1995, Hernandez-Marin & Burbey 2010). Land subsidence is also associated with rain water infiltration through fault zones (Carpenter 1999, Suarez-Placencia 2005, Martinez-Noguez *et al*. 2013). Furthermore, it was found out through simulation that a single well lowering the water table drives land subsidence (Kumarci *et al*. 2008, Ziaje *et al*. 2007). This

research investigates a system with both elements, land subsidence enhanced by a single well and a fault zone acting as hydrologic barrier.

Faults and fractures can influence groundwater flow in aquifer and aquitard layers (Carreon Freyre *et al*. 2005), varying in width from some centimetres to some meters (Murillo-Fernandey *et al*. 1991, Holzer 1977). Kreitler (1977) reported that the faults in the Houston-Galveston area may act as hydrologic barriers. Fluid extraction on one side of a fault causes piezometric surface decline and aquifer compaction on that side of the fault and not on the other. Kreitler (1977) does not, however, completely resolve whether the faults act as hydrologic barriers and control the piezometric surface, he only implies this relationship. Faults may also act as low permeability barriers to fluid flow (Smith 1980), for example when open pore space is filled by mineral precipitation following deformations. Grain size reduction and/or mineral precipitation generally yield fault core with lower porosity and permeability than the adjacent ones (Caine 1996).

Figure 4.26 shows a two-layered system with a clay layer on the top, a sand layer underneath and a 1 m fault zone was set up. The boundary condition (BC) at the top of the system is a Dirichlet BC with a fixed atmospheric pressure. At the bottom, left and right of the domain a fixed Neumann no-flow BC was chosen. As initial condition, full water saturation was assumed. If an inclined fault zone with low permeability is considered, the water level at the left side of the fault presents a deeper decline than on the right side of the fault zone after water extraction of a single well between the no-flow boundary condition and the fault. Also the low permeable fault zone acts as a hydrologic barrier. This is not difficult to understand if the fault zone has a lower permeability. Could it be possible that a fault zone with higher permeability than the aquifer performs as a hydrologic barrier when water is extracted through a well? This study shows that this is possible if some conditions are fulfilled.

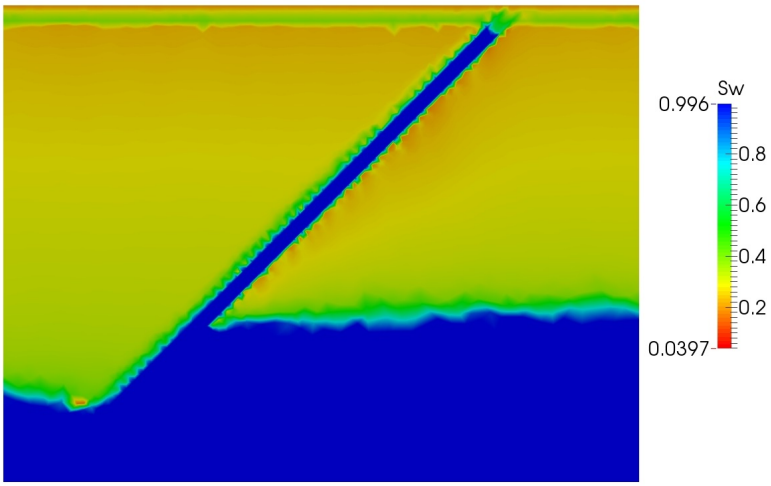

Figure 4.26 Differential water decline at both sides of a fault zone with low permeability after extraction of a single well

The valley of Queretaro city, Mexico, is an example of active land subsidence. Since the 1970s, with the rapid growth of the city, the water demand increased rapidly, and as a result the urban area is affected by differential compaction and formation of a reticular system of faults and fractures, many of them appear on the surface and have caused economical damages in the last 40 years.

Figure 4.27 shows the urban area of the city (light green), faults and fractures (red line in Figure 4.27) and some of the active wells in the city (circles). In many of the cases the wells at both sides of the faults show a considerable difference of the piezometric level. For example, the static level of the well number 612-F at the left side of the fault Tlacote and the well number 1313-A of the year 2011 are 153.9 m and 140 m respectively, which is almost a difference of 14 m. The same behaviour exists also in wells number 1322 and 1638 located at the right and left sides of the fault Epigmenio Gonzales, respectively, where the water level in 2011 were 116 m and 129.5 m, respectively (Table 5).

Table 5 Water table in wells in 2011

Tlacote fault	Well no.	Water level (m)	E. Gonzales fault	Well no.	Water level (m)
right side	2427	133.1	right side	1322	116.0
right side	1313-A	140.0	left side	1638	129.5
left side	612-F	153.9	right side	953	132.2

Usually hydrogeological systems are big and complex because of the heterogeneity of the soil layers, the basement, the fault and the well system, as is the case of the Queretaro aquifer. Besides the complexity of the system, another problem is the lack of data. The study of a natural system like the aquifer in Queretaro, Mexico, is more difficult because of the complexity of the system. It is a faulted and fractured system with irregular and heterogenic stratification and more extensive water extraction in some zones of the aquifer than in others.

Therefore, in this example an idealized system with a configuration similar to the real aquifer in Queretaro was modelled trying to represent the behaviour of the aquifer. The used configuration is a low permeable clay layer on the top, a sand layer underneath and a high permeability fault zone. Also typical values for pyroclastic non-consolidated deposits (TpPyLac) and Quaternary alluvium (Qal) sediments in the aquifer in Queretaro were used for the modeling (Pacheco-Martinez & Azate-Flores 2007, Trejo-Moedano 1989, see Table 1 and 3).

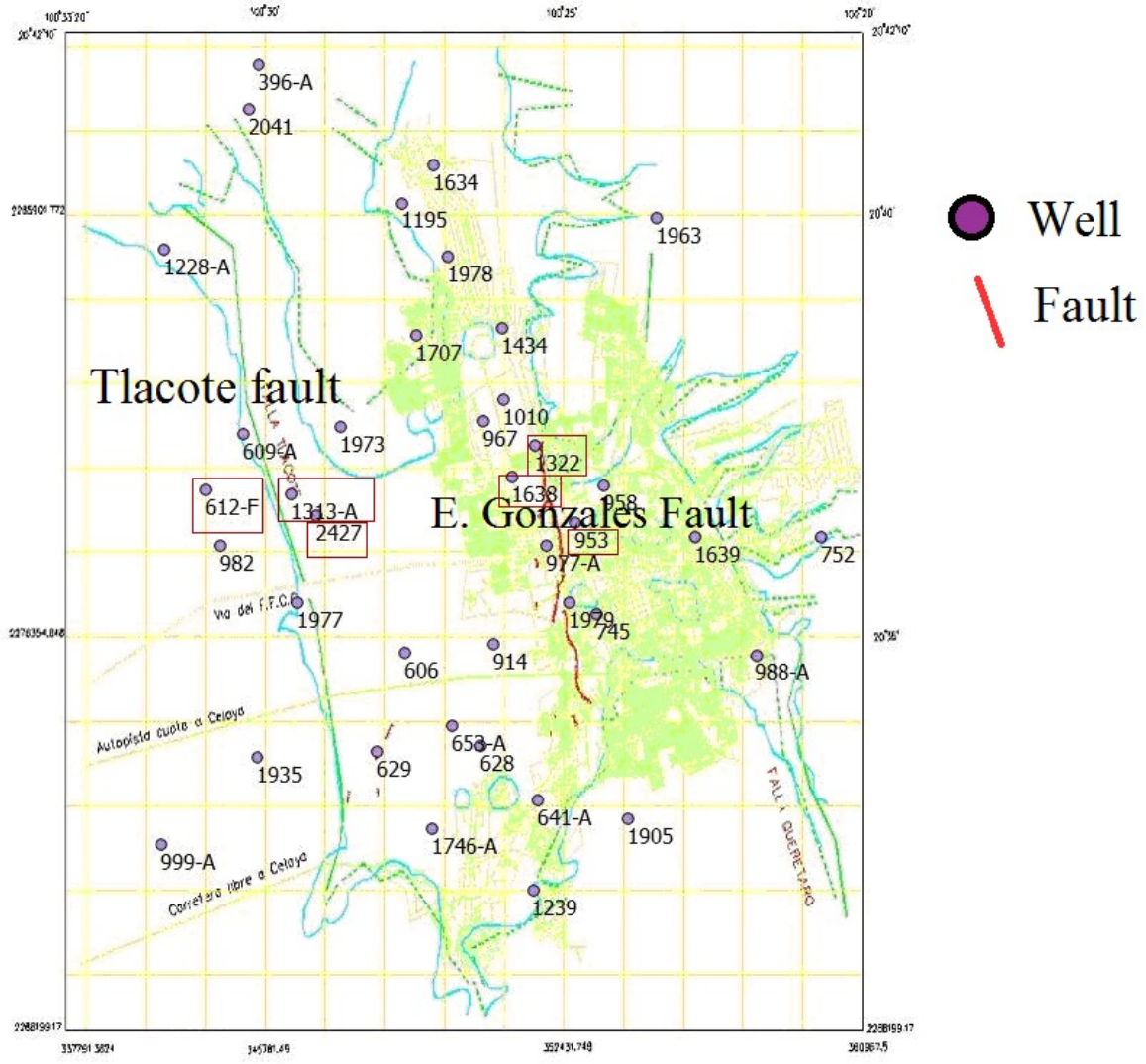

Figure 4.27 Queretaro, urban area and well distribution; faults and fractures location after Pacheco (2007)

The aim of this example is to obtain a better understanding of the relationship of a fault and its permeability and to determine which elements should be present to produce such a hydrologic barrier. Although only idealized hydrogeological systems are modelled, the results explain one of the possible factors of the differences in piezometric level at both sides of the structural discontinuities and help to understand how and under which conditions a fault zone could perform as a hydrologic barrier in the groundwater flow and its influence on land subsidence when this hydrologic barrier is produced. It also serves as a comparison between

the deformation produced by water extraction and fast water infiltration through the fault.

4.3.2 Idealized system and parameters

The same rectangular system used in section 4.2 was chosen. A 2D model of a two-layered system with a clay layer on the top, a sand layer underneath and a 1 m fault zone was set up (Figure 4.28). Different setups were carried out varying the fracture zone inclination, permeability of the fault zone and well position. Three different fault inclinations were analysed, 45°, 90° and 135° degrees with respect to the horizontal. For all simulations, as initial condition, full water saturation was assumed.

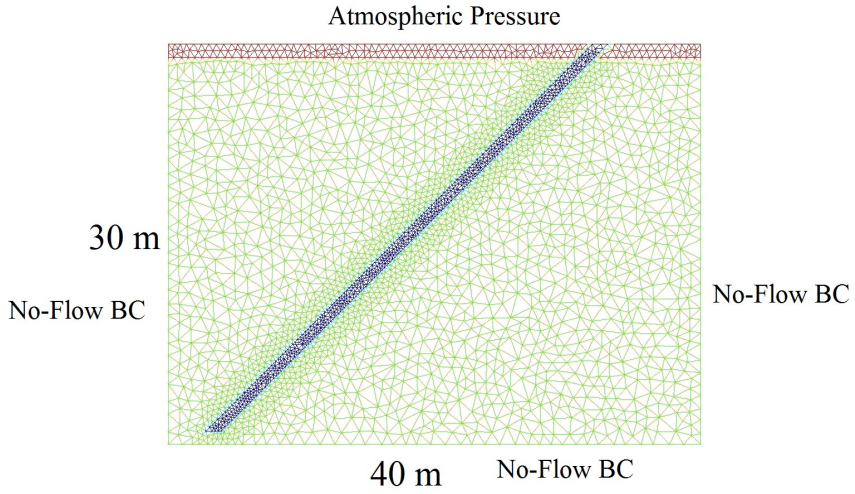

Figure 4.28 Unstructured grid of a 40x30 m system with higher resolution around the fault zone

Displacements are possible along the surface boundary whereas the other boundaries are assumed non-deformable.

4.3.3 Reference case

First a two-layered system without fault and with the same configuration mentioned in the previous section was modelled (Figure 29, left) as a reference to

compare with the results of the other setups. The results of this case are shown in Figure 30, there the normal water depletion cone around a well extraction is illustrated.

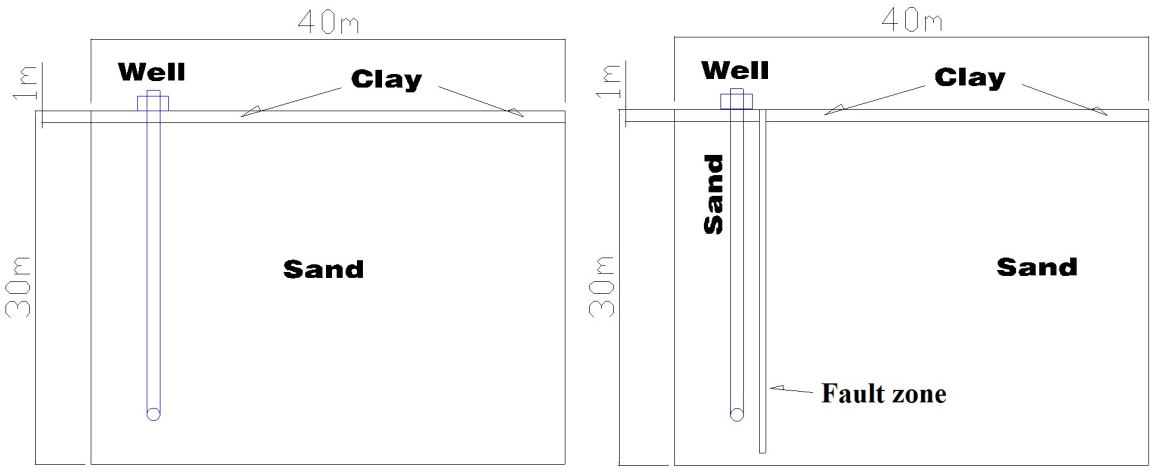

Figure 4.29 Two-layered idealized system: without fault zone (left); with a 90° fault zone (right)

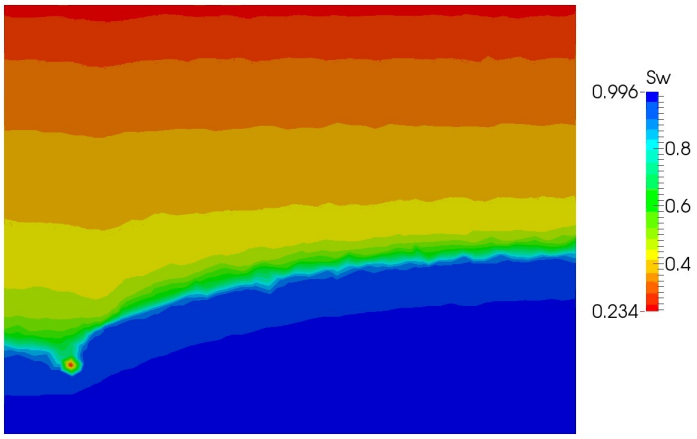

Figure 4.30 Water saturation after water extraction in a system without fault

4.3.4 Vertical fault zone

The first variation to be modeled is the one schematized in Figure 29, right. The well has the same position as in the reference case but now a vertical fault zone is

included. The results of water saturation in Figure 4.31 are quite similar to the reference case, i.e. a vertical fault zone produces almost no difference in the water saturation cone when compared to a system without fault zone.

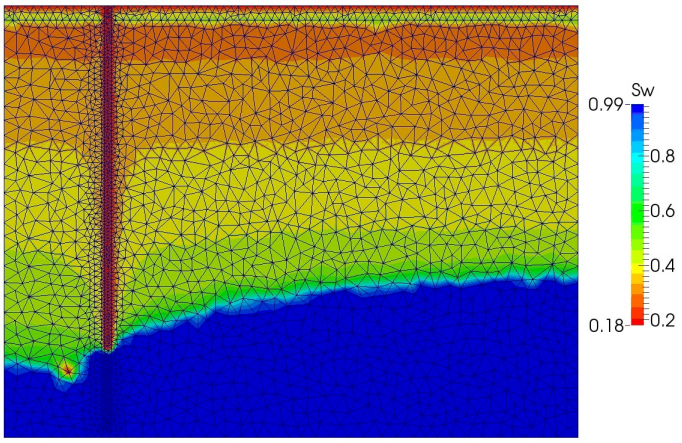

Figure 4.31 Water saturation after water extraction in a system with a vertical fault

4.3.5 Inclined fault zone

The two following simulations are at first with the same system but with a fault zone inclined by 45° and a single well in 25 m depth. There is a short distance between the no-flow BC and the fault zone (Figure 4.32, left). For both cases, the grid resolution in the fault zone and around it is refined (Figure 4.32 and 4.33, right). In the second simulation the fracture has a 135° inclination (Figure 4.33, left). As may be observed in Figure 4.33, left at the bottom, there is a large distance between the well and the fault zone. With the 45° inclined fault zone the bottom of the well is close to the fault and close to the no-flow boundary condition.

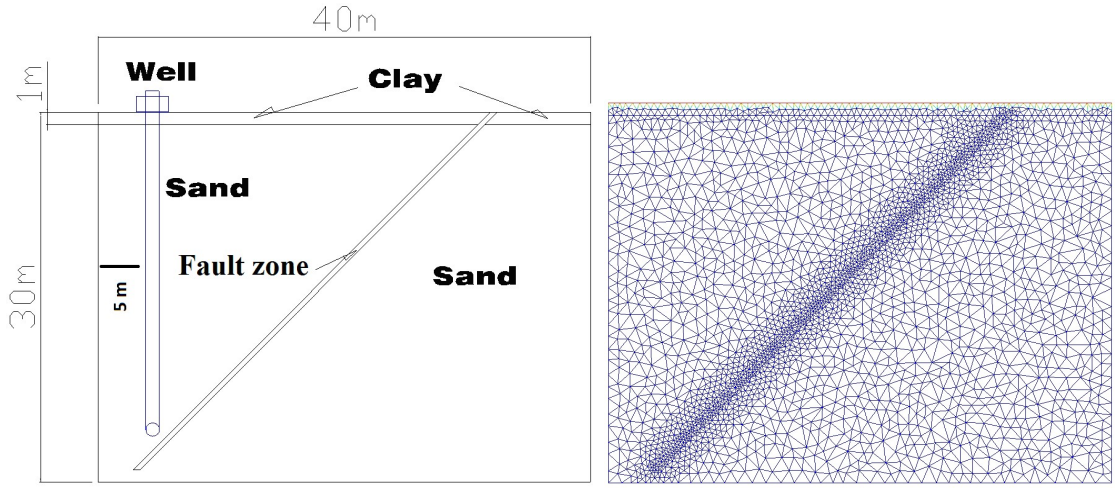

Figure 4.32 Two-layered idealized system with a 45° fault zone (left); grid (right)

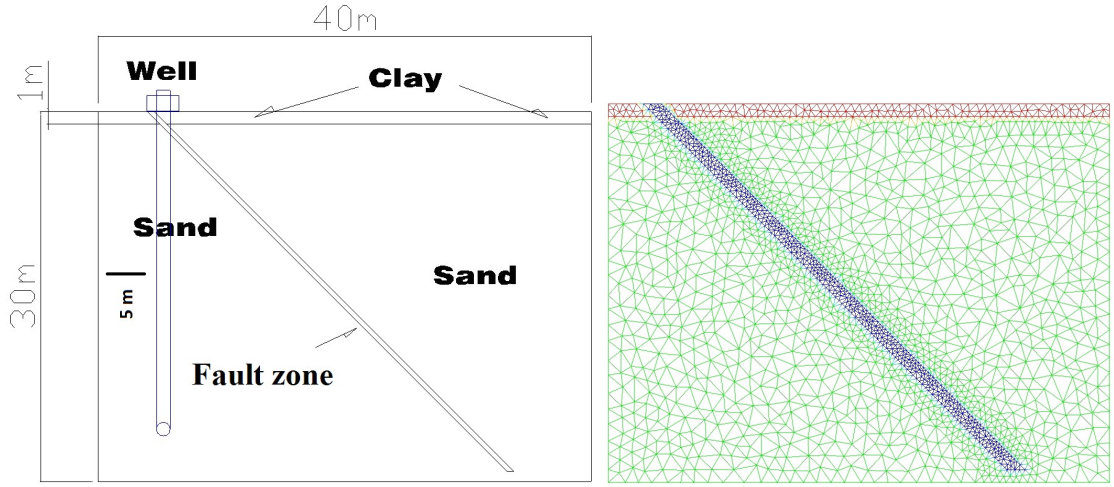

Figure 4.33 Two-layered idealized system with a 135° fault zone (left); grid (right)

First the results of the 135° inclined zone are analysed. Here the depletion cone produced by a single well has no influence on the fault zone with high permeability, i.e. the fault zone does not perform as a hydrologic barrier (Figure 4.34).

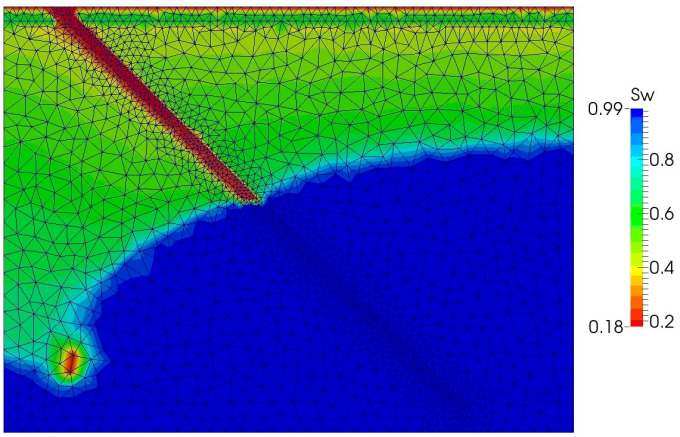

Figure 4.34 Water saturation resulted from a single well extraction in a system with a 135° fault zone

In the case of the system with a 45° inclined, high permeable fault zone (10^{-9} m^2) and a single well extraction Figure 4.35, a, shows a difference of approximately 3.5 m on both sides of the fault zone. The fault zone acts as a hydrologic barrier producing this difference in water levels at both sides of the fault zone and this difference could also increase the differential deformation on the surface.

The factors that produce this barrier effect are: a high well extraction between an impermeable boundary and a high permeable inclined fault where there has to be a short distance between the two and an inclination of less than 90°.

The hypothesis is that the conditions mentioned before are necessary in order to produce this barrier effect. If the well is applied near the fault but not near the no-flow BC, the results show that the barrier effect is not produced. A simulation was performed with the same system but the well was set at the right side close to the fault zone but far away from the no-flow BC. The results show that a typical depletion cone is formed and the fault zone does not act as a barrier (Figure 4.35, b).

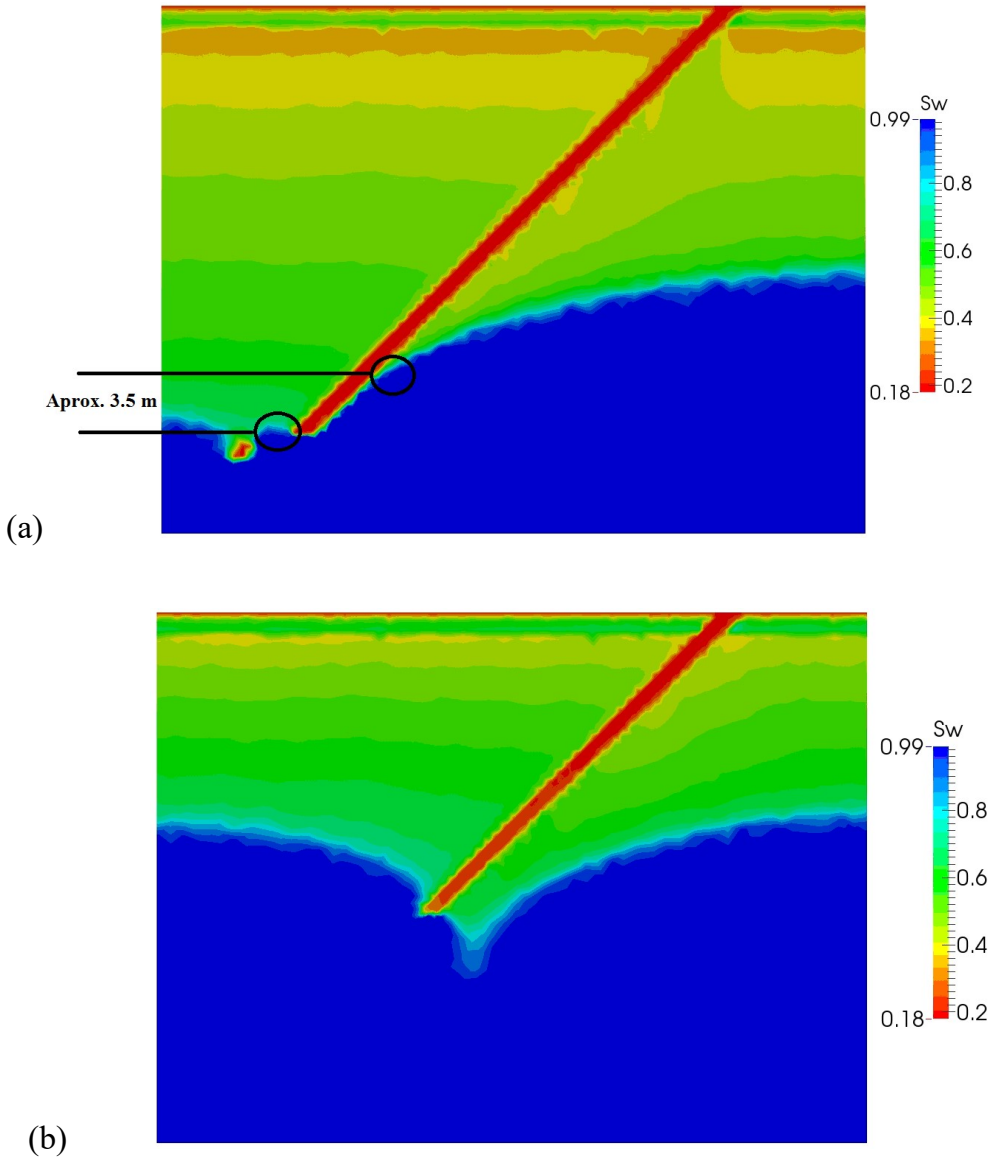

Figure 4.35 Water saturation resulted from a single well extraction in a system with a 45° fault zone; the well is located close to the no flow boundary (left), the well is located far away from the no-flow boundary (right)

In order to ensure that the hydrologic barrier is not produced because of the distance to the no-flow BC, neither because the well is at the right side of the 45° inclined fault zone, another 30x130m system was modeled with the well at the left side near the fault zone but not close to the no-flow BC (Figure 4.36).

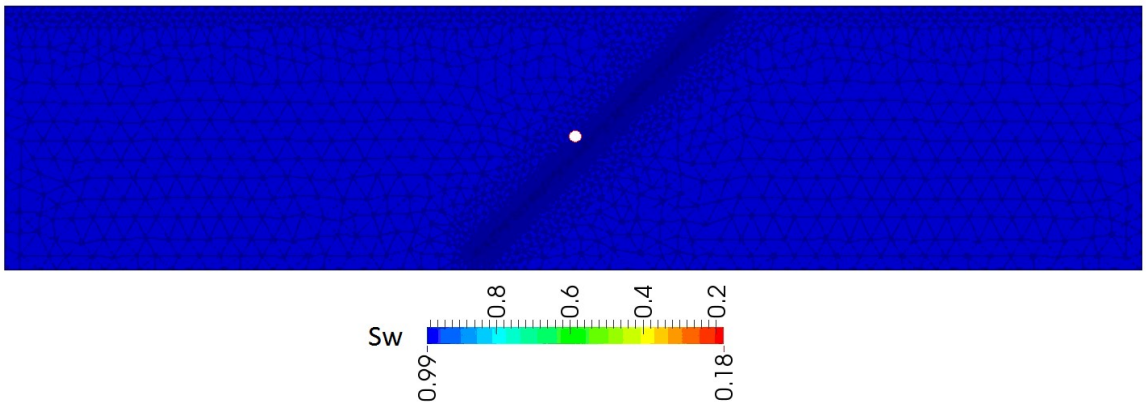

Figure 4.36 Initial condition of modeling a system with a well at the left side and near the fault zone but not close to the no-flow BC

As shown in Figure 4.37, again the hydrologic barrier phenomenon does not appear if the well is near the fault zone and far away from the no-flow BC.

(a)

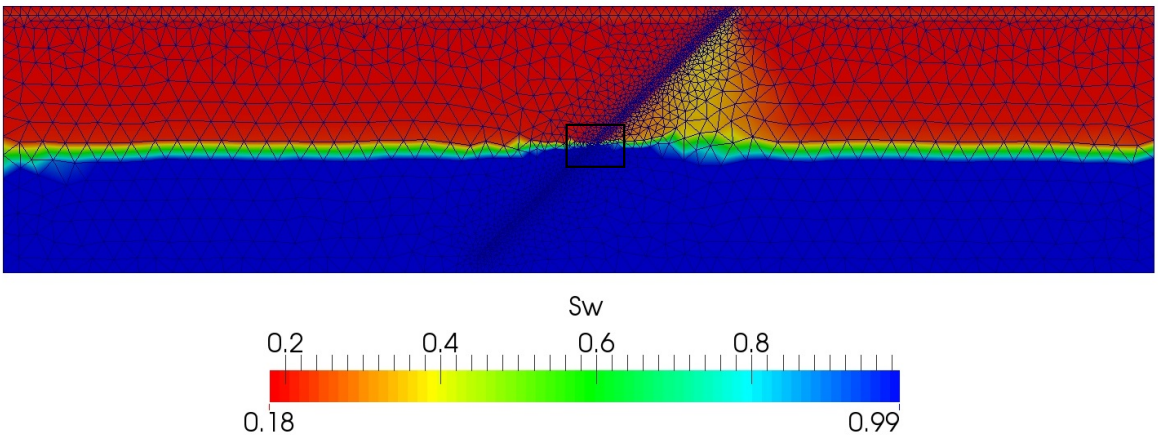

(b)

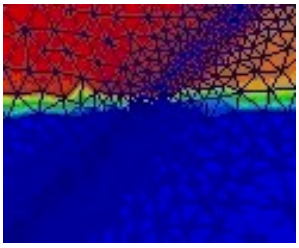

Figure 4.37 (a) Water saturation results of modeling a system with a well at the left side and near the fault zone but not close to the no-flow BC; (b) zoom of fault zone

4.3.6 Deformation caused by barrier effect and fast water infiltration

The results of the case of a system with a 45° high permeability fault zone and a single well extraction exposed in Figure 4.35, a, have been considered for the soil deformation analysis. The lowering of the water table led to a maximum vertical displacement of 0.18 cm (Figure 4.38, a) and a maximum horizontal displacement of 0.06 cm (Figure 4.38, b). The results show that this deformation produced several cut-off points on the surface of the system (Figure 4.39).

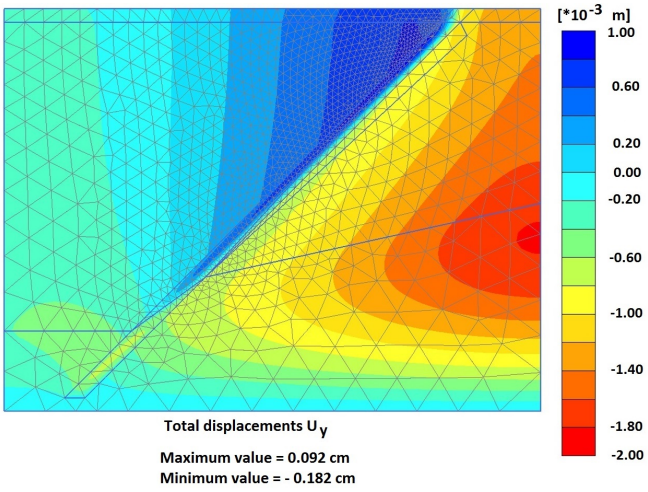

(a)

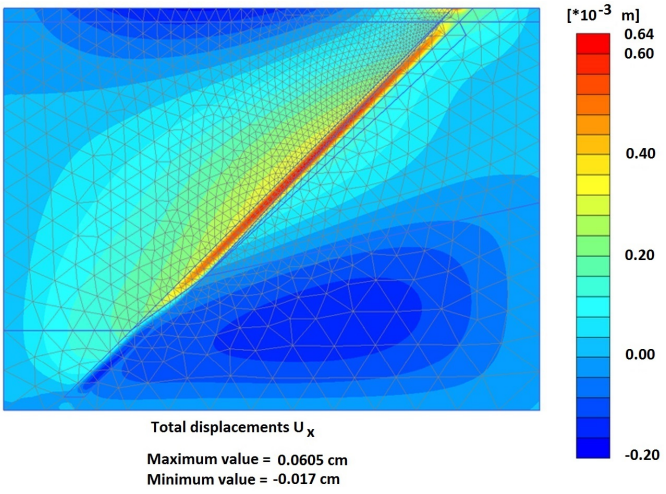

(b)

Figure 4.38 Maximum vertical displacement caused by a single well extraction (a); maximum horizontal displacement caused by a single well extraction (b)

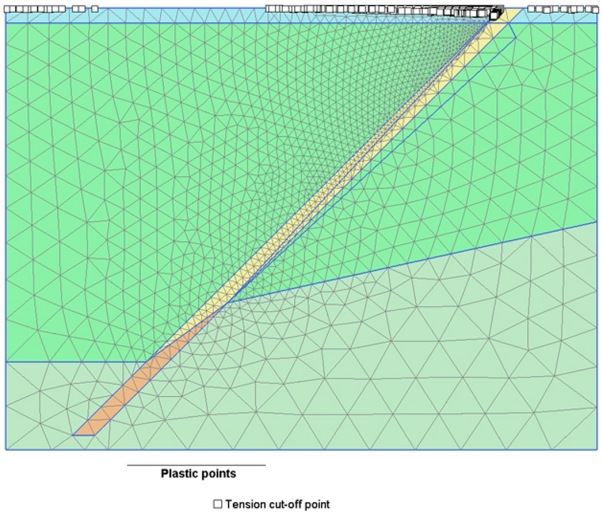

Figure 4.39 Cut-off points on the surface of the system caused by a barrier effect

If after this water extraction, a fast water infiltration through the fault zone is considered which may occur after heavy rainfall, this water infiltration produces additional deformation (Martinez-Noguez *et al*. 2013). Figure 4.40 shows the soil saturation after water extraction by a single well and a 30 minutes fast water infiltration through the fault zone. Figure 3.35, a, represents only the water extraction but in Figure 4.40 also the fast water infiltration is represented.

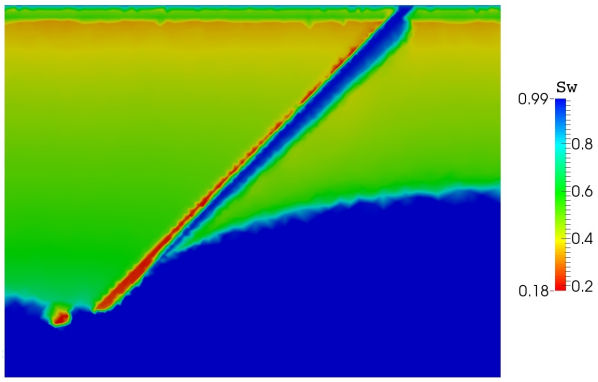

Figure 4.40 Water saturation after extraction and 30 minutes fast water infiltration through a fault zone

This new saturation results have been considered for the deformation modeling. A maximum vertical displacement of 0.65 cm (Figure 4.41a) and a maximum

horizontal displacement of 0.18 cm (Figure 4.41b) were obtained. Both displacements, vertical and horizontal, in the case of additional infiltration are bigger than in the case of a barrier effect produced only by a single water extraction. Horizontal displacements because of infiltration also caused tensional cut-off points and possibly failure points, i.e. new fracture formations.

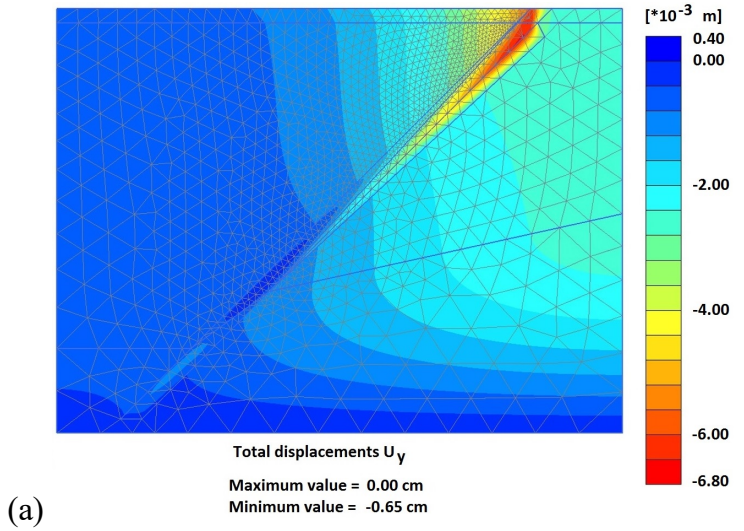

(a)

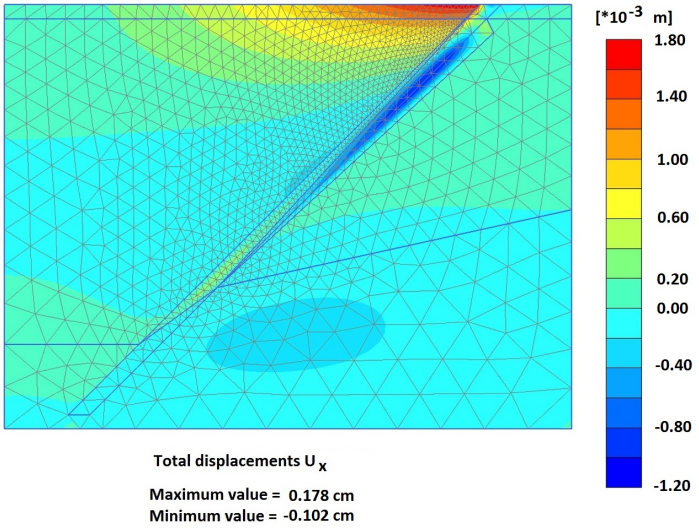

(b)

Figure 4.41 Maximum vertical displacement caused by a fast water infiltration (a); maximum horizontal displacement caused by fast water infiltration (b)

4.3.7 Conclusions

The present study analysed the flow and soil deformation behaviour due to water extraction from faulted aquifer. An idealized porous medium with high permeable fault and single well extraction was analysed. Several configurations for the fault, the location of the well and boundaries were investigated.

The results show that not only an inclined fault zone with low permeability could act as a hydrologic barrier for the water flow in an aquifer but also an inclined fault zone with high permeability. It was noticed that the conditions that produce this hydrologic barrier effect are: a high well extraction between an impermeable boundary condition (e.g. rock) and a high permeable inclined fault where there has to be a short distance between the two and an inclination of considerably less than 90°. Vertical fault zone produces almost no difference in the water saturation cone, when compared to a system without fault zone.

Such barrier effect could be a factor for triggering land subsidence because the different water tables created at both sides of the fault lead to a differential settlement on the surface.

Although a barrier effect produces displacements, especially vertical displacements and cut-off points at the surface, the additional fast water infiltration produces a three times bigger deformation ratio than only the barrier effect and also in a shorter time.

Only an idealized hydrogeological system was modeled and the results explained one factor for triggering land subsidence, differences in piezometric levels around structural discontinuities. This can also occur in natural systems such as in the Queretaro aquifer as the conditions are very similar.

5 Conclusions and outlook

The present study analysed the flow and soil deformation behaviour due to water fast water infiltration and extraction in faulted aquifers through numerical modeling. For the flow a two-phase flow model and for the deformation elasto-plastic models, the Mohr-Coulomb model and the Hardening Soil model, were applied and weakly coupled.

Behaviours of land subsidence were explained numerically and several important results were obtained. Additionally two innovative conceptual models were developed for fault and fracture formation:

- fast water infiltration through a pre-existing fault zone
- barrier effect produced by a fault zone

In this research three examples of numerical modeling were presented. The first application is a model of infiltration through a single-layer system and the impacts on the soil deformation. The second application is a more detailed study of the infiltration and deformation of the soil using a two-layered system. The third application describes a model concept for faulting mechanism after groundwater extraction through a well near a highly permeable pre-existing fault and the impacts on the soil deformation.

A very important result of this research was the development of a conceptual model of a mechanism for the generation of fracturing and triggering of land subsidence: fast rain water infiltration through fault zones and different hydraulic heads.

Through a numerical study this mechanism was explained and also an understanding of the dominant hydrogeological parameters in the evolution of the deformation on the surface caused by a rapid water infiltration through a fault zone was obtained.

In a dry soil as initial condition, if a water column of only a few centimetres (1 and 5 cm) is set on a narrow fault zone, there is no remarkable infiltration through the fault zone because the capillary suction in the clay layer is much stronger than the one of the fault and gravity causes a barrier effect.

If a water column is set on the complete surface, fast infiltration through the fault zone is produced and it propagates not only vertically but also horizontally because of capillarity and gravity forces. It was demonstrated that this rapid infiltration could produce 70 % or more of the annual subsidence ratio. It will produce a rapid increase in the land subsidence and fracture and fault formation and it might damage buildings that are close-by.

In this research it was also found that infiltration into a system with a horizontal surface and with a vertical fracture has no considerable influence on deformation because the water infiltrates directly into the saturated zone. If there is infiltration through the inclined fracture, the displacements, especially the horizontal ones, increase strongly. If there is an inclination on the surface (slope), both horizontal and vertical displacements are considerably increased.

Another important finding was to show that not only an inclined fault zone with low permeability could act as a hydrological barrier for the water flow in an aquifer but also an inclined fault zone with high permeability. It was noticed that the conditions that produce this hydrological barrier effect are: a high well extraction between an impermeable boundary condition and a high permeable inclined fault where there has to be a short distance between the two. A vertical

fault zone produces almost no difference in the water saturation cone in comparison to a system without fault zone. Also the results show that this barrier effect could be a factor for triggering land subsidence.

The main objective of this work was the application of numerical methods to land subsidence. Firstly of all in order to obtain a better understanding of the phenomenon and secondly in order to allow a prediction of the phenomenon in an economical way but with sufficient approximation to permit taking actions. The goal was reached. The numerical modeling performed in this research made the behaviour of land subsidence more clear and explained some aspects of this complicated phenomenon.

The modeling of infiltration through faults and deformation explains possible causes of this deformation and the generation of new faults and fractures so that principally this model could be applied to a real natural system. In this research simplifications were done as the fault was modelled as a continuous porous medium, the flow through the fault was modelled assuming the validity of the Darcy law (Reynolds numbers $Re < 1 \ldots 10$) and the deformation was modelled assuming the fault as a continuous medium. For future work, non-linear flow laws and detailed analysis of soil mechanics with an extended experimental data of the faults should be investigated.

In this work idealized hydrogeological systems were modelled applying values of real soil layers of the natural aquifer in Querétaro, Mexico. Only 2D modeling was performed but the results represent and explain the principal processes properly. For future work a 3D system and other natural systems can be modeled, however sufficient data should be available.

References

Arya,L.M. & Paris,J.F. (1981): A Physico Empirical Model to Predict the Soil Moisture Retention Characteristic from Particle Size Distribution and Bulk Density Data, Soil Sci. Soc. Am. J., 45, pp. 1023-1030

Arroyo,M., Arzate,J., Yutsis,V., Martínez,J., (2002): Estudio integral del recurso agua en los acuíferos del estado de Querétaro, área de geofísica, geología y geotécnia. Reporte Comisión Estatal de Agua (CEA), Querétaro, México

Bastian,P. (1996): Parallele Adaptive Mehrgitterverfahren, Teubner Skripte zur Numerik, B. G. Teubner, Stuttgart

Bastian,P., Birken,K., Johannsen,K., Lang,S., Eckstein,K., Neuss,N., Rentz-Reichert,H. & Wieners, C. (1997): UG - A Flexible Toolbox for Solving Partial Differential Equations, Computing and Visualization in Science (1)
URL:http://cox.iwr.uni-heidelberg.de/ ug

Bastian,P., Chen,Z., Ewing,R., Helmig,R., Jakobs,H. & Reichenberger, V. (2000): Numerical Simulation of Multiphase Flow in Fractured Porous Media, in Chen,Z., Ewing,R. & Shi,Z.C. (eds.): Lecture Notes in Physics, Springer, pp. 52-71

Bear, J. (1972) Dynamics of fluids in porous media. Environmental Sciences Series, Elsevier, New York

Breiting,T., Hinkelmann,R. & Helmig,R. (2000): Modeling of Hydrosystems with MUFTE-UG: Multiphase Flow and Transport Processes in the Subsurface, Fourth International Conference on Hydroinformatics, Iowa, USA

Brooks,R.H. & Corey,A.T. (1964): Hydraulic properties of porous media, in Hydrol. Pap., Vol. 3, Fort Collins, Colorado State University

Burbey. T.J. (2002): The influence of faults in basin-fill deposits on land subsidence, Las Vegas, Nevada, USA. Hydrogeol J 10(5):525–538

Burdine,N.T. (1953): Relative Permeability Calculations from Pore-Size Distribution Data, Technical Report, Petroleum Transactions, AIME

CNA, (2000): Determinación de la disponibilidad de Agua en el Acuífero Valle de Querétaro, Estado de Querétaro: Comisión Nacional del Agua, Subdirección general técnica, Gerencia de Aguas subterráneas

Caine,J.S., Evans,J.P. & Forster,C.B. (1996): Fault zone architecture and permeability structure. Geology; v. 24; no.11; p. 1025-128

Carreón-Freyre,D, Cerca,M., Luna-González,L. & Gámez-González,F.J (2005): Influencia de la estratigrafía y estructura geológica en el flujo de agua subterránea del Valle de Querétaro. Revista Mexicana de Ciencias Geológicas 22(1): 1-18

Carpenter, M.C. (1999): South-Central Arizona. In D. Galloway, D.R. Jones, & S.E. Ingebritsen (Eds.), Land subsidence in the United States: U.S. Geological survey circular 1182 (pp.65-78)

Class,H., Helmig,R. & Bastian,P. (2002): Numerical Simulation of Nonisothermal Multiphase Multicomponent Processes in Porous Media - 1. An Efficient Solution Technique, Adv.Water Resour., 25, pp. 533-550

Coplin,L.S. & Galloway,D. (1999): Houston-Galveston, Texas. Managing coastal subsidence. Land Subsidence in the United States. Circular 1182. U.S. Department of the Interior, U.S. Geological Survey

Distribution of earth's water.
URL: http://water.usgs.gov/edu/earthwherewater.html Accessed at 06.01.2016

Ehlers,W., Avci,O. & Markert,B. (2011): Computation of slope movements initiated by rain-induced shear bands in small-scale test and in situ. Vadose Zone J 10(2):512–525. doi:10.2136/vzj2009.0156

Fracture in Chalco Mexico, Accessed at 06.09.2015
URL: http://www.jornada.unam.mx/2009/06/03/estados/032n1est

Galili,E., Weinstei-Evron,M., Hershkovity,I., Gopher,A., Kislev,M., Lernau,O., Kolska-Horwitz,L. & Lernau,H. (1993): Atlit-Yam: A Prehistoric Site on the Sea Floor of the Israeli Coast. Journal of Field Archeology, Vol 20, No. 2, 133-157

Galloway,D., Jones,D.R. & Ingebritsen,S.E. (1999): Land Subsidence in the United States. Circular 1182. U.S. Department of the Interior, U.S. Geological Survey

Galliway,D. & Riley,F.S. (1999): San Joaquin Valley, California. Largest human alteration of the Earth´s surface. Land Subsidence in the United States. Circular 1182. U.S. Department of the Interior, U.S. Geological Survey

Ganguli, M. (2011): Groundwater withdrawal and land subsidence: A study of Singur Block, West Bengal, India. International Journal of Geomatics and Geosciences. Volume 2, No 2, ISSN 0976-4380

Gerke,H.H. & van Genuchten,M.T. (1993b): Evaluation of a first-order water transfer term for variably saturated dual-porosity flow models, Water Resources Research 29(4), 1225.
URL: http://www.agu.org/pubs/crossref/1993/92WR02467.shtml

Helmig,R. (1997): Multiphase flow and transport processes in the subsurface: A contribution to the modeling of hydrosystems, Springer, Berlin, Heidelberg

Helmig,R. & Huber,R. (1998): Comparison of Galerkin-Type Discretization Techniques for Two-Phase Flow in Heterogeneous Porous Media, Adv. Water Resour., 21 (8), pp. 697-711

Helmig,R. & Cunningham,A. (2002): Multiphase Flow, Transport and Bioremediation in the Subsurface, Course material of IAHR-EGW short course, Lehrstuhl f¨ur Hydromechanik und Hydrosystemmodellierung, Institut f¨ur Wasserbau, Universitäat Stuttgart in cooperation with the Center for Biofilm Engineering, Montana State University, Bozeman

Hernandez-Marin,M. & Burbey,T.J. (2010): Controls on initiation and propagation of pumping-induced earth fissures: insights from numerical simulations. Hydrogeoly J 18:1773–1785

Hinkelmann,R. (2005): Efficient Numerical Methods and Information-Processing Techniques for Modeling Hydro-and Environmental Systems. Springer, Berlin, Germany

Hirono,T. & Wadachi,K. (1995): Environmental Protection Agency. Brief Summary of Land Subsidence in Japan

Holzer,T.L. (1984): Ground failure by ground-water withdrawal from unconsolidated sediments: Geological society of America Reviews in Engineering Geology, Volume VI, p. 67-105

Human settlement in Mesopotamien (Wikipedia, 2015)
URL: http://de.wikipedia.org/wiki/Mesopotamien Accessed 13.05.2015

Ingebritsen,S.E. & Jones,D.R. (1999): Santa Clara Valley, California. A case of arrested subsidence. Land Subsidence in the United States. Circular 1182. U.S. Department of the Interior, U.S. Geological Survey

Ingebritsen,S.E. & Ikehara,M.E. (1999): Sacramento-San Joaquin Delta. The sinking heart of the state. Land Subsidence in the United States. Circular 1182. U.S. Department of the Interior, U.S. Geological Survey

Ingebritsen,S.E., McVoy,Ch., Glaz,B. & Park,W. (1999): Florida Everglades. Subsidence threatens agriculture and complicates ecosystem restoration. Land Subsidence in the United States. Circular 1182. U.S. Department of the Interior, U.S. Geological Survey

Jachens,C.R. & Holzer,L.T. (1979): Geophysical investigations of ground failure related to ground water withdrawal Picacho basin Arizona: Ground Water, vol. 17, no. 6. p. 574-585

Jachens,C.R. & Holzer,T.L. (1982): Differential compaction mechanism for earth fissures near Casa Grande, Arizona. Geol Soc Am Bull 93:998–1012

Jonasson,S.A. (1989): Estimation of the Van Genuchten Parameters from Grain-Size Distribution, in Indirect Methods for Estimating the Hydraulic Properties of Unsaturated Soils, Riverside, California

Kappel,W.M., Yager,R.M. & Miller,T.S.(1999): The Retsof Salt Mine Collapse. Widespread subsidence occurred after a mine collapse in the Genesee Valley, New York. Land Subsidence in the United States. Circular 1182. U.S. Department of the Interior, U.S. Geological Survey

Kreiter,C.W. (1977): Fault control of subsidence, Houston, Texas. Ground Water 15 (3): 203-214

Kumar,C.P. (2002): Modelling of Unsaturated Flow. National Conference on “Modern Trends in Water Resources Development and Environmental Management” 7-8 March 2002, Vellore Institute of Technology, Vellore (Tamil Nadu), pp. 1-9

Kumarci,K., Ziaie,A. & Kyioumarsi,A. (2008): Land subsidence modeling due to ground water drainage using" WTAQ" software. WSEAS transactions on environment and delevopment. Issue 6, Volume 4, 503-512, ISSN: 1790-5079

Kung,K-JS. (1990): Preferential flow in a sandy vadose zone: 1, field observation. Geoderma 46:51–58

Lang,S. (2001): Parallele numerische Simulation instationärer Probleme mit adaptiven Methoden auf unstrukturierten Gittern, Dissertation, Mitteilungen Heft 110, Institut für Wasserbau, Universität Stuttgart

Magaña,V., Pérez,J. & Méndez,M. (2003): Diagnosis and prognosis of extreme precipitation events in the Mexico City Basin. Geofís Int 41(2):247–259

Martinez-Noguez,I., Hinkelmann,R. & Savidis, S. (2010): Modelling Land Subsidence Processes Induced by Fast Rainwater Infiltration Through Fractures into the Unsaturated Zone. Land Subsidence, Associated Hazard and the Role of Natural Resources Development, IAHS Red Book Series, Oxfordshire, Pub. 339, pp. 82-89, paper and oral presentation, ISBN 987-1-907161-12-4

Martinez-Noguez,I., Hinkelmann,R. & Savidis, S. (2012): Numerical Simulation of Infiltration and Land Subsidence in a Two-Layered System with a Fault Zone. 10th International Conference on Hydroinformatics HIC 2012, Hamburg, Germany, reviewed paper and oral presentation

Martinez-Noguez,I., Hinkelmann,R. & Savidis, S. (2013): Fast Water Infiltration, a Mechanism for Fracture Formation During Land Subsidence. Hydrogeology Journal. DOI 0.1007/s10040-013-0971-6

Martinez-Noguez,I. & Hinkelmann,R. (2015): Land subsidence caused by a single water extraction well and rapid water infiltration. Proc. IAHS, 92, 1–6, 2015, doi:10.5194/piahs-92-1-2015

Mayo,A.L. & Koontz,W. (2000): Fracture flow and grownd water compartmentalization in the Rollins Sandstone, Lower Mesaverde Group, Colorado, USA. Hydrogeology Journal, Volume 8, Issue 4, pp 430-446

McClenny,B. (2012): Large sinkhole opened up at Jonesville area home; The Gainesville Sun, Published: Saturday, May 12, 2012 at 9:14 Accessed at 06.01.2016
URL: http://www.gainesville.com/article/20120512/ARTICLES/120519871

Meli,R. & Sanchez,A.R. (1997): Rehabilitation of the Mexico City Cathedral. Structural Engineering International, 9,2. pp. 101-106

Meli,R., Rivera,D. & Miranda,E. (2001): Measured seismic response of the Mexico City Cathedral. Historical Constructions, P.B. Lourenço, P.Roca (Eds.) Guimarães

Mualem,Y. (1976): A New Model for Predicting the Hydraulic Conductivity of Unsaturated Porous Media, Water Resources Research, 12, pp. 513-522

Murillo-Fernández,R., Morales y Monroy,R. & Hernández-Rubio,A. (1991): Agrietamiento lacustre al oriente de la ciudad de México, Sociedad Mexicana de Mécanica de Suelos, México, pp 79-94

Novak,T.P., Hoffman,D.L., & Yung,Y. (2000): Measuring the customer experience in online environments: A structural modeling approach. Marketing Science, 19(1), 22– 42

Osmaniğlu,B., Dixon,T.H., Wdowinski,S., Cabral-Cano,E. & Jiang,Y. (2010): Mexico City Subsidence Observed with Persistent Scatterer InSAR. Journal of Applied Earth Observation and Geoinformation

Pacheco,J., Aryate,J., Rojas,E., Arroyo,M., Yutsis,V. & Ochoa,G. (2006): Delimitation of ground faulure zones due to land subsidence using gravity data and finite element modeling in the Querétaro valley, Mexico. Engineering Geology 84 (2006) 143-160

Pacheco,J. (2007): Modelo de subsidencia del Valle de Queretaro y predicción de agrietamientos superficiales, PhD thesis, UNAM Mexico

Pavelko,M.T, Wood,D.B. & Laczniak,R.J. (1999): Las Vegas Nevada, Gambling with water in the desert. Land Subsidence in the United States. Circular 1182. U.S. Department of the Interior, U.S. Geological Survey

Pham-Van,S. (2009): Application of Different Model Concepts for Simulation of Two-Phase Flow Processes in Porous Media with Fault Zones, Promotion, Technische Universität Berlin

Prokopovich,N.P. (1979): Genetic classification on land subsidence. Saxena, S.K. (ed.). Evaluation and prediction of subsidence. Proc.of the Int. Conf., Pensacola Beach, Florida. January 1978, Am. Soc. Civil Eng., New York, 389-399

Rodríguez-Castillo,R. & Rodríguez-Velázquez,I. (2006): Consecuencias sociales de un desastre inducido, subsidencia. Boletín de la Sociedad Geologica Mexicana. Numero Especial de Geologia Urbana, Tomo LVIII, No. 2, pp. 265-269

Schanz,T., Vermeer, P.A. & Bonnier,P.G. (1999): The hardening soil model: formulation and verification. Beyond 2000 in Computational Geotechnics, Balkema, Rotterdam

Sheng,Z. & Helm,D.C. (1995): Conceptual models for earth fissuring in Las Vegas Nevada, USA. In: Land subsidence. Proceedings of the Fifth International Symposium on Land Subsidence, The Hague. IAHS Publ 234, IAHS, Wallingford, UK, pp 381–387

Suárez-Placencia,C., Escalona-Alcázar,F.J. & Díaz-Torres,J.J. (2005): Desarrollo de grietas en el fraccionamiento Prados de Nextipac, Municipio de Zapopan, Jalisco [Development of cracks in Nextipac Meadows subdivision, municipality of Zapopan, Jalisco]. GEOS 25(2):352–362

Smith,C. (2012): After 37 years at home, sinkhole sends them packing. Gainesville Sun, May 13

Trejo-Moedano, A. & Martinez-Baini,A. (1991): Agrietamiento de suelos zona Queretaro [Soil cracking in the zone of Queretaro]. Sociedad Mexicana de Mécanica de Suelos, México, pp 67–74

Trejo-Moedano,A., (1989): Estratigrafía y propiedades mecánicas del suelo del valle de la zona urbana de Querétaro: Universidad autónoma de Querétaro, ISBN: 968-845-089-8, Querétaro Mexico

Terzaghi,K. (1956): Theoretical soil mechanics; John Wiley and Sons Inc. New York

Tomás,R., Herrera,G., Delgado,J. & Peña,F. (2009): Subsidencia del Terreno. Enseñanza de las Ciencias de la Tierra. Pp. 295-302. ISSN 1132-9157

Van Genuchten,M.T. (1980): A closed-form equation for predicting the hydraulic conductivity of unsaturated soils, Soil Sci. Soc. Am J., 44, pp. 892-898

Verheye,W. (2002): Land use, land cover and soil sciences, vol II: soils of arid and semi-arid areas. Encyclopedia of Life Support Systems (EOLSS), Ramsey, UK, National Science Foundation Flanders–Belgium and Geography Department, University of Gent, Belgium

Villa,E.S., Shelly,E.O., Mooser,F. & Plata,E.L. (2005): Sintesis Geotectonica de la Cuenca de México. TGC Geotecnia, Mexico. D.F.

Waterman,D., Al-Khoury,R., Bakker,J.K., Bonnier,P.G., Burd,H.J., Soltys,G. & Vermeer,P.A. (2004): PLAXIS, 2D, Version 8, Manual. PLAXIS, Delft, The Netherlands. URL: http://www.plaxis.nl/shop/135/info/manuals. Accessed 8 March 2014

Wolkersdorfer,Ch., & Thiem,G. (2006): Ground Water Withdrawal and Land Subsidence in Northeastern Saxony (Germany). Mine Water and the Envirenment, International Mine Water Association. Pp. 91-92

Ziaie,A. & Bagher-Rahnama,M. (2007): Prediction of Single Well Land Subsidence Due to Ground Water Drainage. International Journal of Agricultural Research, 2: 349-358

Settlements close Nile river. Ancient Egypt, Accessed at 06.09.2015
URL: http://www.ancient-egypt.info/2012/03/egyptian-nile-river-and-god-kings-of.html

U.S.G.S., (1999): Land subsidence in the United State: Circular 1182, U. S. Geological Survey. Galloway D., Jones D. R. e Ingebritsen S. E. eds